Automatic generation of Chemical Reactor Networks for Combustion Simulations

Rishikesh Sampat

Technische Universiteit Delft

TU Delft Delft University of Technology

Challenge the future

AUTOMATIC GENERATION OF CHEMICAL REACTOR NETWORKS FOR COMBUSTION SIMULATIONS

by

Rishikesh Sampat

in partial fulfillment of the requirements for the degree of

Master of Science
in Aerospace Engineering

at the Delft University of Technology,
to be defended publicly on Thursday March 29, 2018 at 13:30.

Supervisor:	Dr. A.Gangoli Rao	
	A.A.V.Perpignan, MSc	
	Ir. E.ter Hofstede	
Thesis committee:	Dr. A.Gangoli Rao,	TU Delft
	Dr. D.Lahaye,	TU Delft
	Ir. W.A. Timmer,	TU Delft
	A.A.V.Perpignan, MSc	TU Delft
	Ir. E.ter Hofstede	MTEE

TU Delft Delft University of Technology

ACKNOWLEDGEMENT

This thesis has been a eye-opening journey that has made me grow personally and professionally. This work has been possible because of the support and guidance of my daily supervisors André Perpignan and Eline ter Hofstede. I really appreciate them reading through my thesis and providing valuable comments to improve it. I would also like to thank Dr. Arvind Rao for being my supervisor and giving me the opportunities to be exposed to academic research. Many thanks to Mitsubishi Turbocharger and Engine Europe B.V. for hiring me as a student researcher.

I would like to express my gratitude to my parents, Kirti Sampat and Pankaj Sampat, and my sister, Mrinalini Sampat, for their support and sacrifices that has enabled me to be at this stage in life. I thank my friends and colleagues for their company that helped me get through the difficult times of the journey. Last but not the least I would like to thank Dhirendra Ashar and Vatsal Lilani for believing in me and providing financial support during my Master studies.

Delft, March 2018 R. Sampat

ABSTRACT

Gas turbines are the power house of most modern day aircrafts. Combustion of fossil fuels provides the energy required, but this produces harmful emissions. With ever increasing strictness on emissions regulation, it is becoming even more necessary to design gas turbine combustion chambers with the intent of low pollutant output. Gas turbine engines on the other hand also have the property of dense power output, while at the same time being capable of producing lower emissions than internal combustion engines. This has served as an impetus for Mitsubishi Turbocharger and Engine Europe B.V.(MTEE), to develop a gas turbine, designed around its turbocharger unit, to be used as a range extender on Battery Electric Vehicles(BEV) in the future. The common interest of the Propulsion group at TU Delft, LR and MTEE has resulted in this thesis on researching a computational method to obtain accurate predictions of combustion emissions from a gas turbine combustor.

The method explored is the Automatic CFD-CRN method which decouples calculations of fluid mechanics and detailed chemistry by performing them in a CFD simulation and a Chemical Reactor Network respectively. Accurate prediction of emissions requires a detailed chemical kinetic mechanism to be implemented but doing so, directly in CFD, is prohibitively expensive. Hence CFD is used to obtain the combustion flow field, which is influenced mainly by the evolution of major species, whereas the minor species are obtained from the implementation of detailed chemistry in a CRN derived automatically from the CFD mesh. Such a calculation is feasible because ideal reactors, which are the building blocks of a CRN, have a simplified fluid dynamic model and can hence process the detailed chemistry at an affordable time cost.

A software package implementing the Automatic CFD-CRN process is developed and factors affecting the results from this computational tool are studied in this research work.

NOMENCLATURE

BFS	Breadth First Search
CFD	Computational Fluid Mechanics
CRN	Chemical Reactor Network
DNS	Direct Numerical Simulation
EAR	Excess Air Ratio
FGM	Flamelet Generated Manifold
LES	Large Eddy Simulation
MFC	Mass Flow Controller
MMF	Mean Mixture Fraction
PDF	Probability Density Function
PFR	Plug Flow Reactor
ppm	part per million
PSR	Perfectly Stirred Reactor
RANS	Reynold's Averaged Navier Stokes
SFIRN	Simplified Fluid dynamics by Ideal Reactor Networks

CONTENTS

LIST OF FIGURES

1

INTRODUCTION

Combustion is one of the oldest technologies developed by man-kind. We as human beings have come a long way from the first accidental fire as cavemen to burning fuel in gas turbine engines that propel aircrafts, yet combustion remains an open field with questions remaining to be answered about its occurrence. The energy obtained from combustion comes at the cost of harmful emissions which adversely affects our health and environment. While combustion devices are pivotal to the development of civilization and emissions are an inevitable by-product, it is possible to reduce its negative effects by designing cleaner combustion chambers which emit lesser pollutants. Such design processes require adequate tools which are capable of providing predictions of emissions. This thesis is focused on developing a computational tool for calculating emissions from gas turbine combustion chambers and studying the factors that affect its accuracy.

1.1. BACKGROUND

Gas turbine engines are the primary propulsion systems in aviation today. The main parts of it, as shown in Figure 1.1, are an air intake, compressor, combustion chamber, turbine and exhaust. Current European

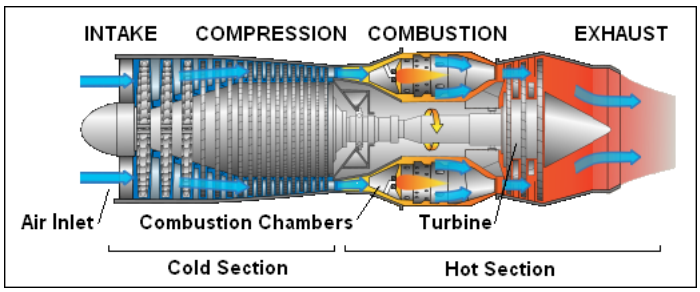

Figure 1.1: Section view of a gas turbine engine[1]

legislation sets challenging goals for the aircraft industry to cut down emissions released by burning fuel in the combustion chamber. Long term goals(2050) include reducing NO_x by 90%, CO_2 by 75%, as compared to a typical new aircraft in the year 2000[13]. Achieving these goals require accurate computational tools in order to model and predict emissions from gas turbine engines to design 'cleaner' combustion chambers.

Mitsubishi Turbocharger and Engine Europe(MTEE) is interested in exploring alternate applications of its turbochargers. A turbocharger is a system consisting of a radial compressor and a radial turbine as shown in Figure 1.2. The future market of Battery Electric Vehicles(BEV) appears to have a demand for range extenders to make less frequent journeys of larger distances and as an emergency backup power supply. A range extender is a system that burns fuel in an engine to run a generator which charges the battery when the charge falls below a critical level. As the range extender will be mounted on a BEV, it is expected that the regulations in the future would require it to have very low emissions. Hence MTEE is developing a micro gas turbine that uses the turbocharger unit to harness power, taking advantage of the potential low emission capability of gas turbine engines while having high power output density to be able to recharge the batteries quickly. In order

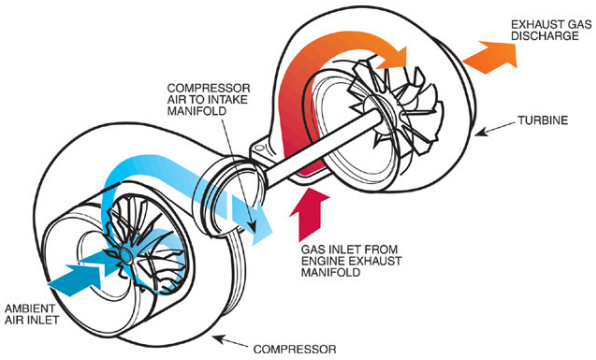

Figure 1.2: Turbocharger[2]

to meet the emission levels, MTEE requires accurate prediction tools during the design phase. This coinciding interest of the Propulsion group at TU Delft Aerospace and MTEE to have accurate emission predictions from gas turbine combustors lead to this thesis.

Computational Fluid Dynamics(CFD) is the generally used tool to predict and study reacting flows in a gas turbine combustion chamber. It is also used to obtain pollutant species output which are called the 'minor species' as they occur in a much smaller amount than the major combustion products of carbon dioxide and water. The current CFD tools have shown to give errors, in minor species concentrations, of several orders of magnitude compared to experimental measurements[17]. One of the reasons for it is that generally, a reduced/simplified chemical mechanism is used to model the chemistry of combustion as implementing a detailed mechanism is prohibitively expensive in CFD due to its size. Also the stiffness of the chemistry makes it difficult to solve along with the non-linear transport equations of CFD.

An alternative approach is that of Chemical Reactor Networks(CRN), in which an equivalent model of the combustor is created using inter-connected ideal reactors as building blocks. As ideal reactors have a simpler system of equations to solve, compared to flow transport equations, detailed chemical mechanisms can be implemented to get a more accurate estimate of chemical species within acceptable computational expense. This research aims at understanding and developing a method to automatically generate a CRN with minimal human interference in the process.

The main goal of the research herein presented is to create valid knowledge to create a computational tool that can automatically generate a CRN for a combustion chamber using the flow field solution by a CFD simulation that implements simplified chemistry.The final deliverable of the thesis is the knowledge as well as a working code of the process of CRN generation and evaluation.

1.2. COMBUSTION

Combustion is a thermochemical process in which the energy stored within the molecules of fuel is released mainly in the form of heat and light. This is used in a gas turbine engine to increase the energy of flowing air. A simple representation of the chemical conversion of hydrocarbon fuel in air is given by Equation 1.1.

$$C_xH_y + a(O_2 + 3.76N_2) \longrightarrow xCO_2 + \frac{y}{2}H_2O + 3.76aN_2 \tag{1.1}$$

This is a representation of a chemical reaction taking place under stoichiometric conditions, i.e just enough air to react completely with the quantity of fuel(C_xH_y). The products may change under rich and lean conditions, i.e when there is excess fuel or excess air respectively and may include other by-products in the form of minor species. The overall chemical reaction is exothermic, hence there is a net release of heat energy which causes an increase in temperature.

1.2.1. TURBULENT COMBUSTION

The flow in a gas turbine combustion chamber is turbulent under most operating conditions. Turbulence can be thought of as a collection of 'eddies' of different sizes. Kinetic energy is transferred from the largest scale to

smaller scales and dissipated at the smallest scale. The transfer of energy occurs due to inherent instability of large scale motions which break down to form small scale motions. The large eddies entrain reactants leading to incomplete mixing in the flow. The small scale eddies, on the other hand, promote small scale mixing and molecular diffusion, allowing chemical reactions to occur. The reactions lead to heat release causing a change in local fluid properties which modifies the turbulent flow. This acts as a feedback loop and there is a constant interaction between turbulent flow and chemical reactions. Thus turbulent combustion is governed by the relative magnitude of the physical and chemical time scales that characterize the transport phenomenon and chemical reactions respectively. When the chemical time scales are comparable to the physical time scales, the rate of evolution of species needs to be taken into account. In cases where infinitely fast chemistry is considered an equilibrium analysis can be done in which species concentrations are calculated from their relation to the equilibrium constants of the reaction.

1.2.2. CHEMICAL KINETICS

Chemical kinetics deals with the calculations for finite rate chemical reactions. Chemical reactions are a result of microscopic collisions between molecules. Based on the number of molecules involved in the collision, a reaction can be classified as Uni-molecular, Bi-molecular and Termolecular. Termolecular reactions are less common and more than 3 molecular collision do not occur due to steric hindrance[26][4].

1. Unimolecular reactions: These are usually a rearrangement or dissociation of a molecule.

$$A \longrightarrow \text{products} \tag{1.2}$$

2. Bimolecular reaction: Most elementary reactions fall under this category, i.e 2 molecules react to form products.

$$\begin{aligned} &A + B \longrightarrow \text{products} \\ &\text{or} \\ &A + A \longrightarrow \text{products} \end{aligned} \tag{1.3}$$

3. Termolecular reactions: These involve 3 bodies. They are usually recombination reactions of the general form

$$A + B + M \longrightarrow C + M \tag{1.4}$$

M is referred to as a the third body and its function is to absorb the internal energy of the newly formed molecule, C, during the collision. Had this body not been present, the molecule would dissociate back to its constituents.

Chemical reaction rate is defined as the rate of consumption of a chemical species in a reaction which in turn indicates the rate of progress of the reaction. Let Equation 1.5 be a chemical reaction.

$$aA + bB \longrightarrow cC + dD \tag{1.5}$$

The rate of reaction is governed by the formulae:

$$\frac{d[A]}{dt} = -k[A]^a[B]^b \tag{1.6}$$

$$k = A(T)e^{-\frac{E_a}{RT}} \tag{1.7}$$

The Equation 1.6 represents the rate of production of species A, where [A] is the concentration of A and [B] is the concentration of species B. In Equation 1.7, k is the rate coefficient, E_a is the activation energy, T is temperature and A(T) is pre-exponential factor as a function of temperature. This relation is also known as the Arrhenius law. Thus the reaction rate is dependent on the temperature through the Arrhenius equation and on the pressure through the influence of pressure on molecular space density which affects the species concentrations. Equations 1.6 and 1.7 are one of the many ways of expressing reaction rates, but this is the most widely used in the field of combustion engineering.

Depending on the level of detail of the mechanism, A and B can directly react to give C and D in a single step reaction as in Equation 1.5, or there can be several intermediate reactions leading to the end result(which

is what occurs in nature). Reactions may be expressed as a gross molecular interaction such as that in Equation 1.8.

$$2H_2 + O_2 \longrightarrow 2H_2O. \tag{1.8}$$

Such reactions are called global reactions and represent an overview of the actual process. This reaction is actually characterized by several sequential processes called elementary reactions which form intermediate species as shown in Equation 1.9.

$$\begin{aligned} H_2 + O_2 &\rightleftharpoons HO_2 + H \\ H + O_2 &\rightleftharpoons OH + O \\ OH + H_2 &\rightleftharpoons H_2O + H \\ H + O_2 + M &\rightleftharpoons HO_2 + M \end{aligned} \tag{1.9}$$

The reactions involving the intermediate species ultimately lead to the conversion of the reactants to the products of the global reaction. This leads to defining a global rate coefficient, which may be different from the rate coefficient of an elementary reaction in the detailed mechanism.

1.2.3. REACTION MECHANISM

Hydrocarbon combustion takes place in several steps. A reaction mechanism is a set of elementary reactions that occur for the reactants to be converted to products. These steps may involve the formation and consumption of intermediate species such as radicals that need not be part of the end product after combustion is completed.

An example of a reaction mechanism is the GRI-Mech 3.0, which is a mechanism developed for natural gas[1] combustion. It is an optimized mechanism that best represents natural gas flames and ignition as currently possible by the Gas Research Institute. It consists of 325 reactions and 53 species and has been optimized for a temperature range of 1000-2500K and 1333.22Pa(10torr) to 1.013×10^6Pa(10 atm) pressure range. Soot formation and chemistry of Selective Non-Catalytic Reburn(SNCR) of NO is not modeled in this mechanism[27]. SNCR is a technology used in industrial furnaces to reduce NO_x and is less relevant for a gas turbine application, so this short coming of the mechanism doesn't affect the research to be performed.

1.3. POLLUTANTS

Some of the products and by products of combustion are harmful for the environment and living beings. These are known as pollutants or emissions. Emissions have been found to be the reason for global warming, ozone layer depletion, acid rain, lung diseases and cardiovascular issues. The main emissions of concern in the gas turbine aspect are CO, NO_x and soot. For the research to be conducted, CO and NO_x will be the considered pollutant species and hence are further elaborated.

1.3.1. CARBON MONOXIDE

Carbon Monoxide(CO) can be poisonous if inhaled as it forms a complex compound with the hemoglobin in blood and reduces the capability of oxygen absorption for biological energy production and metabolic activity. It could lead to unconsciousness, nausea and death[28].

FORMATION

In order to understand the formation of CO, it is necessary to understand the process of combustion of a hydrocarbon. The explanation is provided using methane as a fuel and in successive steps.

1. Combustion at high temperatures(>1000K) relies on radicals to react with fuel molecules. The important radicals are O, OH,H and HO2. These radicals are produced during ignition or by pyrolysis in the preheat zone. These radicals attack fuel molecules and cause them to dissociate, in this case from CH_4 to CH_3.

$$\begin{aligned} O + CH_4 &\rightleftharpoons CH_3 + OH \\ OH + CH_4 &\rightleftharpoons CH_3 + H_2O \\ H + CH_4 &\rightleftharpoons CH_3 + H_2 \\ HO_2 + CH_4 &\rightleftharpoons CH_3 + H_2O_2 \end{aligned} \tag{1.10}$$

[1] Natural gas is a fuel primarily consisting of methane, CH_4

2. Next, the intermediate, CH_3 oxidizes to form CH_2O.

$$\begin{aligned} CH_3 + O_2 &\rightleftharpoons CH_2O + OH \\ &\rightleftharpoons CH_3O + O \\ CH_3 + O &\rightleftharpoons CH_2O + H \end{aligned} \tag{1.11}$$

   CH_2O by itself doesn't cause further chain branching, but is responsible for the production of H atoms, which in turn, take part in chain branching reactions as shown in Equation 1.12, as part of the hydrogen oxidation mechanism, that sustains the combustion reactions by the radicals hence produced.

$$\begin{aligned} H + O_2 &\rightleftharpoons OH + O \\ O + H_2 &\rightleftharpoons OH + H \\ OH + H_2 &\rightleftharpoons H + H_2O \end{aligned} \tag{1.12}$$

3. CH_2O undergoes further oxidation and dissociation to produce CO, i.e

$$CH_2O \longrightarrow HCO \longrightarrow CO \tag{1.13}$$

4. CO in turn oxides through several reactions to form CO_2 which is the end product of complete combustion. This step is also the major source of heat release in the combustion process.

Although the above process has been presented specifically for methane oxidation, the process is quite similar for higher hydrocarbons as during their oxidation, the fuel molecules first break down into simpler alkyls and undergo a similar process.

The global reaction for the oxidation of CO is as given in Equation 1.14

$$CO + \frac{1}{2}O_2 \rightleftharpoons CO_2 \tag{1.14}$$

The main elementary reactions involved in this conversion are given in Equation 1.15

$$\begin{aligned} CO + OH &\rightleftharpoons CO_2 + H && \text{E}_a\text{=32.18 kJ/mol, 1000-2000K[29]} \\ CO + O_2 &\rightleftharpoons CO_2 + O && \text{E}_a\text{=200 kJ/mol, 1000-2000K[29]} \\ CO + O + (M) &\rightleftharpoons CO_2 + (M) && \text{E}_a\text{=12.5 kJ/mol, 1000-2000K[29]} \end{aligned} \tag{1.15}$$

The reactions in Equation 1.15 are relatively slow, which makes it possible for some of the CO produced to not be oxidized to CO_2 before it leaves the combustion chamber, often due to lower temperatures or low residence time. Thus CO emissions obtained at the combustion chamber exhaust are due incomplete oxidation.

1.3.2. NITROGEN OXIDES

NO_x, which is a combination of NO, N_2O and NO_2, has been found to cause photo-chemical smog, acid rain and generate ozone[2] by chemical reaction in the troposphere. In the stratosphere NO_x chemically reacts with ozone, hence depleting the ozone layer leaving the earth's surface vulnerable to the excess ultraviolet radiation from the sun. Consequently, NO_x reduction has become one of the primary focus of advances towards cleaner gas turbine combustion[4].

FORMATION MECHANISMS

NO_x has been found to be formed by the Thermal Pathway, Fenimore mechanism, NNH mechanism, N_2O route and Fuel NOx pathway[30].

1. **Thermal NO_x:**
   Its formation is described by the extended Zeldovich mechanism[31]. It is governed by the following equations:

$$O + N_2 \rightleftharpoons NO + N \qquad \text{E}_a\text{=319 kJ/mol, 2000-4000K[29]} \tag{1.16a}$$

$$N + O_2 \rightleftharpoons NO + O \qquad \text{E}_a\text{=26.2 kJ/mol, 300-3000K[29]} \tag{1.16b}$$

[2] Tropospheric ozone is considered a pollutant which can cause stunted growth in crops as well as be poisonous to humans.

$$N + OH \rightleftharpoons NO + H \qquad E_a\text{=0 kJ/mol, 300-4000K[29]} \tag{1.16c}$$

The triple bond in the Nitrogen molecule is very strong and hence Equation 6.12 has a high activation energy(319 kJ/mol). It is the rate limiting step in the Zeldovich mechanism and has a high reaction rate above 2000K, which gives it the name 'Thermal NO_x'.

A common way of calculating the NO concentration is to assume that the N atoms are in a quasi steady state. This is because Equation 1.16b and Equation 1.16c have been found to be much faster than Equation 1.16a, thus the N atoms which are a product of Equation 1.16a are almost instantly consumed. So the concentration of NO is expressed as,

$$\frac{d[NO]}{dt} = k_1[O][N_2] + k_2[N][O_2] + k_3[N][OH] \tag{1.17}$$

$$\begin{aligned} \frac{d[N]}{dt} &= k_1[O][N_2] - k_2[N][O_2] - k_3[N][OH] \\ \frac{d[N]}{dt} &= 0 \\ \therefore k_1[O][N_2] &= k_2[N][O_2] + k_3[N][OH] \\ \therefore \frac{d[NO]}{dt} &= 2k_1[O][N_2] \end{aligned} \tag{1.18}$$

The value of $[N_2]$ can be measured by probes or calculated by equilibrium analysis, but [O] has been shown to be under-predicted by an equilibrium assumption[32] as it is an unstable species.

$$[O] = \frac{k_{H+O_2}.k_{OH+H_2}.[O][H_2]}{k_{OH+O}.k_{H+H_2O}.[H_2O]} \tag{1.19}$$

A more reliable prediction can be obtained by a partial equilibrium calculation as shown in Equation 1.19. It is calculated using the concentrations of O_2, H_2 and H_2O which can be better predicted by calculations or measurements as they are stable species[4]. The most accurate method would be to perform the calculation without any assumptions of equilibrium and derive the concentrations of the concerned species from a chemical kinetic mechanism.

2. **Prompt/Fenimore NO:**
Prompt NO_x is formed by the following rate limiting reaction,

$$CH + N_2 \rightleftharpoons HCN + N \qquad E_a\text{=86.47 kJ/mol, 1000-4000K[29]} \tag{1.20}$$

The CH radical is formed by a precursor, C_2H_2, which is formed in fuel rich conditions. This mechanism has a much lower activation energy than the thermal pathway and is hence formed at lower temperatures(<2000K)[4]. In the presence of oxygen, the N atoms produced react to form NO.

The mechanism was discovered by experiments by Fenimore [33]. He measured the NO concentrations in the post flame and primary reaction zones. The measurements indicated the formation of NO in the primary reaction zone which was contrary to the prediction from the Zeldovich mechanism, according to which NO_x should be found only in the post flamezone due to the high temperature requirements for the reaction. Thus in [33] it is concluded that the Prompt NO_x may be a significant contributor to the total NO_x especially under fuel rich reaction conditions.

3. **NNH mechanism:**
This deals with the reaction of dissociation of NNH to H and N_2. The reactions involved are:

$$NNH \rightleftharpoons N_2 + H \qquad E_a\text{=0 kJ/mol[29]} \tag{1.21a}$$

$$NNH + O \rightleftharpoons NO + NH \qquad E_a\text{=0 kJ/mol[29]} \tag{1.21b}$$

The forward reaction rate of Equation 6.14 is found to be more or less independent of temperature but the reverse reaction rate increases especially at high temperature conditions in flames due to the increase of H species concentration. The pathway can lead to increase of NO concentration by an order of magnitude in a methane/air flame at 1800K[34]. The reverse reaction of Equation 6.14 is rapid enough to establish equilibrium of NNH, which results in NNH concentrations to be high enough to be important in bimolecular reactions such as the NO producing Equation 1.21b.

4. **N_2O mechanism:**
   This is similar to the thermal mechanism, wherein O attacks N_2 molecules, but in this case it occurs in the presence of a third molecule M and leads to the formation of N_2O in Equation 6.16.

$$O + N_2 + (M) \rightleftharpoons N_2O + (M) \qquad E_a\text{=0 kJ/mol[29]} \tag{1.22}$$

   This reaction is promoted at high pressures as it is a three body reaction and has a low activation energy, making it an important contributor to NO_x under lean premixed gas turbine combustor conditions. This is because Thermal NO_x is reduced due to lower temperatures and Prompt NO_x by lean conditions[35]. Subsequently the reaction in Equation 1.23 produces NO.

$$N_2O + O \rightleftharpoons NO + NO \qquad E_a\text{=116 kJ/mol, 1370-4080K[29]} \tag{1.23}$$

5. **Fuel NO_x:**
   This is formed by the reaction of fuel bound nitrogen found in fuels such as coal. This is less relevant from a gas turbine perspective which employs cleaner hydrocarbon fuels such as natural gas and kerosene compared to coal and biomass.

1.4. EMISSIONS PREDICTION BY CFD

Turbulent combustion is common in modern combustion devices such as gas turbine combustors and furnaces. In order to model it computationally, conservation equations of mass, momentum, energy and species need to be solved. The extent of modeling required to represent the flow field depends on the resolution of the scale at which the calculations are performed as shown in Figure 1.3. The wave number is inversely proportional to the length scale considered, i.e. larger the wave number, smaller is the length scale. If the

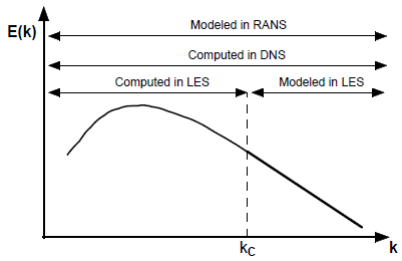

Figure 1.3: Turbulence energy spectrum plotted as a function of wave numbers. RANS, LES and DNS are summarized in terms of spatial frequency range. k_c is the cut-off wave number used in LES (log-log diagram)[3]

resolution of the grid is high enough to capture the smallest scale of flow, no extra modeling is required and this method is known as Direct Numerical Simulation(DNS). On the other hand, if the grid is not that well resolved, turbulence needs to be mathematically modeled. Such techniques are Reynold's Averaged Navier Stokes equations(RANS) and Large Eddy Simulation(LES). RANS calculates a temporal mean value of the quantities, as shown in Figure 1.4, and hence the increase in resolution of the grid shall reach an asymptotic value of improvement in results, as once the essential mean flow phenomenon is captured there would be no added benefit obtained by refining the mesh. Thus RANS simulations may be done on relatively coarser meshes as compared to LES or DNS and time averaging makes it less expensive to solve, which makes it the preferred method of combustion simulations for a lot of practical combustion devices.

$$\frac{\partial}{\partial t}(\bar{\rho}) + \frac{\partial}{\partial x_i}(\bar{\rho}\widetilde{u_i}) = 0 \tag{1.24a}$$

$$\frac{\partial}{\partial t}(\bar{\rho}\widetilde{u_j}) + \frac{\partial}{\partial x_i}(\bar{\rho}\widetilde{u_i}\widetilde{u_j}) = \Big[-\frac{\partial \bar{p}}{\partial x_j} + \frac{\partial \bar{\tau}_{ij}}{\partial x_i} + \bar{\rho} g_j\Big] - \frac{\partial}{\partial x_i}(\bar{\rho}\widetilde{u_i"u_j"}) \tag{1.24b}$$

$$\frac{\partial}{\partial t}(\bar{\rho}\widetilde{\phi_k}) + \frac{\partial}{\partial x_i}(\bar{\rho}\widetilde{\phi_k}\widetilde{u_i}) = \Big[-\frac{\partial \bar{J}_i^k}{\partial x_j} + \bar{\rho}\widetilde{S}_k\Big] - \frac{\partial}{\partial x_i}(\bar{\rho}\widetilde{\phi_k"u_j"}) \tag{1.24c}$$

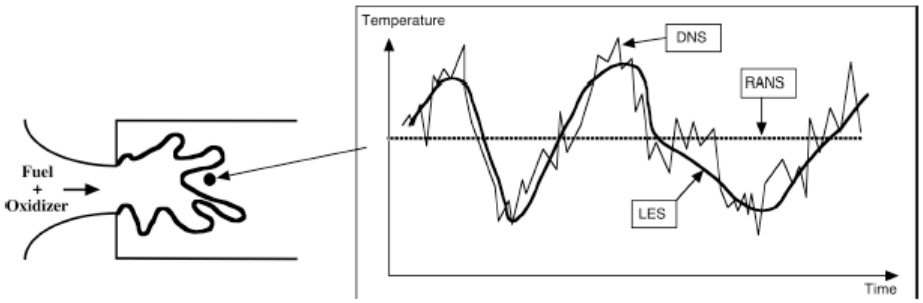

Figure 1.4: Time evolution of local temperature computed with DNS, RANS or LES in a turbulent flame brush[3]

$$\widetilde{f} = \frac{\langle \rho f \rangle}{\langle \rho \rangle} \tag{1.25a}$$

$$\langle f \rangle = \frac{1}{n_{samples}} \sum_{n=1}^{n_{samples}} f_n \tag{1.25b}$$

$$f" = f - \widetilde{f} \tag{1.25c}$$

Equation 1.24 is the set of RANS governing equations and Equation 1.25 represents the fluctuations, f", which is the fluctuation relative to density weighted mean. The introduction of turbulence to the transport quantities gives rise to certain unresolved terms in the system of equations, leading to a closure problem. To solve the closure problem several models exist. It may also be noted that the second term on the left hand side of Equation 1.24b, makes the system highly non-linear. This adds an element of expense to the convergence of the numerical solution.

The evolution of chemical species takes place through a series of elementary reactions involving intermediate species end products. A group of such chemical equations is expressed in a detailed chemical kinetic mechanism, such as GRI Mech 3.0 which is composed of 53 species and 325 reactions. Detailed chemical kinetic mechanisms may cover reactions with a time scale varying from nanoseconds to seconds as shown in Figure 1.5. This difference in time scales makes the system of equations 'Stiff'. Reaction time scales may

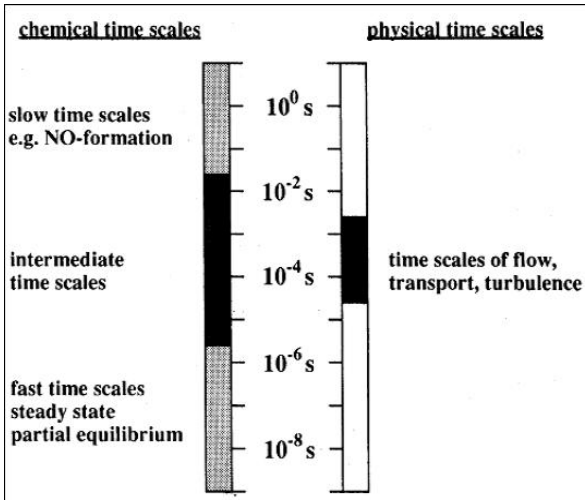

Figure 1.5: Time scales in turbulent reacting flows[4]

largely vary due to the nature of the reactions involved and the occurrence of different reactions under varying temperature conditions in the domain. To capture the changes in species with fast reaction rates a small time step is required, but these species reach a steady state early in time. On the other hand, species varying slowly can be solved with a large time step but need to be integrated up to a larger absolute time. This puts a constraint on the system to use small time steps(for fast reactions), and solve till a long absolute time, i.e large number of iterations(for slow reactions). Hence solving stiff differential equations can be expensive.

Some methods often used to deal with this involve variable time stepping, in which the integrator uses small time steps till the fast varying species become steady, after which a large time step is chosen.

A combination of large number of species in a detailed reaction mechanism, Stiffness of chemistry and non-linearity of the momentum equation, leads to a prohibitive computational expense for simulations of practical combustion systems. Hence in a lot of Computational Fluid Dynamics(CFD) methods for combustion simulations, reduced chemical mechanisms which involve fewer species are used[36]. It is quite common to perform CFD simulations with the assumption that the chemical time scales are much smaller or comparable to the turbulent time scale, in order to reduce the stiffness issue. In reality, the evolution of pollutant species, such as NO_x, have a slower mechanism, time scales of the order of a few seconds, and the turbulence, having a time scale of the order of 10^{-4}s as shown in Figure 1.5, which requires the introduction of an extra source term for NO_x.

A common method of calculating NOx emissions in CFD is post processing. The reactions involved in NOx production are slower compared to other reactions as well as the turbulence rate. For this reason, nitrogen oxide mass fractions are not calculated directly during the CFD simulation as it would be too expensive to obtain a well converged solution. ANSYS Fluent provides the option of calculating NOx concentrations as a post processing operation to the CFD solution. Transport equations for nitrogen oxides are solved, which have the possibility of including models for taking into account fluctuations due to turbulence. Properties such as temperatures and mass fractions of intermediate species involved in the production of NOx such as O, OH,O_2 are obtained from the pre-calculated CFD solution, hence the post processing results are only as good as the CFD performed prior to it. One of the drawbacks is that the intermediate species concentration used may not be accurate as they were calculated using some form of simplified chemistry, depending upon the model used. Recalculating all the species at the cell centers of the CFD domain would be a better solution, but that would result in a highly non linear and stiff system of equations with large dimensions due to the transport of quantities(convection and diffusion terms) and the large number of species involved respectively. Hence the assumptions are necessary in this method. From literature it is seen that the Fluent post processing tool gives large deviations from experimental NOx values when used for cases giving out sub 10ppm levels of NOx such as that in Flameless combustion[17]. It is also mentioned explicitly in the ANSYS Theory Guide that the available equilibrium models for estimating the concentration of O atoms, which are necessary for NO species calculations, under predicts the NOx concentration values[37].

1.4.1. FLAMELET GENERATED MANIFOLD

Flamelet Generated Manifold(FGM), is a turbulence-chemistry modeling method used in CFD simulations for combustion. As the name suggests, it is based on a laminar flamelet model. FGM was first presented by Oijen and Goey [38] as a method to reduce the cost of computation for combustion and currently being widely explored by different combustion groups at TU Delft and elsewhere in the Netherlands. A turbulent flame is assumed to be composed of several laminar flamelets. In the FGM method, several flamelets are pre-calculated for different conditions and a multidimensional table, i.e a manifold is assembled using them. This enables the expression of the variation of a large number of chemical species in a few scalar variables that characterize the flamelets. Transport equations of these scalar variables are solved along with the fluid dynamic equations in the CFD simulation, instead of solving transport equations for many species. The species mass fractions can be obtained by a post processing lookup operation from the manifolds using the calculated values of the scalar variables.

LAMINAR FLAMELET

The flamelet model considers a turbulent flame to be an ensemble of laminar flamelets. A commonly used flamelet model is the counter-flow flamelet as shown in Figure 1.6. In this particular model, the fuel and air streams are injected from opposite directions and meet at a stagnation plane. Such a flame can be characterized by the strain rate which can be altered by either altering the speed of the jets or changing the distance between them. The flamelet model uses finite rate chemistry, but the chemistry is assumed to faster than the smallest turbulence time scale. This assumption means that reactions take place in a thin flame zone and only processes taking place perpendicular to the flame front are of consequence. This allows for the reduction of the flame to a 1D problem [39]. This is a reasonable assumption for major species for heat release which are produced by faster reactions, but may be incorrect for slower mechanisms of NO and CO production.

MANIFOLD

The FGM method generates manifolds that relate certain scalar properties to flame quantities such as species and temperature, to be used as look-up tables in a post processing operation. A flamelet, in FGM, is character-

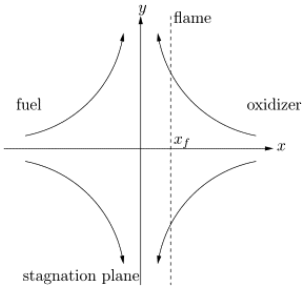

Figure 1.6: Non premixed flamelet

ized by a scalar progress variable. To improve the accuracy, several progress variables, representing different phenomenon may be used to represent the same 1D flame. This reduces a problem described by a large number of species to solving transport equations for 2 or more scalar quantities. This is where the FGM method is different from a standard flamelet approach. Instead of parameterizing a flamelet by one variable, such as strain rate, to identify the flamelet and another variable such as mixture fraction to derive the location along the flamelet, it uses the distribution of two or more scalar variables that vary along the same flamelet. The idea is that each state in each flamelet will have a unique combination of the multiple scalar variables, meaning that for a given combination of scalar variables there exists only one location in the entire ensemble of varying flamelets.

In the FGM implementation in ANSYS Fluent, typically a progress variable, C, and Mixture fraction Z are used as scalar variables. C is expressed as a combination of mass fractions of certain species and Z indicates the amount of composition that originated from the fuel stream. A flamelet is uniquely defined by the combination of C and Z that exists, i.e C(Z). C and Z form two axes of a 2D plane and the third axis contains information of a species and temperature from the flamelet. This process is repeated for different flamelets by varying the strain rate starting from low to high till flame extinction occurs. This is used to fill the 3D space of each manifold, there being a separate manifold for every variable to be represented(i.e species+temperature). The regions where no flamelet curve exists in the C-Z plane, i.e point between flame extinction and unburnt state are represented using the extinguished flamelet[40]. Thus the manifolds are constructed. The CFD solver solves a transport equation for the progress variables, i.e C and Z in the above mentioned case and a source term for C is supplied from the FGM. Once a solution is achieved for the domain, the species can be retrieved by a look up process in the manifolds using the values of C and Z for each location.

The progress variable in FGM is chosen such that it captures the reaction zone defined by the heat release, but minor species reactions continue way beyond this zone. Hence choosing a progress variable that is suitable for capturing both major and minor species is challenging and leads to inaccurate minor species prediction. Usually the progress variable captures energy production well and is a combination of CO_2, CO, H_2O and H_2 species mass fractions. Such a progress variable is not suitable to capture the minor species and it is better to resort to the post processing method by solving a transport equation as described earlier to obtain NOx predictions.

MINOR SPECIES

Minor species such as NOx and CO are formed through chemical reactions that are typically slower than the heat release reactions in combustion. One of the primary assumptions in the FGM method is the usage of laminar flamelets which are modeled such that they use finite rate chemistry, but the chemistry is assumed to faster than the smallest turbulence time scale. This means that the flames can adjust instantaneously to varying strain rates. The assumption fails for slower reactions such as those for NOx and CO formation, and hence these species would be less accurate if obtained from the FGM derivation.

Another limitation of FGM is the progress variable expression. Usually the progress variable is built for mass fractions of species to be able to express heat release reactions, but this may not be a correct indication for slower producing reactions, i.e even when the progress variable is near its upper limit, which indicates fully reacted, the reaction may still be taking place. Van Oijen and De Goey [41] have investigated the inclusion of NO in the progress variable along with the other major species. The progress variable, C, is expressed as

$$C = \frac{Y_{H_2}}{M_{H_2}} + \frac{Y_{H_2O}}{M_{H_2O}} + \frac{Y_{CO_2}}{M_{CO_2}} + \alpha\frac{Y_{NO}}{M_{NO}} \tag{1.26}$$

where Y_i is the mass fraction and M_i is the molar mass of the i^{th} species. α a number indicating the contribution of NO to the scalar, C. The results showed acceptable accuracy, i.e comparable to a NOx post processor which solved a separate transport equation, when the value of α was large enough(α=10). In other cases, the NOx post processor was found to be slightly more accurate than direct lookup in the manifolds. For extremely large values of α the FGM process would tend to a NOx post processor as the progress variable only represents the NOx production. The disadvantage of that would be that the progress variable is no longer a good indicator for the evolution of heat and major species which are the drivers of combustion.

Hence, although FGM is an attractive approach for computation of combustion, it has limitations in predicting minor species which are of interest for pollutant prediction. This makes it interesting to explore other approaches that may have the potential for better predictions.

1.5. EMISSIONS PREDICTION BY CHEMICAL REACTOR NETWORKS

One of the main bottlenecks of CFD for combustion is the high non linearity of the momentum conservation Equation 1.24b, in the RANS system of equations. Eliminating this equation would greatly simplify the system and would be computationally easier to solve the stiff chemistry. This brings us to the concept of ideal reactors.

A PSR is a 0D ideal reactor model. Also known as Well-Stirred Reactor(WSR) and Continuously Stirred Tank Reactor(CSTR), this reactor model considers perfect mixing of reactants within the control volume, and hence there are no spatial gradients of species and state within the reactor. It is 0D because it has no spatial variables and hence the momentum equation is not defined and solved for. A schematic diagram of a PSR is shown in Figure 1.7. A PSR has Da=0.

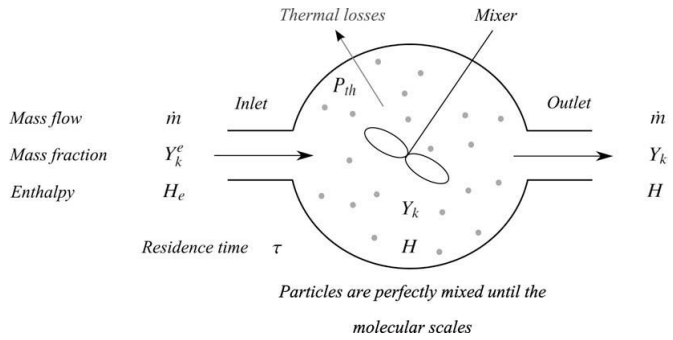

Figure 1.7: Schematic diagram of a PSR[5]

Experimental reactors that try to achieve this model use high velocity inlet jets and have been used to study aspects of combustion such as flame stabilization, NO_x formation and auto-ignition[26].
The reactor is considered in steady state. The governing equations are the conservation of mass, species and energy. In the following set of equations , the conservation of mass is implicit as the reactor is considered in steady state and the rate of mass entering the system is equal to the rate of mass leaving it. Hence, only conservation of species and enthalpy is presented.

Species Conservation

$$\dot{\omega}_i MW_i V + \dot{m}(Y_{i,in} - Y_{i,out}) = 0 \qquad \text{for} \qquad i = 1,2,..\text{N species} \tag{1.27}$$

$$\dot{\omega}_i = f([X_i]_{cv}, T) = f([X_i]_{out}, T)$$

$$Y_i = \frac{[X_i]MW_i}{\sum_{j=1}^{N}[X_j]MW_j} \tag{1.28}$$

Enthalpy Conservation

$$\dot{Q} = \dot{m}\Big(\sum_{i=1}^{N} Y_{i,out}h_i(T) - \sum_{i=1}^{N} Y_{i,in}h_i(T_{in})\Big)$$

where, (1.29)

$$h_i(T) = h^o_{f,i} + \int_{T_{ref}}^{T} C_{p,i}\,dT$$

In Equations 1.27,1.28 and 1.29, $\dot{\omega}_i$ is the rate of increase of molar concentration of species i, Y_i is the mass fraction of species i, MW_i is the molecular weight of i, V is the reactor volume. In Equation 1.29 $\dot{Q}$ is the heat transfer rate due to heat loss/addition from the walls, h_i is the specific enthalpy of the i^{th} species, $h^o_{f,i}$ is the absolute specific enthalpy of formation of the i^{th} species, $C_{p,i}$ is the specific heat capacity of the i^{th} species.

So we have N+1 variables(N species and Temperature), N equations from mass and species conservation combined and 1 equation of energy conservation.The system is solved for species mass fractions and temperature. Due to the steady state assumption, it is a system of nonlinear algebraic equations. Depending on the chemical system involved the system may be stiff for example due to different time scales of different species reactions and convergence may be difficult to achieve. This may require more sophisticated numerical methods than the standard used Newton's method.
It is common to characterize a PSR by its residence time defined as,

$$t_R = \frac{\rho V}{\dot{m}} \tag{1.30}$$

where the mixture density is calculated from ideal gas law,

$$\rho = \frac{P(MW)_{mix}}{R_u T} \tag{1.31}$$

The above mentioned model of the PSR is a theoretical one. The practical implementation of a PSR has a system of Ordinary Differential Equations(ODE) that are time dependent. These equations are solved towards a steady state by marching in time. The reason for this approach is that achieving convergence for the algebraic system of equations mentioned in 1.27, 1.28 and 1.29, is difficult due to the stiffness of the problem at hand. This was the general approach found in common thermo-chemical solvers such as Cantera and KPP.

1.5.1. CRN IN LITERATURE

If the entire combustion region is represented by a single ideal reactor, the representation of the fluid flow would be flawed due to the simplified flow field representation. This would mean that the chemistry would be calculated at incorrect thermodynamic conditions. Chemical Reactor Networks(CRNs) may be a solution. As the name suggests, CRNs are networks formed by interconnecting several ideal reactors, each having their own properties. By distributing the computation of reactions over several ideal reactors, it is possible to better represent the flow field by running each reactor at suitable conditions, hence capturing the variations due to the flow field in the domain. The main advantage of a CRN is the feasibility to include detailed chemistry. This is possible due to the simplification of the fluid dynamics, which reduces the non linearity of the combustion problem and converts the system of partial differential equations to a system of ordinary differential equations having a 0D element as its building block, making convergence computationally more feasible.

As in every system, there are limitations. The simplification leads to a loss of information of the flow. The flow field is preserved in the form of the mass flows exchanged between different reactors, hence capturing reactor inter-connectivity accurately is crucial to be able to represent the combustion chamber domain that was intended to, in the form of a CRN.

Ideal chemical reactors have been used to model gas turbine combustion chambers by engineers, since as early as the 1980s. For example, Touchton [6], model's a combustion chamber using three PSRs in series, to produce real time prediction of NO_x based on gas turbine input and output parameters, which in turn was fed to NO_x abatement systems such as Selective Catalytic Reduction(SCR) to have better pollution control. The numerical simulations were carried out for a combustor with steam injection at the combustion chamber inlet, in a combined cycle. The steam injection was to reduce NO_x by reducing the overall flame temperature. The reactors were arranged as shown in Figure 1.8. The first reactor was considered to have a very low

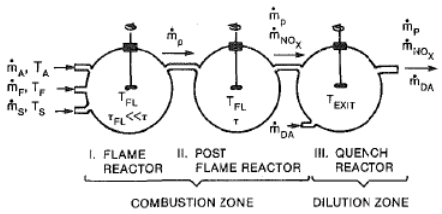

Figure 1.8: Conceptual model of combustor[6]

residence time and the fuel was burnt using a global chemical mechanism establishing a global equilibrium of the major species and temperature. NO_x production was modeled in the second reactor, which was the post flame reactor, as only thermal NO_x was considered the main source in-order to keep the final expression simple. This model was modified from a previous work wherein NO_x concentration was expressed as a function of residence time and reaction rate. The modification was to replace the residence time with an effective residence time to account for the choking of the system at the first stage nozzle. The third reactor was for dilution wherein the products were mixed with dilution air and all reactions are considered to be frozen by the sudden drop in temperature. The model was run for single burner tests and then compared to field data of the GE MS9001E and MS7001E gas turbines which used the same combustion chamber. R_{STM} was defined as the steam injection effectiveness, given by the ratio of NO_x mass after steam injection to that before steam injection. The ratio is on a dilution free basis at a constant fuel flow. The values of R_{STM} correlated best when plotted against steam to fuel ratio. The errors were found to be within ±5% of the field measured NO_x data. Thus the 3-PSR model was concluded to be a reliable algorithm for control of NO_x abatement technologies. Although the data correlated well for a particular type of comparison(R_{STM} v/s steam-to-fuel ratio), deviations were found in the correlation of NO_x emissions index to combustor inlet temperature. The results are good for the control of the system, which requires a relative agreement between NO_x ratio and steam injection, but not very suitable for absolute NO_x concentration calculation.

Another example is the work of Rizk and Mongia [7]. This has a more detailed reactor network model. The network was created on the basis of engineering knowledge such as the occurrence of mixing of different air-fuel streams in the combustor, lean blow out and dilution. This model consisted of a number of reactors in series and parallel as shown in Figure 1.9. Three arbitrary parameters were defined to keep the defini-

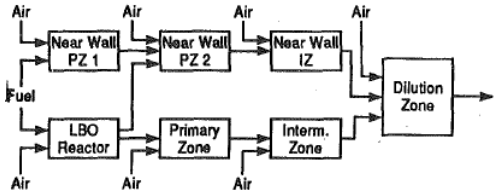

Figure 1.9: Combustor flow model[7]

tion of reactors similar for different combustors, as well as define a particular combustor uniquely. It used a detailed chemical kinetic mechanism for the pyrolysis and oxidation of propane by Westbrook and Dryer [42]. An extended Zeldovich mechanism was included for NO_x prediction. This model was run for different parameters such as equivalence ratio, residence time and system pressure to obtain predictions for NO_x, CO and UHC. This data was fit to obtain analytical expressions, and these expressions were validated against operational data from gas turbines. A good fit was obtained. The advantage of this model was that it provided the capability to observe the process of pollutant formation within various regions of the combustor giving better insight for reducing the emissions. The utilization of a detailed mechanism made the prediction more realistic, although better results were obtained after the inclusion of spray evaporation and heterogeneous mixing models.

Rizk and Mongia [43] went on to improve upon [7] by trying to reduce the empirical input to the system. They performed a 3D CFD calculation of a combustion chamber using a 4-step reaction scheme. The CFD result was divided into several sub-volumes, although the exact method and basis of division was not mentioned. Each subvolume's average flow field was used as an input to the models developed in [7], hence yielding the distribution of NO_x, CO and corrected temperature field in the combustion chamber. Hence a 3D CFD was used as an input to a model developed from a CRN. This method gave detailed pollutant formation data with minimal empirical assumptions.

Andreini and Facchini [44] used the CRN concept in conjunction with ESMS, which is a gas turbine system simulation code wherein each component is defined as a black box with its own model. They obtained NO_x predictions for emission reduction technologies on conventional diffusion flame combustors, lean premixed combustors and RQL combustor. The code was able to predict trends with acceptable accuracy.

Faravelli *et al.* [8] used a CRN to study the interaction between flue gas recirculation, staged combustion and Selective Non-Catalytic Reburn(SNCR) to achieve NO_x reduction. The combustor, as shown in Figure 1.10 was modeled as a 1D reactor network with several reactors in series as shown in Figure 1.11. The primary

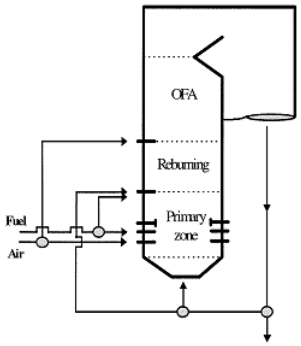

Figure 1.10: Schematic of furnace boiler[8]

zone was represented by a single PSR, the reburning zone by a PSR followed by a PFR[3] and a post combustion zone by a PSR followed by a PFR. The splitting of the residence time between the PSR and PFR, in the reburn-

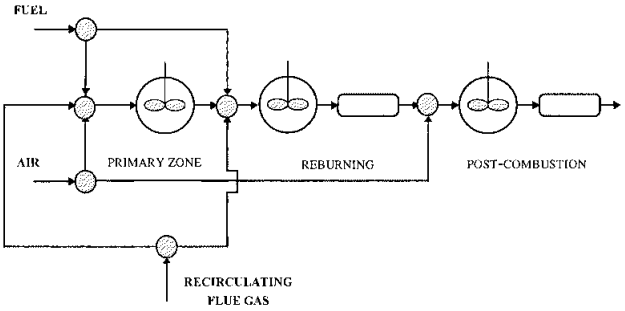

Figure 1.11: CRN for furnace boiler[8]

ing zone and post combustion zone, was based on the expected mixing in the zones. Each PSR was operated at a kinetic average flame temperature of the zone determined from previous CFD studies and experimental measurements. One of the main difference from a gas turbine combustor was that the flame zone was modeled as an isothermal PSR and not adiabatic as there was a heat exchanger present to boil water in this zone. A detailed chemical mechanism was implemented. The results showed a maximum error of 20ppm or 16% compared to experiments. The model also successfully predicted the anomalous trend of DeNO$_x$ reduction with increase in reburning. The reactor network was modeled using knowledge gained from CFD simulations of the combustion chamber. This was done manually, based on the operator's understanding and selection of regions to collectively represent as an equivalent reactor in the domain.

Novosselov *et al.* [9] performed a manual CFD-CRN analyses on a lean premixed gas turbine combustor with a pilot burner. They used a 3D CFD simulation to gain knowledge of certain critical parameters. A 31 element CRN was constructed manually based on these factors such as velocity profiles, rate of entrainment in various zones and fluctuations in flame temperature. The CRN was solved using a detailed chemical kinetic scheme. It was done so for full load operating conditions with variable pilot flows ranging from 35% to 200%. Based on the results presented in Figure 1.12, they concluded that the CRN tool provided good insight into the pollutant formation chemistry behavior and may be used for parametric design of combustors as its computation time was several orders of magnitude less than that of the simplest CFD used to solve for emissions. Although the normalized results appear to be quite accurate, there is still about a 20% error in the worst case scenario in Figure 1.12. It is also surprising to see that they achieve a relatively accurate solution with just 31 reactors, whereas other authors report a number in excess of 300. This could possibly be because the elements used by Novosselov *et al.* [9] consist of both PSR and PFR, whereas other authors only use PSRs. The process in the current case is a manual one, and hence a more strategic placement of reactors was possible from the analysis of CFD data. An objective comparison of the time taken by the CFD-CRN method and CFD for emissions was not reported.

Lebedev *et al.* [10] improved upon this reactor model by performing a similar procedure, on the combus-

[3] PFR:Plug Flow Reactor; It is a 1D ideal reactor which has perfect mixing along a cross section and no mixing along the axis, i.e species are transported only by advection along the axis.

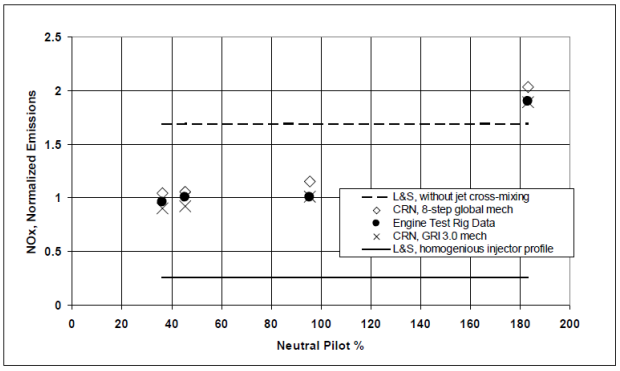

Figure 1.12: Comparison of measured and predicted NO_x emission. Normalization is based on the engine test rig NO_x emission of 95% pilot, which is close to the 100% neutral pilot condition[9]

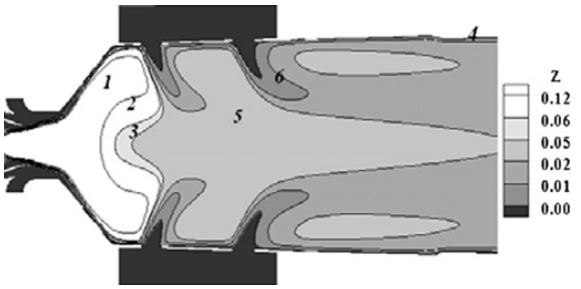

Figure 1.13: Schematic of methane fueled CIAM-M combustor with mixture fraction distribution[10]

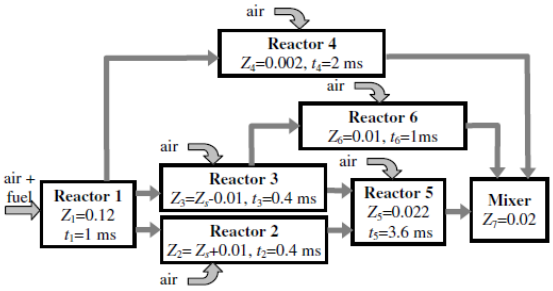

Figure 1.14: CRN for CIAM-M combustor[10]

tor of a CIAM-M gas turbine, but using the mixture fraction and residence time as critical parameters, which made the process more objective, although the actual generation of connected reactors was manual. The system was simulated for both methane and kerosene fuels. The mixture fraction field from CFD is shown in Figure 1.13. The reactor network is shown in Figure 1.14. The model had a disadvantage of being applicable to only the given type of combustor which was a conventional diffusion flame combustor. The emission of pollutants for different operating conditions was calculated and compared to experimental results. The process was done for different detailed kinetic schemes for methane and the results were found to be highly sensitive to the mechanism used. The results are shown in Figure 1.15. The DS reaction mechanism predicts NO_x bet-

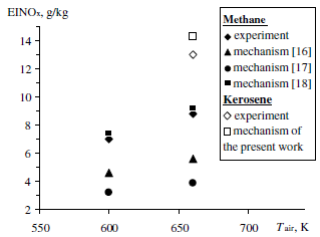

Figure 1.15: Comparison of results([16]:Konnov's mech, [17]: GRI mech 3.0, [18]:DS mech)[10]

ter than the GRI-mech 3.0 because the DS kinetic model gives a stronger prediction of prompt NO_x in the fuel rich zone and a larger conversion of NO to NO_2. The concept of using the residence time as one of the main parameters of splitting the domain is notable in this work, unlike several previously mentioned works where it was used as a means of validation only. The DS mechanism shows the least error($\approx$ 1%) whereas the GRI-mech 3.0 shows an error of about 60%. This has been justified as a characteristic of the mechanism but may also probably be because of the few number of reactors used to represent a fairly complex flow phenomenon.

Park *et al.* [11] simulated a lean premixed gas turbine combustor using the CFD-CRN method for different operating conditions. A 3D CFD simulation was done. Based on the simulation results, flame behavior and combustor boundary conditions, a CRN was generated. The domain was divided into reactor zones based on

temperature, velocity and flame area density. This was done manually based on the user's discretion of the aforementioned parameters. The study shows that CFD-CRN approach could accurately predict NO_x emissions for an industrial DGT5 combustor, although some limitations such as deviations from experimental data at higher combustor loads and high inlet temperature conditions were reported as shown in Figure 1.16. A largest error of about 30% is seen at near half load on a hot day.

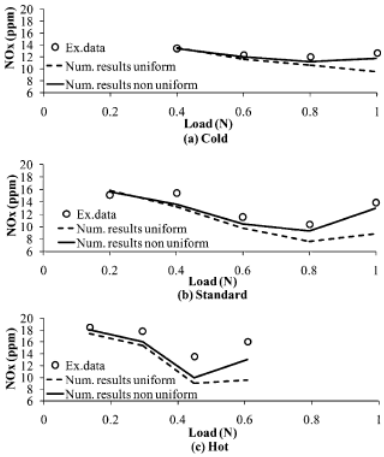

Figure 1.16: NO_x emissions for cold, standard and hot ambient conditions[11]

The CRN concept has also been used to study flameless combustion, which is a low NOx combustion concept. Rao *et al.* [12] used reactor network modeling to model an atmospheric combustion test rig for flameless combustion operating on natural gas.The network was designed based on engineering inferences from PIV measurements. This was claimed to be a simplified analysis hence only a simplified heat transfer model was incorporated. The results are shown in Figure 1.17 and 1.18. The CO emissions were over predicted

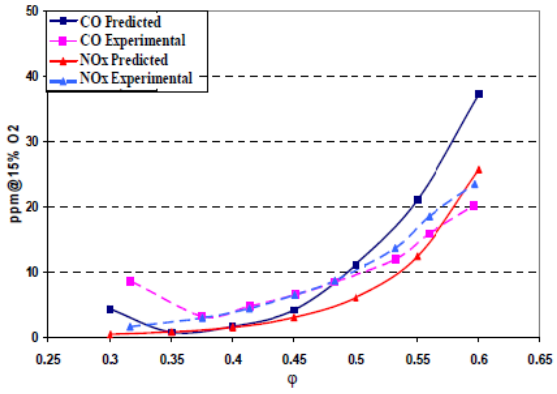

Figure 1.17: Combustor NO_x and CO variation due to equivalence ratio[12]

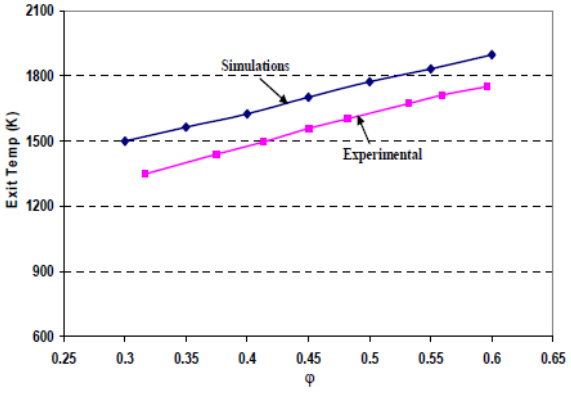

Figure 1.18: Variation of combustor exit temperature with equivalence ratio[12]

and NO_x emissions were under predicted compared to experiments. The temperature predicted by the CRN was also higher. These were attributed to the simplified heat transfer model and the inability to account for change in recirculation due to change in inlet air temperature and equivalence ratio.

The CRN concept has been explored at TU Delft, Faculty of Aerospace Engineering by Rosati [45] and Talboom [46]. Rosati [45] used theoretical modeling to study the crucial parameters of the combustion process of the system being investigated. This knowledge from the investigation was used to arrange ideal reactors in a network in which a detailed kinetic mechanism was implemented. The motive of the project was to develop a tool to obtain quick and accurate emission predictions as compared to CFD methods. The simulations were performed for a lifted jet in hot coflow flame, the Delft Jet Hot Coflow(DJHC) flameless furnace and the premixed combustion chamber of the Advanced Hybrid Engines for Aircraft Development(AHEAD) project. The schematic of the hybrid engine concept is shown in Figure 1.19. The method was found to be not very suitable for the lifted flame case, but good agreement with experimental results was found for the flameless furnace

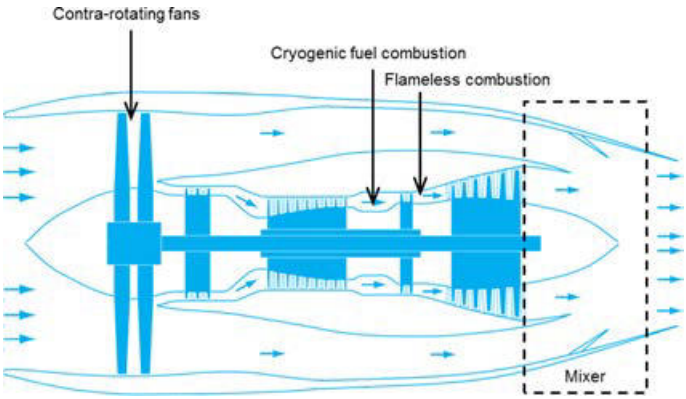

Figure 1.19: Schematic of hybrid engine concept[13]

and premixed combustion chamber. Talboom [46] performs a CRN analysis for both, the premixed as well as flameless combustor of the AHEAD project. The CRNs are generated based on CFD simulations done by previous researchers and knowledge obtained from [45]. The model was extrapolated for the engine at cruise condition and a study was performed to obtain the optimal energy split between the two engines to obtain minimum emissions. In the case of kerosene combustion, the fuel was assumed to be in the gaseous phase.

1.5.2. AUTOMATIC CRN IN LITERATURE

The manual process of CRN generation, relies on operator specified mas flows and reactor properties which at times may be subjective. The CRN generation process can be made more objective and repeatable by automating it. Detailed chemistry may be used in the combustion calculation by decoupling the fluid dynamic and chemical kinetic calculations. The fluid dynamic calculation is performed with simplified chemistry, just enough to predict the effect of reactions on the flow field. This is then post processed using a network of ideal reactors(CRN) that include a detailed chemical mechanism. This decoupling is possible as the minor species are assumed to have a small influence on the flow field[14][15]. A larger number of reactors is better to retain the flow field data as more mass flow controllers can be defined in different spatial directions and more reactors can be defined at different thermodynamic states allowing for variations which would have been averaged and represented as a single value in a case with lesser reactors. It is possible to setup a CRN with a few reactors(<100) manually, based on engineering analysis of CFD data, but to be able to generate large number of reactors from CFD, an automatic method is required to keep the CRN generation easily repeatable and have reliable mass flows. The information obtained from CFD to generate a CRN is:

- mass flow between reactors is calculated as a sum of mass flows between cells in reactors.
- the temperature and initial species mass fraction.
- the volume of the reactors, calculated as a sum of the volume of the constituent cells.

To reduce such operator dependence and make the process more repeatable and objective while still taking advantage of the data from the CFD simulation, researchers took a step towards automating the CRN generation process. Benedetto et alBenedetto *et al.* [14] analyze a 320MW furnace, which is shown in Figure 1.20, using a CFD input of the reacting flow to generate a CRN. The CRN was generated by grouping cells of a CFD mesh based on a temperature-stoichiometry correlation. Each cluster was modeled as an ideal reactor. The choice of a PSR or PFR was based on the randomness of the flow characterized by the saggital angle of the velocity vector as shown in Figure 1.21 and Figure 1.22. The saggital angle is taken for velocity vectors at a particular cross section of the flow. A small saggital angle characterizes a region with flow having a predominant direction and can be represented by a PFR. A more random distribution of the saggital angle having larger values indicates that the region can be represented by a PSR. One of the major assumptions was that the minor species have small influence on the flow field and temperature distribution, hence the CFD calculation used a reduced mechanism, just enough to predict effect of reactions on the flow field. This method was automated except for the step where the operator had to subjectively decide the minimum number of reactors required to represent each zone. This needed to be eliminated in future works. Falcitelli *et al.* [47] summarize the algorithm introduced in their previous work, of automatically generating a CRN from CFD data. A simplified chemical kinetic scheme was used to evaluate the CFD and the same mechanism was used in the CRN

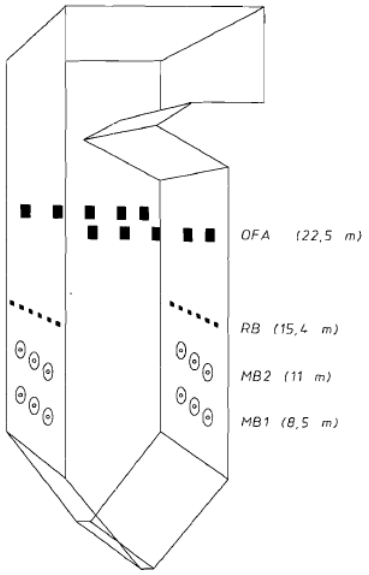

Figure 1.20: The Monofalcone furnace boiler[14]

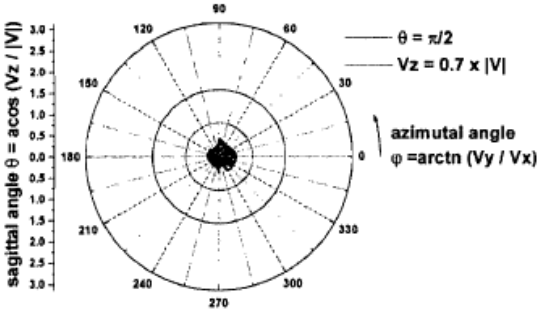

Figure 1.21: Velocity distribution of region with directional flow[14]

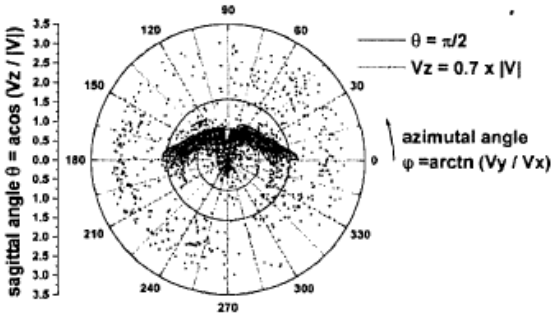

Figure 1.22: Regions with random velocity distribution[14]

to verify its validity with respect to the flow field. The verification was done by comparing the concentration distribution of major species, giving a satisfactory agreement for a network with over 400 reactors.

Faravelli *et al.* [15] proposed the Simplified Fluidynamic by Ideal Reactor Network(SFIRN) approach. A 3D CFD of a gas/oil fired 75 MW furnace was done to generate a temperature-stoichiometry distribution. The cells were grouped by dividing the stoichiometry axis into three zones(rich reducing zone, lean oxidizing zone and mixing zone). The amplitude and position of this division along the axis was left to discretion of the operator. The cells in each of the parts were clustered to form an ideal reactor and the flow randomness determined whether it was a PSR or a PFR. The furnace was divided into different regions (first and second burner levels, reburning, over-fire air ports level) in an arbitrary manner. Figure 1.23 shows the CRN representing the furnace. A detailed kinetic model was used with the focus of predicting NO_x. The NO_x9911 scheme was used which included models for the oxidation of hydrocarbon for a wide range of operation conditions. The validity of the CRN was checked by comparing the residence time to that calculated from CFD. A good agreement with experiments was obtained for both the absolute value of NO_x with as well as its trend with a maximum error of about 10% from the experimental values. It was mentioned that the SFIRN didn't correctly account for effect of turbulent fluctuations on the chemistry, but it was argued that the effect was of significance only for high activation energy reactions(>335kJ/mol) and that only a few such reactions were present. Also a sensitivity analysis was said to have revealed a lower importance of these reactions to the output result, although these results haven't been cited or presented. The authors also report a typical solution time of about half hour on a Pentium II PC. The SFIRN method is quite promising and could form the base algorithm of the tool to be developed during the thesis. There is a degree of subjective decision making such as the arbitrary division of the furnace and the thresholds for dividing the stoichiometry axis which should be made more objective.

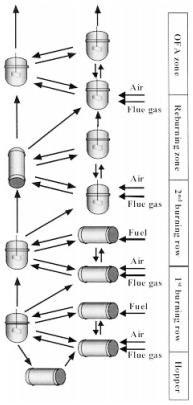

Figure 1.23: CRN representing the furnace[15]

The SFIRN approach was also applied by Frassoldati *et al.* [16] for cases of strong swirling confined flames. A study to find the number of reactors beyond which the NO_x emission is independent of that number is also done as shown in Figure 1.24. A comparison of NO_x concentrations from experiments, CRN model and Fluent NO_x postprocessor(FLUENT6.0) for different swirl numbers, is shown in Figure 1.25. As can be seen in both of the aforementioned figures, a good agreement with experimental data was obtained, both in trend and absolute value. The results are quite promising and the case being that of a confined swirling flame, is

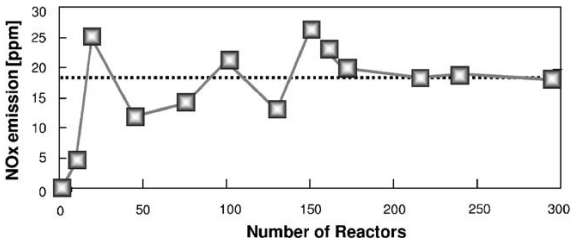

Figure 1.24: Trend of NO_x calculated emissions increasing the number of reactors. Dotted line:experimental results[16]

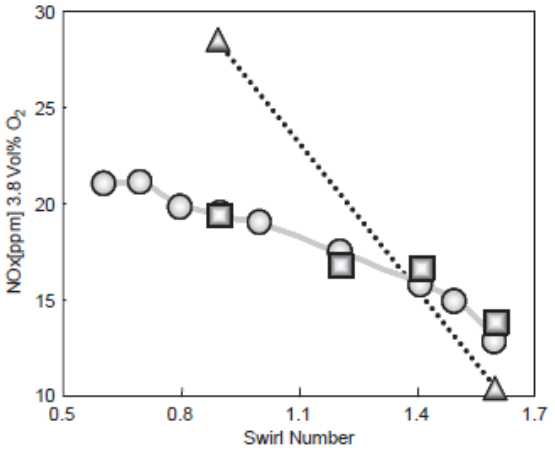

Figure 1.25: NO_x emissions at different swirl numbers. Circles:experimental measurements. Squares:CRN predictions. Triangles: Fluent NO_x postprocessor(FLUENT6.0)

similar to that of a gas turbine combustor. The experimental results seem to be point value data at the exit of the domain considered. The paper does not state how exactly a single number for the CRN calculated NO_x emission of the chamber was obtained but it seems to be an average at the domain exit. If it is so, it must be kept in mind that there may be higher variations in the value of NO_x concentration within the flame, for which a comparison to experiments was not presented.

The research work being described further on was done specifically on gas-turbine combustors, unlike most of the previous work involving CFD-CRN which was done on furnaces. Fichet *et al.* [5] improved upon the algorithm of [47] by using mixture fraction-progress variable distribution for clustering based on chemistry and physical splitting based on streamlines rather than simple geometric connectivity. Each reactor was modeled as a PSR and the operation temperature of the PSR was recalculated, rather than using the CFD prediction, in-order to account for temperature variation due to the detailed mechanism. This was contrary to other previous works [47],[16]. The reasoning given for this is that a temperature difference of around 50K(which is about 3% for a flame of around 1500K), may not affect the flow in terms of mass fluxes, but would surely affect the NO_x concentration due to its exponential dependence on temperature. The PaSR model was not implemented to keep the CPU time within acceptable limits. Thus turbulent fluctuations

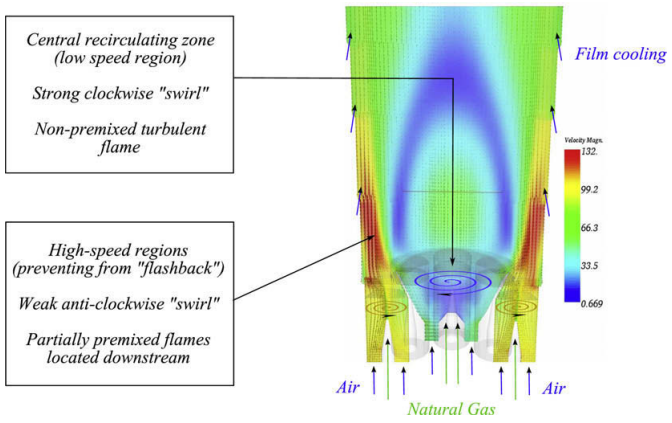

Figure 1.26: Industrial flame tube configuration[5]

were not considered. The simulations were done for a combustor of an industrial gas turbine as shown in Figure 1.26. The network was tested for independence from number of reactors and it was found that a minimum of 369 reactors gave a consistent solution. Consistency was measured by the agreement of mixture fraction and temperature field with CFD calculations. The NO_x emissions calculated by the CRN are in good agreement with experiments. A value of 42.8 dry volume ppm was predicted for a measured value of 44 dry volume ppm which is an error of about 3%. The method is a stark improvement over previous methods in terms of incorporating more details of the fluid flow in the CRN. On the other hand, the method involves the solving of extra transport equations to obtain the streamlines, which moves away from the motive of having simpler calculations. The paper also steers away from using isothermal reactors, unlike most researchers in the past which would mean longer computation time.

Results for a flameless burner were also presented by Cuoci *et al.* [17]. The author's improved upon the method of [47] and took into account the effect of turbulence fluctuations on temperature. They also implemented a simplified PaSR model. The results though, were not satisfactory as shown in Figure 1.27. The

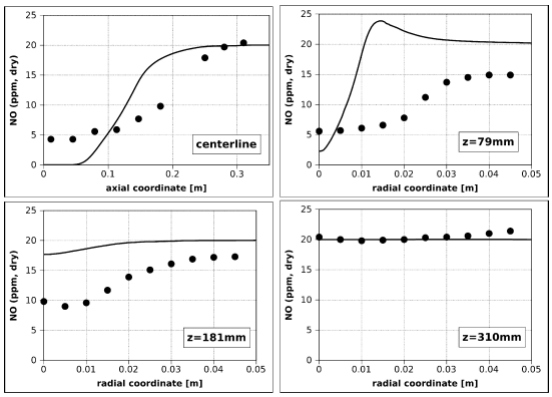

Figure 1.27: Comparison of experimental measurements(symbols) and numerical predictions(lines) of NO mass fraction[17]

largest deviation of NO_x prediction was as high as 300% of the experimental measurements and was attributed to poor temperature field prediction from CFD.

One of the advantages of generating CRNs automatically over manual methods is reduced amount of user input and tuning. For example, in a manual situation, if a CRN is setup for a particular operating condition of the combustion chamber by tuning the mass flows exchanged, for a slightly different condition, either the entire network needs to be created and tuned from scratch or just use the existing network accept the modeling errors, because for a different operating condition, the mass flows between different regions in the combustion chamber will change and sol will other properties such as temperature and residence time. The automatic generation allows for generating a new CRN quite easily and although not always the most optimal CRN is produced, the networks always have a common standard and algorithm of generation which is objective and not dependent on the operators perceptions and approximations.

A chronological order of the developments of CRNs to represent combustion chambers found in literature, have been presented in tables 1.1,1.2 and 1.3. The tables summarize the literature that was referred, in a qualitative form. It's purpose is to serve as a reference guide to get a quick overview of the type of work done done in the field of CFD-CRN over the years.

Table 1.1: Development timeline of CFD-CRN

Year	Author	University	Application	Fuel	Mechanism	Description
1984	Touchton [6]	General Electric Co.	SCR-DeNOx, Gas turbine steam combined cycle, Can combustor used in GE MS9001E and MS7001E	Methane	Global mechanism,NO_x by empirical relation	Combustor modeled by 3 CSTRs in series based on existing engineering knowledge to be able to control steam injection for NO_x reduction. NO_x emission empirical relation is derived updated with an empirical correction to the residence time to account for mixing effects and with another correction for NO_x reduction by steam injection.
1993	Rizk and Mongia [7]	Allison Gas Turbine,GM	Conventional gas turbine combustor	Kerosene	Westbrook and Dryer [42]	CRN model created, implementing detailed reaction mechanism, to extract analytical equations that represent processes within the combustor. Numerical studies done on CRN to see the effect of factors such as residence time and fuel-air inlet ratio. This results in 3 input parameters that need to be given to the model to represent a combustor. The network is run to check critical phenomenon of blowout conditions and near wall effects. The equations hence formulated are later used to predict emissions under different operating conditions. Droplet evaporation models also included. Reactors arranged manually based on engineering judgment.
1993	Rizk and Mongia [43]	Allison Gas Turbine,GM	Conventional gas turbine combustor	Kerosene	Westbrook and Dryer [42]	A 3D CFD solution of a gas turbine combustor is obtained. The emissions are predicted using the semi-analytical model developed in [7]. The model parameters need not be guessed, but are given from the CFD data output, reducing empirical or engineering estimates of flow parameters. Initial manual CFD-CRN.
1997	Faravelli *et al.* [8]	Politecnico di Milano	320 MW industrial furnace boiler with advanced reburning, ENEL	Heavy oil	NC796	Furnace combustion simulated using Equivalent Reactor modeling. Reactor Network modeled manually based on engineering knowledge gained from previous CFD results.
2000	Benedetto *et al.* [14]	Universita degli Studi di Pisa	Monfalcone #3 boiler, 320MW oil and opposite wall fired steam generator,ENEL	Oil	Ranzi *et al.* [48]	New objective design approach developed. CFD calculation performed using simplified chemistry and CRN automatically extracted based on temperature-stoichiometry distribution. Minimum number of reactors in each zone manually specified. Detailed chemical kinetics implemented on the CRN. PSR and PFR based on velocity vector distribution.

Table 1.2: Development timeline of CFD-CRN(2)

Year	Author	University	Application	Fuel	Mechanism	Description
2000	Faravelli *et al.* [15]	Politecnico di Milano	75 MWe gas/oil fired furnace with reburning, Cassano power plant	n-heptane +benzene, methane	NO_x9911	SFIRN (Simplified Fluidynamic by Ideal Reactor Network) approach. Flow field and Temperature field calculated by 3D CFD. Network of reactors built automatically based on stoichiometry and temperature distribution. The burner was divided arbitrarily into zones and the T-ϕ distribution was divided into 3 parts based on empirical knowledge.
2002	Falcitelli *et al.* [49]	Universita degli Studi di Pisa	5 MW and 10 MW Glass melting Furnaces	Heavy oil	NC796[8]	CFD-CRN concept applied.
2002	Falcitelli *et al.* [47]	Universita degli Studi di Pisa	320 MW furnace boiler	Oil	Westbrook and Dryer [42]	Algorithm for automating CRN generation presented and implemented on Furnace boiler. Paper specifies the criteria and method of enforcing the criteria for the automatic 3D CFD domain splitting to create a CRN.
2004	Andreini and Facchini [44]	University of Florence	Gas turbine combustion chambers-Conventional diffusion, Lean Premixed and RQL	Natural gas	GRI 2.11,GRI 3.0, Warnatz Mech	ESMS(Gas turbine system simulation code) coupled with CRN to predict emissions from gas turbine combustors. No CFD involved, more or less 1D simulations throughout with manual CRN arrangement.
2005	Frassoldati *et al.* [16]	Politecnico di Milano	High swirling confined flame, TECFLAM	Methane	GRI 3.0	Paper presents CFD simulations for flames of high Swirl number. Along side, the automatic SFIRN method was also implemented to create a CRN to predict and study NO_x emissions.
2006	Novosselov *et al.* [9]	University of Washington	DLE industrial gas turbine, lean premixed, swirl stabilized at dump plane, annular augmented backside cooled combustor. Solar Turbines	Natural Gas	GRI 3.0	3D CFD used to gain knowledge of flow and temperature field. Domain divided into zones manually based on empirical methods and CRN constructed wherein detailed kinetics is implemented.
2008	Schutz *et al.* [50]	DLR	FLOX combustor[51]	Natural Gas	GRI-3.0[27]	CFD of FLOX combustor. Cells replaced by a PaSR and detailed mechanism implemented. CO and NO_x evolution analysed.
2008	Rao *et al.* [12]	Technion	FLOXCOM combustor	Natural Gas	GRI-3.0[27]	Combustor simulated by manually generated CRN based on PIV experiments. NO_x production is analysed.

Table 1.3: Development timeline of CFD-CRN(3)

Year	Author	University	Application	Fuel	Mechanism	Description
2009	Lebedev *et al.* [10]	Central Institute of Aviation Motors,Russia	CIAM-M gas turbine diffusion combustor	Methane, Kerosene	Konnov's mech[52],GRI-Mech3.0[27],DS mechanism[53]	Reactor model to predict emissions from combustor in diffusion mode.3D CFD+manual CRN generation. CRN distribution done on the basis of stoichiometry and residence time observed from CFD results.
2010	Fichet *et al.* [5]	EIFER, Germany	Industrial gas turbine combustor	Natural gas	GRI 3.0	Improved splitting criteria of CFD field with better flow field categories for the automatic generation CRN from 3D CFD domain. Sensitivity of NO_x emission to air humidity and change in gas turbine load studied.
2013	Lyra and Cant [22]	University of Cambridge	Lean premixed flame	Methane	GRI 3.0	Automatic generation of CRN from CFD results. Simulations done for 3 different equivalence ratios. Results compared to PLIF experimental results. Solution of temperature and mass fractions of species obtained by solving system of equations for reactors in CANTERA. Sensitivity analysis performed to determine optimal number of reactors in network. **MHI sponsored project**
2013	Cuoci *et al.* [17]	Politecnico di Milano	Turbulent jet flames, MILD combustor	Methane, Syngas	GRI-3.0	Better modeling of turbulence in automatically generated CRN as described in [47]
2013	Park *et al.* [11]	Konkuk Univ, Seoul	DGT5 based, test combustor	Methane	GRI-3.0	Manual empirical splitting of CFD domain to obtain CRN.
2015	Amzin and Cant [54]	Bergen University College, Norway	Pilot stabilized turbulent bunsen flame	Methane	GRI 3.0	Assessment for premixed combustion. Sensitivity analysis wrt number of reactors and turbulence schemes presented. **MHI sponsored project.**
2015	Rosati [45]	TU Delft	(a)AHEAD project premixed combustor (b)Delft Hot Jet Coflow furnace(c) Lifted jet flame	Methane	GRI-3.0[27]	Aim to get quck and accurate emission prediction.Manual CRN calibration using engineering knowledge and theoretical models. Analysis also done for lifted jet in hot coflow flame but not successful due to reduced turbulence modeling in CRN. No CFD, only reactor network for both fluid and chemical analysis, natural gas as fuel.
2016	Talboom [46]	TU Delft	Hybrid combustor(Lean Premixed+ Flameless) of the AHEAD project	(a)LH2-Kerosene (b)LNG-Kerosene	C2_NOx, GRI-2.11, GRI-3.0[27], Kerosene mech[55],	CRN analysis to investigate the effect of varying energy fraction over both combustors on emissions. Manual CRN generation based on knowledge from CFD.

1.6. RESEARCH OUTLINE

The research objective is to create a computational tool to predict emissions of a combustion chamber, with a better accuracy than that obtained directly by CFD simulation. The success of the CFD-CRN method relies on how the CFD cells are clustered to form a CRN, and how well the CRN represents the actual physical domain. This conversion from CFD to CRN should hence be influenced by the criteria used to cluster the cells. In literature, most notable studies used the same clustering criteria considering temperature and stoichiometry. From the works in open literature, it was found that the effects of different clustering criteria on the emissions predicted by the CFD-CRN method were not well explored. This lead to the formation of the research question for this project,

Does the clustering criteria have an effect on the emissions predicted by the CFD-CRN method and how does this effect vary with the choice of criteria?

A program was written in Python to perform the CFD-CRN process. The CFD simulations were performed in ANSYS Fluent by André A.V. Perpignan for different operating conditions of a lab-scale combustion chamber. The Python program was used to automatically generate CRNs based on different clustering criteria to study their effects on the NOx and CO emission being calculated.

1.7. OVERVIEW

An overview of the forthcoming chapters is provided in this section. Chapter 2 describes the methodology of Automatic CFD-CRN as seen in literature. Based on this, a Python code is developed. The clustering algorithm of agglomerating CFD cells into ideal reactors is explained in Chapter 3 followed by an explanation of the CRN solver in Chapter 4. Chapter 5 presents a test case combustion chamber, used to study the CFD-CRN method. It describes the CFD simulation provided to generate the flow field, which in turn is used to produce a CRN. Chapter 6 presents an analysis of emissions obtained by the developed CFD-CRN code. The sensitivity of emissions prediction to the choice of clustering criteria is studied. To provide a better understanding of the influence of criteria, an analysis of pollutant formation within the combustion chamber is presented. The research conclusions are summarized in Chapter 7 and recommendations for future studies and usage of the tool are listed in Chapter 8.

2

AUTOMATIC CHEMICAL REACTOR NETWORK

The Automatic CFD-CRN method involves post processing a CFD simulation of a combustion chamber. The cells of the CFD mesh are agglomerated into a network of ideal reactors and a detailed chemical mechanism is used to calculate the species concentration in each reactor. This should allow for accurate calculation of minor species, especially those classified as pollutants such as NOx and CO. This chapter elaborates on the algorithms used for clustering and solving the CRN as presented in open literature. Based on these methods an in-house CFD-CRN code was developed.

2.1. SIMPLIFIED FLUID DYNAMICS BY IDEAL REACTOR NETWORKS

This section presents the algorithm used by the different studies based on the Simplified Fluid dynamics by Ideal Reactor Networks(SFIRN) method. The term is coined in [15] and is based on the concepts initially developed in [14]. Benedetto et al[14] aimed to create a more objective methodology of creating CRNs from CFD simulations and did so by automating the process. This concept was further improved by [15],[47],[5] and [17] in succession. The final output of these studies is a software called KPPSMOKE, also referred to as KPP(Kinetic Post Processor), which is an object oriented software capable of calculating minor species emissions from combustion chambers using detailed chemical kinetic schemes, as a post processing operation on CFD simulations done with simplified/reduced chemistry.

The main idea behind the methodology is to decouple the calculations of fluid mechanics and chemical kinetics so that it is feasible to implement a detailed chemical kinetic scheme in order to obtain a good prediction of minor species. CFD is suitable for fluid flow calculations and CRNs are better suited for solving detailed chemistry. Combining the two in sequential order as shown in Figure 2.1, yields a system in which CFD is performed using a simplified chemistry scheme and a CRN is generated based on the simulation result. The temperature, initial estimate of species and mass flow exchanged between reactors of the CRN are

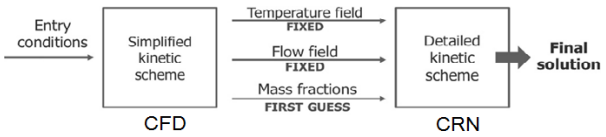

Figure 2.1: CFD-CRN[18]

taken from the CFD result. Finally the CRN is solved using a detailed chemical kinetic mechanism and a prediction of mass fractions of species is obtained. This process has an assumption that minor species do not contribute significantly towards heat release in combustion and hence do not affect the flow field, which allows CFD calculations to be performed with simplified/reduced chemistry such that major heat release reactions are captured, to determine the flow, and post process the flow field with detailed chemistry, without the chemistry changing the flow field.

An overall layout of the KPP software is presented in Figure 2.2. The main components are the CFD input, Clustering and CRN solver. The CFD simulation for a turbulent reacting flow is the basis for generating the

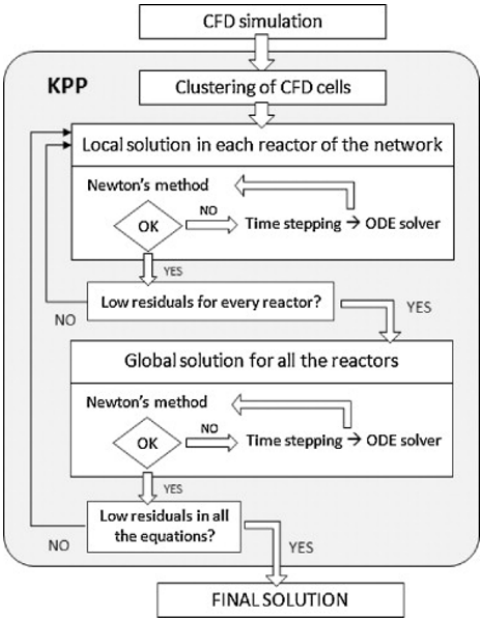

Figure 2.2: KPP algorithm[19]

CRN. The cell centre data, comprising of properties such as temperature, pressure, cell volume, species mass fraction is extracted from the data file of the simulation. Another important aspect of the simulation is the inter-cell connectivity, which is obtained from the mesh topology. The topology is obtained as a relative function of reactor positions without involving any absolute spatial locations, making the process applicable to 1D, 2D and 3D CFD simulations. This connectivity is also the source of mass exchange between cells and is required to determine the mass flow between reactors in the eventual CRN. The information of the flow field, in the CRN, is captured by the mass flow exchanged between reactors. This is because the CRN is composed of zero dimensional reactors and hence there is no definition of direction within a reactor, as a result of which there is no definition of momentum conservation in the reactor.

Cells with similar physical/chemical properties are grouped together to reduce the computational problem to a tractable size when a detailed chemical scheme is used. Zones where large gradients of temperature and composition exist, are crucial for differentiation from a chemical kinetics perspective. However, there are less critical cells which may be similar from a kinetics perspective and can be clustered together. Cells of cold or frozen flow are chosen as the first points of grouping the cells into a single equivalent reactor. This reduces the computational effort and memory requirement, making it feasible to perform mass balance over a large number of species as those involved in a detailed scheme[56]. Hence a CFD simulation of a combustion domain consisting of a few million cells can be reduced to a system of 10^3-10^5 0D ideal reactors. Benedetto *et al.* [14] perform the grouping by first dividing the combustion chamber into a few zones manually, based on the combustion process expected and then automatically grouping the cells with respect to temperature and stoichiometry in each zone to form reactors. Falcitelli *et al.* [47] cluster the cells in multiple stages without any manual intervention.

1. Chemical splitting: Rough classification of mesh cells based on temperature and stoichiometry values, regardless of geometrical properties.

   Classification based on ΔT and $\Delta\lambda$ intervals. T has uniform spacing. The distribution of λ is given as,

$$\begin{aligned} \lambda_n &= \lambda_{feed} + n\Delta\lambda \qquad n \in \{0,-1,-2..\} \\ \lambda_n &= \lambda_{feed}\frac{1}{1-n\Delta\lambda} \qquad n \in \{1,2..\} \end{aligned} \tag{2.1}$$

$$\lambda_{feed} = \frac{\text{total feeding air}}{\text{stoichiometric air required by fuel feed}} \tag{2.2}$$

2. Physical splitting: Classes are subdivided further seeking for all clusters of geometrically connected cells.

3. Number of zones produced in step 2 depends on ΔT and $\Delta\lambda$ that are chosen by operator. The maximum number of cells in the network, N_{max} is defined by the operator. To further reduce the number of zones, clustering is done based on the unmixedness of the cells.

$$\begin{aligned} Z_{tot} &= \text{unmixedness index} \\ Z_{tot} &= \frac{1}{N}\sum Z_i \end{aligned} \tag{2.3}$$

where, Z_i is the binary unmixedness index of the i^{th} species defined as,

$$Z_i = \frac{\bar{Y}_i - \bar{Y_i^2}}{\bar{Y}_i(1-\bar{Y}_i)} \tag{2.4}$$

with

$$\begin{aligned} \bar{Y}_i &= \frac{\sum_j Y_{i,j}\rho_j V_j}{\sum_j \rho_j V_j} \\ \bar{Y_i^2} &= \frac{\sum_j Y_{i,j}^2\rho_j V_j}{\sum_j \rho_j V_j} \end{aligned} \tag{2.5}$$

where Y is the mass fraction, ρ is the density and V is the reactor volume. If number of zones in step 2>N_{max}:

   (a) Classification of first N_{max} cells kept as is. Cells beyond that, assigned to existing zones one by one.

   (b) First the cells are arbitrarily assigned to their neighbors.

   (c) Next the increment of unmixedness is evaluated.

$$\Delta Z_{tot} = (n+1)Z_{tot} - nZ_{tot} \tag{2.6}$$

   (d) This is done for all neighboring classes. The combination that corresponds to minimum increase in Z_{tot} is performed.

4. The above process is done for each excess cell till all of them are reclassified.

Frassoldati *et al.* [16] arbitrarily divide the CFD domain into different geometric regions, the number of which is specified by the operator. As the clusters need to represent PSRs, the distribution of Temperature and excess oxygen(Λ) of the constituent cells is checked by the standard deviation of the values. The clusters with larger standard deviation are split into two parts. This process is repeated iteratively till the total number of reactors reaches the maximum number of reactors, defined by the operator. This is also the clustering method used by Cuoci *et al.* [17], which is further extended by repeating the process iteratively until convergence, i.e the point when changing the dimension of the network no longer affects the solution. Fichet *et al.* [5] apply slightly different chemical splitting criteria to better capture different aspects of the combustion regime. They further improve the clustering by applying a more detailed physical criteria which captures flow patterns such as recirculation occurring in the chamber. Chemical splitting: Mixture fraction(Z) and progress variable(C) from turbulent combustion modelling used as parameters.

- Z intervals expressed in geometrical series focusing on near stoichiometric regions.
- C includes information of temperature distribution and kinetics, is generated as an arithmetic series.

Physical splitting: A streamline,Γ, is considered. Fluid tracers 'Tr' and 'a', are placed on the streamline.

- Tr(constant with time) differentiates air from fuel jets as defined by inlet boundary conditions.
- a(fluid age, increases with time) used to describe recirculation zones.

The value for these tracers is calculated by solving transport equations for each of them in post processing. These steps ensures each zone has common physics without any geometrical or empirical criteria.

The clustering algorithm of KPP is such that it avoids

- geometrical irregularities i.e. prevent agglomeration of cells that are not geometrically connected,
- non smooth transition between zones with very different volumes.

The reactor state quantities are obtained from the constituent CFD cell quantities in the following manner:

- Volume: obtained as a sum of cell volumes
- Interlinking flows: obtained as a a sum of mass flows between constituent cells of reactors
- Mass diffusion coefficient
- Temperature and initial composition: volume average of the clustered cells.

The domain is clustered with different number of clusters starting form a certain number and increasing the number of clusters till a further increase in clusters doesn't affect the final solution of minor species. This gives a grid independent solution.

Once the cells are clustered, the resultant reactors are assigned a state defined by physical and chemical properties. The volume of the reactor is computed as a sum of that of the constituent cells. The temperature and species mass fractions in most cases[14][17] are obtained by a volume average or a weighted average over the those of the constituent cells. In some cases[16][15] the temperature of operation of the reactor is calculated as a kinetic average of the cell temperatures using a weight of NO_x formation contribution of each cell,

$$T = \frac{\int_0^\infty f(T).T.NOx(T,\lambda,\tau).\tau(T).dT}{\int_0^\infty f(T).NOx(T,\lambda,\tau).\tau(T).dT} \tag{2.7}$$

where, f(T) is the normalized temperature distribution, T is the local temperature, τ is the residence time and NO_x(T,λ,τ) is the NO_x mole fraction, formed in a cell at temperature T, equivalence ratio λ and residence time τ. NO_x function is previously tabulated. In [47], the temperature, $\overline{T}$, is computed by enthalpy conservation.

$$\sum m_i \int_{T_i}^{\overline{T}} C_p(T)dT = 0 \tag{2.8}$$

In [5], the initial state of the reactor was computed using Favre averaging of physical variables. The exchange of mass between reactors, in all cases, is calculated as a sum of mass flows between cells of different reactors according to the given flow field.

In earlier studies[8],[14],[49],[16] the type of reactor, PSR or PFR, was assigned based on the randomness in distribution of velocity vectors. If the velocity vectors had a dominant direction it would be a PFR and if the distribution is more random it would be a PSR. In more recent studies such as in [17][22][5], only PSRs are used. A clear explanation for using only PSRs was not given in the literature, but it may be to reduce computation complexity by not having to solve 2 different types of systems of equations(PSR:ODE and PFR:PDE) simultaneously. Besides a PFR can also be resolved as a series of PSRs operating at different conditions.

Turbulence-Chemistry corrections are taken into account in [17]. As temperature has a non-linear effect on the reaction rate constant, temperature fluctuations due to turbulence may have a significant effect, especially on reactions of high activation energy. These reactions are crucial for NO_x formation. Hence to tackle this, a PDF describing the time variation is considered to include the effect of turbulence. The corrected reaction rate during the post processing is expressed as,

$$\overline{k}_j = \int_{T_{min}}^{T_{max}} k_j(T)P(T)dT = C_j k_j(\overline{T}) \tag{2.9}$$

where, $\overline{k}_j$ is the mean turbulent rate constant of reaction, k_j(T) is the instantaneous value, P(T) is the PDF of temperature and C_j is a correction coefficient. As the temperature is kept constant during the post processing phase, this correction of reaction rate constant needs to be done only once before starting the evaluation of the reactors. P(T) is assumed to be a two moment β function. The calculation of the temperature fluctuations requires the temperature variance, σ^2, to determine T_{max} and T_{min}. This is done by solving an extra transport equation for variance along with the CFD calculation. The effect of turbulence on composition fluctuation is not considered. To account for non- perfect mixing, the PSR is split into an inert part and a reactive part. The chemical reactions are allowed to progress and are calculated in the reactive part. The split is obtained by,

$$\gamma = 2.13(\frac{\nu\epsilon}{\kappa^2})^{1/4} \tag{2.10}$$

where, γ is the volume fraction of the reactive part, ν is the laminar kinematic viscosity, ϵ is the rate of dissipation of turbulent kinetic energy and κ is the turbulent kinetic energy. So each reactor has an effective volume of γV_g, where V_g is the geometrical volume. [17] is the only study in which the effects of turbulence are considered in the CRN and significantly better results were seen than in cases without the correction.

All the previous implementations of this concept in literature tried to solve the entire system simultaneously in one system of equations(global method). KPP applies a strategy of solving the problem piece-wise and marching it towards the steady state solution and once it is close enough, it uses a global method to speed up the calculation. The piece-wise solution is done at two levels:

1. First it is done locally, by solving each reactor independently in successive order. The reactor is solved as a steady state mass balanced reactor as shown in Equation 2.11

$$M_k \omega_{ki} = \sum_{j=1}^{N_R} D_{kj} \omega_{ji} + f_{ki} + \Omega_{ki} V_k \tag{2.11}$$

where, M_k is the output mass flow from the k^{th} reactor, D_{kj} is the mass flow rate from from the jth reactor to the kth reactor, f_{ki} is the mass flow of species i entering the k^{th} reactor from the external environment, i.e boundary condition, Ω_{ki} is the formation rate of i^{th} species and V_k is the volume of the k^{th} reactor. M_k and D_{kj} are extracted from the CFD solution in the post processing phase. They are constrained by the conservation of mass

$$M_k = \sum_{j=1}^{N_R} D_{kj} + \sum_{i=1}^{N_C} f_{ki} \tag{2.12}$$

Equation 2.11 can be re-written as

$$g_{ki} = \sum_{j=1}^{N_R} (D_{kj} - M_k \omega_{kj} \delta_{kj}) \omega_{ji} + f_{ki} + \Omega_{ki} V_k = 0 \tag{2.13}$$

And in compact form as

$$g(\omega) = -C\omega + f + R(\omega) \tag{2.14}$$

The local solution of each reactor is obtained by assuming states of other reactors to be fixed, hence the inlets to the reactor will be fixed as shown in Equation 2.15.

$$[C_{in}(\omega) + f]_{old} - C_{out}(\omega) + R(\omega) = 0 \tag{2.15}$$

Instead of having one system of $N_c \times N_s$ equations, there are N_c systems each of N_s equations solved independently. Inlet transport values are updated after each iteration, one iteration consisting the calculation for all reactors. In some case, the Newtonś method is not robust enough, in case of which a local time-stepping method is used.

$$m\frac{d\omega}{dt} = [C_{in}(\omega) + f]_{old} - C_{out}(\omega) + R(\omega) \tag{2.16}$$

This ODE system is integrated till low enough residuals are obtained. Once the residuals are small enough it switches to a global solver.

2. The global solver solves all the reactors simultaneously and starts with a time stepping integration.

$$m\frac{d(\omega)}{dt} = -C\omega + f + R(\omega) \tag{2.17}$$

This is done using the implicit backward Euler method so that it converges even under the stiff conditions of the system. If the residuals of the Time stepping are small enough, meaning that the solution is closer to the final steady solution, the calculation is accelerated by switching over to a global Newton´s method. Time step integration is slower and more expensive but is more stable in reaching the solution than the Newton's method, hence Global Newton's method diverges, it switches back to time stepping.

The validity of the network is checked by different methods in different studies. In [57], it is done by comparing the residence time distribution computed by CFD and that by CRN. A pulse tracer(0.1 s) is introduced in the ERN and its time is calculated to be the residence time in each reactor in [14]. The reactor types are changed till a satisfactory agreement is obtained. Falcitelli *et al.* [47] perform a verification step for the correlation of the generated CRN to the CFD field by running the CRN with the same reduced chemical mechanism used for the CFD solution. The fields of O_2 and CO_2 are compared, which are not expected to differ much as they are the major species and are representative of the combustion process. So if the fields calculated with CRN is in coherence with the CFD field, it is verified that the CRN representative of the case simulated by CFD.

2.2. PSR ENERGY CALCULATION

A PSR may be referred to as 'isothermal' or 'adiabatic' depending on the way the energy calculation is handled. An 'isothermal' PSR is one in which the temperature is maintained constant throughout the calculation by not solving the energy conservation equation. In an 'adiabatic' PSR the energy equation is simultaneously solved in the system of equations and external heat transfers may be specified as source terms. Using an isothermal PSR in a CRN may be beneficial as the non-linearity introduced in the chemical source term due to the exponential dependence of reaction rate on inverse of temperature, is lost by making it a constant term thereby reducing the computational cost of convergence. One may argue that a change in species concentrations may result in a change in enthalpy release and the change in temperature should be accounted for. However, as mentioned by Faravelli *et al.* [15], one of the reasons why Automatic CFD-CRN is possible, i.e the process of decoupling fluid mechanics and chemical kinetics, is because the minor species do not cause much of an enthalpy release and it is the major species that are mainly responsible for heat release. The process assumes that the CFD simulation is adequate enough to give a good estimate of major species and hence the temperature and flow field established. Using this reasoning, Cuoci *et al.* [17] have performed simulations in KPP and have obtained some promising results. One of the properties of the isothermal model would be that the better resolved the temperature field is in the CRN, the better would it represent the case. This means that in general more reactors especially in regions of higher temperature gradients would be better.

Fichet *et al.* [5], used adiabatic reactors to recalculate the temperatures as they say that although the variations in temperature(~50K) may not be high enough to affect the flow field, the exponential dependence of reaction rate coefficient on temperature by Arrhenius' law may affect the NOx concentrations.

As the computational tool was developed in a new framework, the isothermal reactor model was used due to its lower complexity. There is the possibility of extending the software to calculate energy by including the respective equations in the solver.

2.3. OUR AIM

In the framework of the current project, the aim was to develop a computational tool for predicting emissions. Due to the shortcomings of conventional CFD, the use of CRNs were explored in a literature, of which the most notable works were presented in previous sections, and the Automatic CFD-CRN method used by the KPPSMOKE software, was found to be the most suitable. This method has minimum reliance on the operator's specified parameters and in theory is generic enough to be applied on any type of combustor and complexity of flow. As long as a CFD simulation can be performed for a combustor with reasonable accuracy of prediction of major species, the method can be applied to it.

It was seen in Literature that the effect of the criteria used for clustering on the final result was not well studied. In order to achieve a flexibility for the clustering process and the criteria itself, the CFD-CRN method was implemented in-house in this project. A Python code package was written. Cantera has been chosen as the chemistry solver for this code. Its suitability and features are explained in the next section.

2.4. CHEMISTRY SOLVER

Cantera[58] is an open source chemical kinetics and thermodynamics software package. It can be used in Python, C++, C and a few other languages. Its main advantages are reliable chemistry bookkeeping, flexibility with different mechanisms and it also has an in built reactor network solver. Cantera was chosen as the solver for this project because it is open source and contains the functionality required from a chemistry solver. The Cantera library has two main sections in its structure as shown in the Figure 2.3. The bookkeeping layer is capable of files containing information about reaction mechanisms, transport properties,

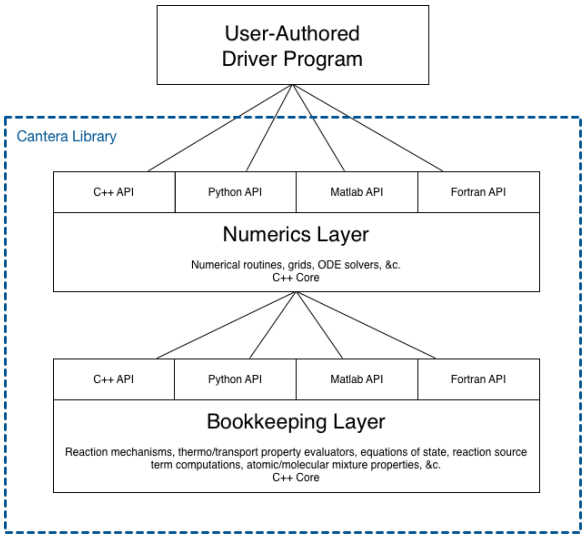

Figure 2.3: Cantera Structure[20]

thermodynamics data , etc, used to define states for a thermo-chemical problem. The numerics layer, is the part which is interfaced to the SUNDIALS library and is responsible for solving the system of equations using suitable numerical methods. Cantera accesses the CVODES solver of SUNDIALS in order to solve systems of stiff Ordinary Differential Equations, such as those defined for a reactor network.

2.4.1. CRN USING CANTERA IN LITERATURE

Researchers in the past have used the Reactor Network solver of Cantera to represent combustion chambers and solve for minor pollutant species. Perpignan *et al.* [21] used CRNs to predict emissions from a Flameless combustion chamber meant for a gas turbine engine. The CRNs are manually created, i.e the connections between reactors and reactor thermo-chemical states are manually specified to represent the combustion chamber. This information is derived by analyzing a CFD simulation performed beforehand as shown in Figure 2.4. The corresponding CRN is shown in Figure 2.5. The CRN method proved to give better prediction

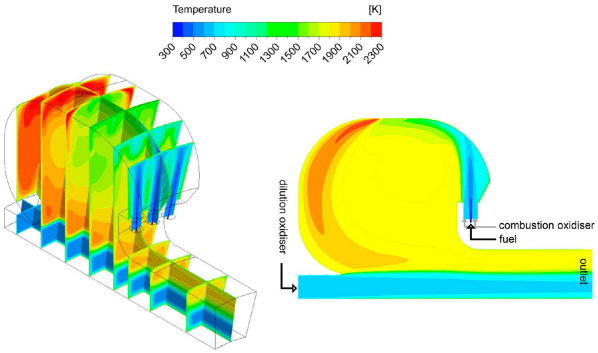

Figure 2.4: CFD simulation of combustion chamber[21]

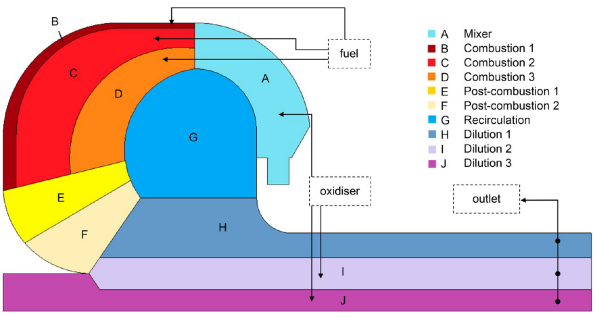

Figure 2.5: CRN representation of combustion chamber[21]

of pollutants than that from CFD methods as shown in Figure 2.6 and fig 2.7. The NOx production was found to be dominated by the prompt NOx pathway. The author's conclude that a combined use of CFD and CRN is a better way predicting emissions than using either in isolation.

Lyra and Cant [22] implement the same general kinetic post processing described in [15][14]. The difference is in the following steps:

1. The type of reactor, i.e. PSR or PFR, is allocated based on the local mean velocity derived from CFD as an ensemble average over the CFD cells. If this value is low, the reactor is modelled a PSR, else if it is high, it is modelled as a PFR. The limiting value of the mean velocity is fixed at 15% of the maximum velocity in the CFD solution.

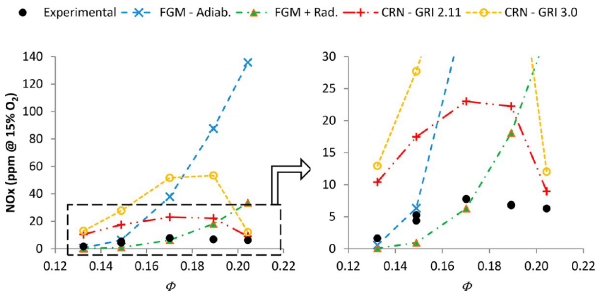

Figure 2.6: NOx emissions[21]

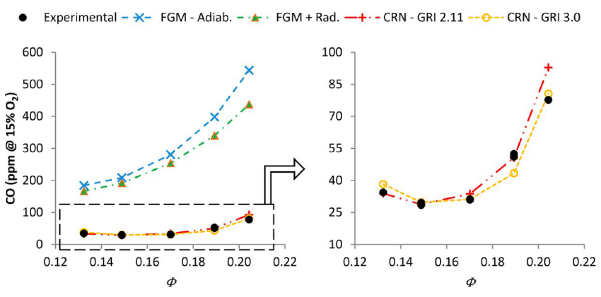

Figure 2.7: CO emissions[21]

2. The temperature field is updated and calculated along with the species concentrations in the ERN. The convergence of the calculation is checked based on the change in temperature between successive iterations.

A similar procedure is also adopted in [54]. Lyra and Cant [22] have implemented the Equivalent Reactor Network method for lean premixed methane/air flames. The configuration, as shown in Figure 2.8, has a premixed methane-air jet flowing into a cylindrical combustion chamber. The sudden expansion of the jet in the larger diameter combustion chamber induces a recirculation zone. Simulations are performed for 3 flames denoted as Flame A, B and C having equivalence ratios of 0.43, 0.50, 0.56 respectively. ERN simulations

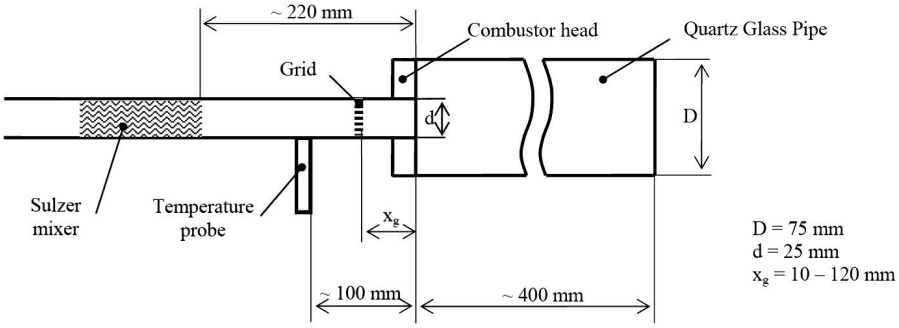

Figure 2.8: Schematic representation of combustion chamber[22]

were performed using an in-house reactor network code in which Cantera was used as a chemistry solver. The author's used both PSRs and PFRs to build the reactor network. The code they developed produces ERNs automatically based on the algorithms in open literature[16]. The network is solved by solving each reactor individually in successive order, such that the solution from one reactor is passed on to the next reactor. This iterative process is continued till a global steady state is achieved. This calculation method takes into account flow effects such as recirculation without the need for any explicit specification for the same. The ERN method proved to give accurate predictions of emission of NOx and CO as shown in Figure 2.9 and Figure 2.10. A sensitivity analysis for the number of reactors required to represent the domain was done and increasing the number of reactors yielded better results till a grid independent solution was reached. This is also what one would expect because more reactors would be able capture variations in the species profiles but once the major flow phenomenon are captured, further increase in reactors may not yield a significant improvement. The author's also mention that the number of reactors required depends on the flame topology and complexity of the flow. In this particular simulation, abut 20% of the reactors were PSRs and the rest were PFRs. The largest network reported has 500 reactors and simulation cost was approximately 7 CPU hours on a standard desktop PC.

2.5. IN-HOUSE CODE

The software developed is a combination of the CFD-CRN concept as seen in literature along with Cantera as the chemistry solver to obtain emissions predictions. The CFD simulations that are required as an input are performed in ANSYS Fluent. The Python code implements the following steps:

- Read CFD data

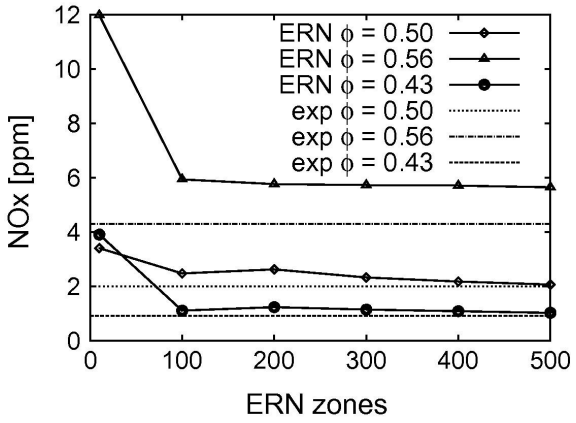

Figure 2.9: NOx concentrations for Flame A, B and C respectively[22]

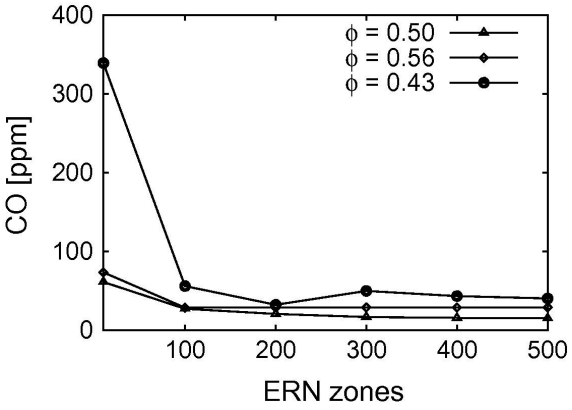

Figure 2.10: CO concentrations for Flame A, B and C respectively[22]

- Clustering CFD cells into equivalent reactors
- Solving the CRN while using Cantera for chemistry calculations.

The CFD case and data are read in rich text format as opposed to the standard binary format for ease of programming. This may be improved upon in the future by converting the code to accept binary files as it will make file handling faster and more compact. Some visualization tools were also created to be able to get some visual feedback about the structure of the CRN and distribution of properties within it. The code is able to export files in a format acceptable by Paraview. The CRN reactor centers can be visualized in 3D space along with the distribution of properties such as temperature and species composition. A 2D view can also be seen which is the CRN data projected onto an axial plane of the CFD domain. The CFD-CRN code layout is shown in Figure 2.11 and the CRN clustering and solution processes are explained in the forthcoming chapters.

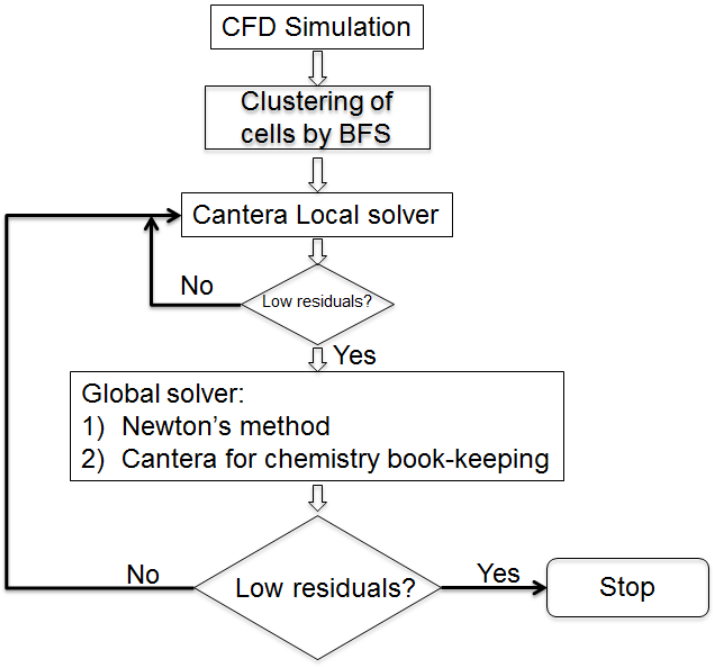

Figure 2.11: Layout of CFD-CRN code

3

CLUSTERING

From the point of view of accuracy, it is best to replace every CFD cell with a PSR and solve the resulting CRN. This would provide the highest resolution and capture the maximum flow physics, but would place a huge computational demand, especially on the amount of memory required when a detailed chemical kinetic mechanism needs to be implemented. Hence the CFD domain needs to be reduced to a an equivalent system of a suitable size.

3.1. CLUSTERING CONCEPT

In this project, the reduction is required to be done automatically, removing the dependence on operator's interpretation of the CFD results and manual skills, to a large extent. The idea, is to group cells that are similar from a chemical kinetics point of view. This grouping or clustering needs to be done such that the states of the so formed reactors are physically consistent with the original CFD system. Some of the requirements that arise for the clustering method:

- Ensure similarity of cells being grouped together.
- Ensure cells being clustered are geometrically connected.
- Ensure conservation of transport properties during conversion from CFD to CRN domain.

Similarity needs to be quantified, Usually it is done by grouping cells having a quantity within a certain range of each other. This means that when lower number of reactors are required, the range needs to be relaxed which may lead to clustering of "less similar" cells. This is a trade-off, making it an optimization problem of lower number of equations to solve versus accuracy of the system.

3.2. GRAPHS FOR CRN

The process of clustering should be applicable across a wide range of geometries and should be independent of the type of coordinate system. The absolute location of the reactors in space is not relevant for clustering. The crucial data from the CFD solution is the inter-connectivity between cells and the information exchanged at common faces. This may be used to extract their proximity to each other, the direction of mass flow and the amount of mass flow exchanged. These requirements fit perfectly for the application of graphs.

Graphs are mathematical structures used to model pairwise relations between objects. A graph is made up of nodes/vertices which are connected to each other by edges. The edges may be directed, which means that an edge connecting 2 nodes would have a preferred direction towards a particular node, or undirected in which case all vertices are treated equally. In computer science, graph theory has been extensively used and there have been algorithms developed for graph traversal, searching and sorting. This provides a good base for the application, which is to travel through the CFD cells and group similar cells together. The CFD cell centers can be represented by nodes and edges represent common faces between 2 cells, thereby representing the connection. The graph is constructed from the ANSYS Fluent case file, by exploring all faces mentioned in the file. From the face notation, the related cells are found and the information is stored as a dictionary. A dictionary is a linked list representation in Python. It is convenient because the graph is expected to be sparse,

i.e each vertex is connected to only a few vertices compared to the total number of vertices. This notation is more memory efficient than a matrix notation for this particular application.

3.3. CLUSTERING ALGORITHM

This section describes the process of clustering CFD cells to generate a CRN. It involves traversing through the graph of CFD cells, checking for fitness of clustering criteria, updating the quantities of reactors formed by clustered cells and the actual act of combining cells and generating a new graph of reactors which forms the CRN.

3.3.1. GRAPH TRAVERSAL

In order to cluster similar cells, they need to be 'searched' in the graph. Graphs have standard algorithms defined for searching and sorting and the advantages of each algorithm have been well studied in the past[59]. The graph traversal algorithm should be such that every move has a significant chance of encountering, not only a similar cell based on physical/chemical property, but also a geometrically connected one to the cluster as it would be inconsistent to group physically unconnected pockets in the CFD domain. In this particular case, an efficient way of searching similar cells while ensuring that they are geometrically connected is to search a cell's nearest neighbors first before proceeding deeper into the graph. For this particular purpose, The Breadth First Search(BFS) algorithm was chosen. The BFS traversal is one in which cells nearest to the start point are explored first. Hence during the traversal cells at the same distance from the start point, or in other words at the same depth in the graph, are considered equally for traversal and the algorithm proceeds to the next 'depth level' only after the full 'breadth' of the current 'depth' is completely explored. The very nature of the BFS ensures that the nearest cells are explored first which increases the chance of encountering geometrically connected cells sooner during the traversal.

An overview of the clustering algorithm is presented in Figure 3.1. The graph is searched by the BFS algorithm, the pseudo code for which is shown in Algorithm 1. The algorithms relies on the color of the cell to identify if the cell is unexplored, explored or queued represented by white, black and gray respectively. All cells are initiated as white. The search starts from a predefined start point, which is obtained from a list of locations, to allow for the start point to be changed after every iteration so that the resultant clustered graph is independent of the start location. The first cell initiates as a reactor. The currently unvisited neighbors of the cell, denoted by the color white, are added to the Queue and their color is changed to gray. Queue is a data structure which follows the First In First Out(FIFO) principle, i.e. the elements stored first exit the queue first. The current cell undergoes a 'Fitness test'. If a cell passes the test, it is added to the current reactor else, a new reactor is created with this cell as the first constituent. In either case, once the cell is explored, its color is changed to black. This process continues till the graph is fully searched, i.e the Queue is empty. This is one iteration of the entire CRN generation process.

Algorithm 1 BFS algorithm

```
1:  s = startpt
2:  s.color = Gray
3:  Q = null list
4:  ENQUEUE(Q,s)
5:  while Q ≠ null list do
6:      u = DEQUEUE(Q)
7:      for each v ϵ G.Adjacent[u] do
8:          if v.color == White then
9:              v.color = Gray
10:             ENQUEUE(Q,v)
11:     Do[Clustering]
12:     u.color = Black
```

3.3.2. FITNESS

The Fitness test is carried out by a fitness function and certain other conditions. The following conditions need to be met to pass the 'Fitness test':

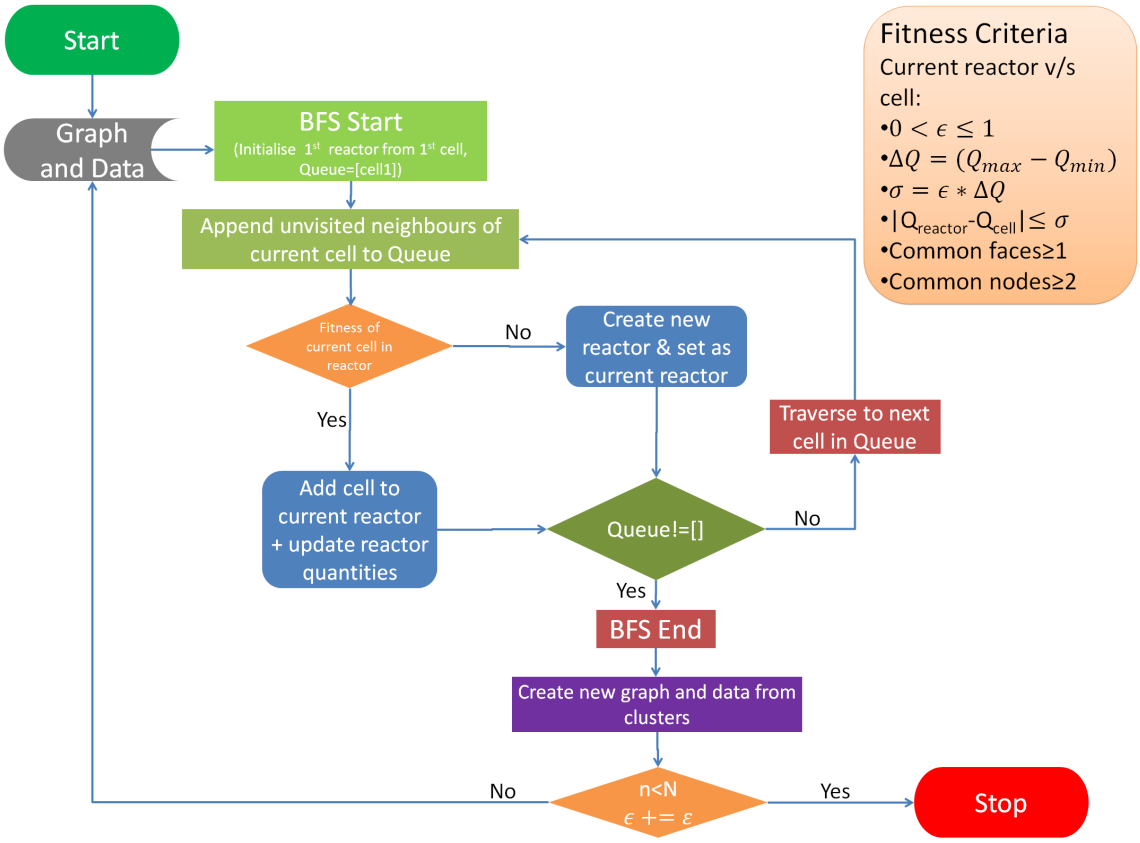

Figure 3.1: Clustering Algorithm overview

1. a check for common faces or nodes. This is an additional check over the BFS traversal to ensure clustering of geometrically connected cells into reactors. The cell to be added is checked for having at least one common face or 2 nodes with the reactor.

2. A user defined list of criteria for clustering is entered while starting the program. These quantities should satisfy a fitness criteria as shown in Figure 3.1. At the beginning of the process the difference between the maximum and minimum value of the quantity in the CFD domain is obtained. A tolerance, σ, is defined as shown in Equation 3.1, where ϵ should be $0 < \epsilon < 1$.

$$\begin{aligned} \sigma &= \epsilon * (Q_{max} - Q_{min}) \\ |Q_{reactor} - Q_{cell}| &\leq \sigma \end{aligned} \tag{3.1}$$

   Within the Fitness function, the absolute difference of the value of the quantity in the reactor and that in the cell is checked to be less than σ. The value of ϵ is increased conditionally at the end of an iteration, which effectively relaxes in the clustering criteria and increases the range of values that may be accepted as 'similar' for a particular reactor. The value of ϵ is universal, which means its is the same for all criteria in all reactors.

3. Other derived criteria can also be coded into the program. These are quantities which are not directly available from the CFD solution but can be derived by some mathematical operations on the pre-existing quantities. One such implemented criteria is the angle between the velocity vectors.

3.3.3. UPDATING QUANTITIES IN EACH REACTOR

Upon clustering a cell into a reactor, the values of quantities within the reactor needs to be updated so as to define the state of the reactor as an agglomerated representation of the constituent cells. The algorithm used to update the reactor quantities while maintaining physical consistency is shown in Figure 3.2. The PSR model does not take into account any spatial dimension, which means velocity has no meaning and definition in this system and hence there is no difference between total and static thermodynamic values for a PSR.

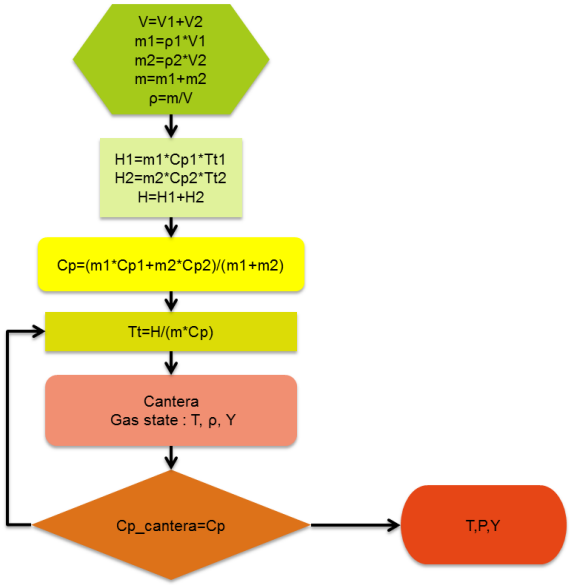

Figure 3.2: Algorithm used to update reactor quantities while clustering

The PSR model ignores the existence of a dynamic component of a quantity. Hence one may either assign a static value to the PSR and acknowledge the difference to the assumptions within the PSR model or assign the total values, but in this case, the chemistry will be calculated at total temperature and pressure values, which is again a deviation from chemical kinetic formulation. In this code, the updated state is calculated while taking into account conservation of total enthalpy so that there is physical consistency during the clustering process but static value of temperature, obtained by subtracting the dynamic component from the total temperature, is used while defining the gas state in a reactor. The dynamic component is composed of the contribution of velocity to the enthalpy, which is obtained by a mass average of velocity components over the constituent cells.

3.3.4. CLUSTERING

The clustering starts off with a graph representing the CFD cells. The BFS traversal is used to scan through the graph for similar cells. The traversal begins from a designated start point which can be specified. This starting cell is used to generate the first cluster centre. The next cell is checked for Fitness. If it is found to be fit enough to group with current cluster, it is added, else this cell is used to generate a new cluster. This process is continued till the entire graph is explored. If a cell is added to a cluster, the average cluster quantities are updated to account for this addition. The cluster inter-connectivity is important to retain the CFD flow field in the CRN. This is done by having the correct amount of mass flowing between reactors, and this mass flow is obtained from the CFD simulation. ANSYS Fluent stores mass flows for each face. Hence it is necessary to keep an account of the faces in a cluster. The only faces that matter to a cluster are those shared with other clusters, in other words they are the bordering faces. Thus a record of bordering faces of each cluster is maintained. The face list of each cluster is updated when a cell is added by taking a symmetric difference of the face lists of the cluster and cell, which means that the result consists of the face present in either the cell or the cluster, not in both. The common faces are the interior faces and are 'dissolved'. Similarly, a record of cells(referring to cells from the original CFD simulation) in a cluster is maintained, which is done by simply recording the cells in the cluster and the cells to be clustered in a list where cells common to both sources are listed only once.

The clustering iterations are carried out till the number of reactors is less than the threshold specified as a user input. If the number is larger than the threshold, the Fitness comparison tolerance is relaxed conditionally so as to allow more cells to agglomerate in the next iteration. The above process is repeated on the new graph in the next iteration, where 'cell' would refer to the elements of the current clustered graph and 'reactor' would refer to the elements formed by clustering the nodes of the current graph. The successive iterations result in a graph with the nodes representing the final reactor centers. The pseudo-code of the clustering process is shown in Algorithm 2.

Algorithm 2 Clustering algorithm

```
1: function FITNESS(Q_u, Q_c, faces_u, cells_u, faces_c, cells_c)
2:     cond = |(Q_u − Q_c)/(Q_max − Q_min)|
3:     if cond<=tol and (fcom ≠ ∅ or ncom ≥ 2) then
4:         return True
5:     else
6:         return False
7: function CLUSTERING
8:     if Fitness==True then
9:         Re-valuate Quantities
10:        Update cluster average values
11:        Cell list: Union of u and c lists
12:        Face list: Symmetric difference of u and c lists, i.e. only faces present either in u or c not in both
13:    else
14:        Create new cluster center
15:        Initialize new point in graph
16:    Update 'neighbours' directory
```

3.4. FEATURES

This section mentions some of the features and capabilities of the clustering program.

- Multiple criteria: The clustering can be done based on multiple criteria, Eg: a combination of Temperature and Velocity or even more. The decision of clustering is taken only if each criterion individually satisfies the Fitness test. This means that the more the number of criteria the more difficult it is is to reduce, meaning that the tolerance needs to be relaxed more to reach the target number of reactors.
- Reduction: The algorithm can reduce the graph size through successive iterations up to any specified number. An extreme case of reducing the CFD domain of 10^6 cells to 1 reactor was also successfully tested.
- Time: The algorithm can reduce about a million cells to 100 reactors in about 45 minutes.
- Generality: The representation of the cells and reactors in the form of a graph makes the process independent of the type of mesh(structure/unstructured) as the cells are related based on inter-connectivity and not defined based on their locations in space.

4

CHEMICAL REACTOR NETWORK SOLVER

Cantera was used as a chemistry solver in this project. This chapter describes its solving capabilities, how it was applied in the project, limitations and steps taken to overcome them.

4.1. CANTERA MODELS

Cantera has several object based models which can be assembled together to form a reactor network. The main models are:

- Ideal Gas Reactor: It is a closed reactor which is by default a constant volume system. It can be set to have moving walls, and hence a changing volume. The reactor contains a gas, the state of which is defined by Temperature, Density and mass fraction of species contained. Although, there are several ways in which the state of a gas can be defined, Cantera uses these quantities as independent variables while solving the equations. All other quantities are derived. The state variables of an IGR are mass, volume, temperature and species mass fraction.

- Reservoir: It is an infinite resource of predefined gas whose remains constant during calculations. It can be used as a source or a sink.

- Mass flow controller: Governs mass flow from one reactor/reservoir to another reactor/reservoir. It is insensitive to pressure difference, i.e. it would allow mass flow from lower pressure to higher pressure. The mass flow is specified while defining the controller and if the mass flow is negative, the value is taken to be zero. A Mass Flow Controller, hereafter referred to as MFC, is a Cantera object which allows flow in one direction at a predefined mass flow rate.

- Valve: It is an object that allows mass flow through it proportional to the pressure difference across it. The valve coefficient is the proportionality constant which needs to be defined. If the pressure difference is negative, the mass flow is zero, hence it is a one way valve. It is defined as:

$$\begin{aligned} \dot{m} &= k_v(P_1 - P_2) \qquad \text{if } P_1 > P_2 \\ \dot{m} &= 0 \qquad \text{else} \end{aligned} \tag{4.1}$$

- Reactor Network: A group of reactors is solved by inserting it in a ReactorNetwork object in Cantera. It can accept one or more reactors, and solves them simultaneously in one system of equations.

A PSR can be modeled by placing mass flow controllers as inlets and outlets of an Ideal Gas Reactor. The theoretical PSR model is a time independent system of nonlinear equations. Due to the stiffness associated with chemically reactive systems, such a setup would be difficult to converge. Hence Cantera, sets up a time dependent system of Ordinary Differential Equations(ODE). This system is solved by advancing it in time and at $t=\infty$ a steady state should be achieved which would be the theoretical PSR model.

4.1.1. CANTERA GOVERNING EQUATIONS

This section presents the governing equations used by Cantera to solve a ReactorNetwork object.

Mass Conservation

$$\frac{dm}{dt} = \sum_{in} \dot{m}_{in} - \sum_{out} \dot{m}_{out} \tag{4.2}$$

Species Conservation

$$\frac{d(mY_k)}{dt} = \sum_{in} \dot{m}_{in} Y_{k,in} - \sum_{out} \dot{m}_{out} Y_k \tag{4.3}$$

$$m\frac{dY_k}{dt} = \sum_{in} \dot{m}_{in}(Y_{k,in} - Y_k) + V\dot{\omega}_k MW_k \tag{4.4}$$

where, Y_k is mass fraction of species k, $\dot{\omega}$ is the production rate of species k from reactions and MW_k is the molecular weight of k.

Energy Conservation

$$mC_v\frac{dT}{dt} = -\dot{Q} + \sum_{in} \dot{m}_{in}(h_{in} - \sum_k u_k Y_{k,in}) - \frac{pV}{m}\sum_{out} \dot{m}_{out} - \sum_k V\dot{\omega}_k MW_k u_k \tag{4.5}$$

where, C_v is specific heat at constant volume, u_k is specific internal energy of species k, p is the pressure of the reactor, h_{in} is the enthalpy of inlet stream and $\dot{Q}$ is the heat loss from the reactor. These set of equations form a system of the form

$$\begin{aligned} \dot{y} &= f(t, y) \\ y(t_0) &= y_0 \end{aligned} \tag{4.6}$$

'y' is the dependent variable and t is the independent variable in a general equation. Y_k may exist in the source term $\dot{\omega}$ in Equation 4.4, as a term with power not equal to unity. 'T' in Equation 4.5 appears in the species production term as an exponential factor, due to Arrhenius' equation. Thus the above equations cannot be generally written as a linear polynomial of y and its derivatives, making it a non-linear system. The non-linearity may be reduced if 'T' is kept constant and the energy equation not solved.

4.1.2. ODE INTEGRATION

This system is integrated as follows:

$$y_{n+1} = y_n + \int_n^{n+1} f(t, y)dt \tag{4.7}$$

Cantera calls CVODES to solve differential equations and it is done so using the Backward Differentiation Formulation(BDF) as it is a stiff system of equations. The general formulation of BDF is,

$$\sum_{k=0}^{s} \alpha_k y_{n+k} = h\beta f(t_{n+s}, y_{n+s}), \tag{4.8}$$

where h denotes the step size and

$$t_n = t_0 + nh. \tag{4.9}$$

As the function, f(t,y), is evaluated at the latest time, t_{n+s}, this becomes an implicit method. The value of s depends on the specified value. CVODES varies it from 1 to 5 such that a stable calculation occurs. Due to this implicit nature, for each time step, the function, f(t,y) in the RHS in Equation 4.8 needs to be evaluated using a linear approximation. This is done using a Newton Raphson scheme.

4.1.3. LIMITATION

There is an inbuilt option to solve reactor networks in Cantera. This solves all the reactors simultaneously by assembling all the governing equations in a matrix leading to a AX=B type of problem as shown in Equation **??**. The limitation is that the size of the matrix 'A' is limited by the RAM available. This is because Cantera, which uses SUNDIALS[60] for the ODE integration, is capable of only calling upon the dense solver, because the governing equations are written such that all the matrices are treated in a dense manner. In reality the Jacobian matrix is sparse as each reactor is connected to only a couple of other reactors, compared to the total number of reactors in the system. As the aim is to use a detailed reaction mechanism, GRI Mech 3.0 with

53 species, the system is limited to a couple of hundred reactors. For example, a network of 5000 reactors using GRI Mech 3.0 mechanism(53 species) would have 55 variables each, i.e 275000 variables. When the Jacobian is created, it would be of the size 275000x 275000. Each variable is a floating point which occupies 64 bit memory, so this Jacobian would occupy at least $8x275^2$MB, i.e 605 GB of RAM memory. This is quite a large RAM requirement. Hence an alternative solution strategy needs to be used which can treat this matrix as a sparse one.

4.1.4. REACTOR NETWORK MODEL

From literature it is seen that at least 5000 reactors are required even for simple flames to obtain a 'grid independent' solution from the CRN when starting from about a million CFD cells, which is the size of a typical RANS simulation of a section of a combustion chamber as shown in Figure 4.1. A larger number of reactors allows for greater resolution, thereby being able to represent regions of different composition and temperature by different reactors. A more resolved CRN would give better prediction of emissions, as temperature and composition gradients are better represented as opposed to being smeared by inclusion in the same reactors, as is the case of a few/lower number of reactors. This is why the choice of aiming for large number of reactors is done during this project. Cantera framework limits the size of the CRN due to constraints of RAM required and prevents the use of reactors of the order 10^3, needed to achieve grid independence. In order to

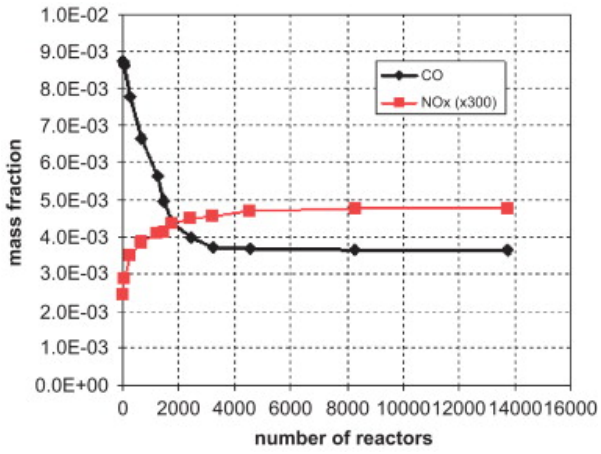

Figure 4.1: Grid independence of CRN[15]

work around Cantera's limitation of handling large reactor networks, the reactors are physically decoupled from each other and are solved in iterations. Each PSR is composed of an Ideal Gas Reactor at its core connected to inlet and outlet reservoirs as shown in Figure 4.2. There may be multiple inlet and outlet reservoirs, each reservoir being connected by one mass flow controller and 2 valves, one in each direction, to the Ideal Gas reactor. The reservoir state is synchronized with the state of the neighboring reactor, connected to the current reactor in the network. Instead of solving all the reactors simultaneously, each reactor is advanced in time by small time steps. After each iteration, the boundary reservoirs to each reactor are updated to the state of the neighboring reactors, which serves as a virtual coupling between reactors, and the process is repeated till convergence. Thus each reactor is a system in itself where its inlet and outlet conditions, i.e source and sink reservoirs, are updated after each iteration.

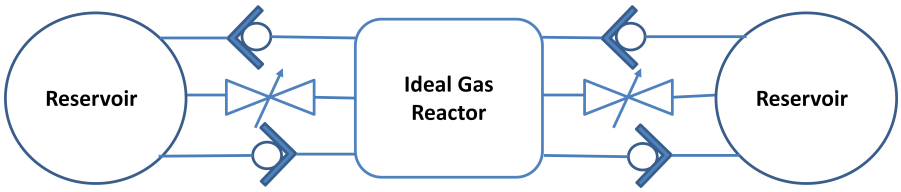

Figure 4.2: PSR model in Cantera

The reactor graph is explored. Neighbors to each reactor are checked for common faces, faces being those of the constituent cells that were clustered together from the CFD domain. Common faces are checked for

the associated mass flow from the CFD data. The mass flow is taken into account only if it is an outflow from the current reactor, so if it is an inflow it will turn up as an outflow when the neighboring reactor turns up as the current reactor during the iterations. This ensures that a particular mass flow is accounted for only once in the entire set of iterations. The total mass flow from one reactor to another is a sum of all outwards mass flow, and this total mass flow is assigned to the mass flow controller between them in that direction. The sum of mass flow through all outward MFCs from a reactor is the total mass flowing through that reactor.

The model also has the choice of using a feed forward and feedback valve in parallel to every MFC. The reactors start off with an initial composition of species having a certain total mass. As the iterations progress, the composition changes, but the mass of each reactor may also change. The PSRs are set up such that the inlet and outlet mass flows are fully balanced by the MFCs which prevents the mass from changing, as there is no excess mass flow to or from the reactor. The valves serve the purpose of temporarily allowing excess mass flow in either direction during the transient calculations, while ensuring that the system is fully balanced with the initially specified mass flows by having zero mass flow through the valves at steady state. The presence of valves enables reduction in pressure differences between reactors and hence leads to all the reactors having about the same pressure which is near to the inlet pressure, as is the case in constant pressure combustion such as that in a gas turbine engine.

4.2. BOUNDARY CONDITIONS

The boundary conditions are given a definition similar to their corresponding counter parts in ANSYS Fluent, which also happen to be the most widely used definitions in CFD in general. The BCs that are handled in the code are Mass flow inlet, Outlet, Periodic BC and Wall.

1. **Mass flow Inlet:** The value of the zone to which the inlet faces belong are looked up manually from the CFD simulation and hard coded into program. The face type is looked up from the standard Fluent boundary condition ids. For every inlet face, the corresponding mass flow rate is looked up from the data dictionary. A reservoir is defined, which is a Cantera object, and its state is hard coded using the inlet conditions that were specified for the CFD simulation. So if the face belongs to the Fuel Inlet zone, the Reservoir is defined to the Temperature Pressure and Composition(Species mass fractions), of the inlet fuel. Eg: CH4 at 300K and 1 atm. Similarly if the face belongs to the Air Inlet zone, the Reservoir is initiated to the inlet Air conditions. This specification is case dependent and needs to be manually specified in the program. The zone ids are quite readily available in ANSYS Fluent and are clearly stated.

2. **Outlet:** Faces are identified to be an outlet boundary condition and the mas flow rate is searched from the data dictionary. This is used to define the corresponding mass flow controller. A valve is modeled, such that it is a feed forward one to release excess mass indicated by the build up of excess pressure. The MFC and valve flow into a Reservoir, defined at ambient conditions, i.e air at STP[1].

3. **Periodic BC:** A periodic condition has 2 faces associated with it, a periodic face and a shadow face. In Fluent, a positive mass flow indicates flow from periodic to shadow face and a negative mass flow indicates flow from shadow face to periodic face. It is important to capture this boundary condition in the CRN because a lot of combustion chambers are axisymmetric and often only a small sector is simulated with periodic boundary conditions on the cut out faces. This is especially important in flows with swirl about the axis. First these faces are identified and specified as pairs. Next, mass flow controllers are defined according to the direction of flow, but this is done only if the periodic face and shadow face belong to different reactors.

4. **Wall:** This is a boundary condition for heat flux. Although it is not actively used in the current project, it is an option kept for when temperature is recalculated in the CRN. The heat loss through the wall is obtained from the CFD simulation. Every face defined as a wall has a heat flux passing through it which is calculated in the CFD simulation. This is used to initialize the Cantera 'Wall' object, where the wall is between the reactor in which the cell is and a Reservoir defined at ambient conditions.

4.3. MASS IMBALANCE

To satisfy conservation of mass in a CFD simulation, the mass flowing into the cell should be equal to the mass flowing out. In practice, the cells from the CFD simulation have a certain amount of mass imbalance, i.e the

[1] Standard Temperature and Pressure

total inflow and outflow mass flow rates associated to a cell have a difference equal to a certain tolerance set in the CFD solver which is accepted to be a converged solution as even the smallest difference would be equal to machine precision and not exactly zero. When several such cells are agglomerated, the mass imbalance adds up and the resultant reactor has a relatively large mass imbalance. In order to be able to solve the reactor, the mass flows need to be corrected. If each reactor is corrected individually, it would not ensure the conservation of mass throughout the network, and while creating the code, it was seen that such an approach lead to an imbalance in major species obtained at the exhaust of the combustor from the CRN when compared to the CFD solution, which should not be the case as the preliminary assumption includes the correct prediction of major species by CFD.

A better way of solving this problem is to correct the mass flows of all the reactors simultaneously. A system of equations is setup, where the independent variables are the total outflow from the reactors. The total mass flowing out from a reactor may be flowing into several neighboring reactors. Hence, the inflow into a reactor is a fraction of the total outflow from the neighboring reactor and this fraction is calculated from the mass flow of the original CFD solution and kept constant. The equation set up is a balance of total inflow and outflow of a reactor, for a system of N number of reactors in Equation 4.10, the matrix form of which is shown in Equation 4.11.

$$M_k - \sum_{j \neq k}^{N} \alpha_{kj} M_j = \sum f_k \tag{4.10}$$

$$\begin{bmatrix} \alpha_{11} & -\alpha_{12} & -\alpha_{13} & -\alpha_{14} & .. & .. \\ -\alpha_{21} & \alpha_{22} & -\alpha_{23} & .. & .. & .. \\ -\alpha_{31} & -\alpha_{32} & \alpha_{33} & .. & .. & .. \\ : & : & : & .. & .. & .. \end{bmatrix} \begin{bmatrix} M_1 \\ M_2 \\ : \\ : \end{bmatrix} = \begin{bmatrix} \sum f_1 \\ \sum f_2 \\ : \\ : \end{bmatrix} \tag{4.11}$$

where M_k is the total outflow from k^{th} reactor, M_j is the total outflow from j^{th} reactor, α is the fraction of outflow from j^{th} reactor flowing into k^{th} reactor and f_k is any other source of mass inflow. As can be seen, all mass flows, M, are defined as an outflow from a reactor. This results in a AX=B type system where A is a NxN matrix and B is a vector of source terms. In the current code, B contains the boundary inflow mass flow values. The solution to the system is found giving the total outflows as a result. The coefficients from the matrix A are used to assign the correct fractions of the total outflows to the corresponding mass flow controllers. For every mass flow rate there are two corresponding MFCs, one outflow MFC in the PSR model of the current reactor and its associated inflow MFC in the PSR model of the adjacent reactor, due to the decoupled method of solving the CRN as explained earlier.

The pseudo code for mass flow correction is mentioned in Algorithm 3. It shows the process of calculating the inlet mass flow fractions, solving the system of equations and finally correcting the mass flows in each mass flow controller.

Algorithm 3 Mass Imbalance correction

```
coeffmat=null square matrix; diagonal size=number of PSR
f: boundary condition mass flows. Inflow is positive
while Creation of MFC from r1 to r2 do
    coeffmat[r1][r1]+=mflow
    coeffmat[r2][r1]-=mflow
for p from 0 to Number of PSR-1 do
    factor=coeffmat[p][p]
    for q from 0 to Number of PSR-1 do
        coeffmat[q][p]=coeffmat[q][p]/factor
A=coeffmat
B=f
function SOLVE(A,B)
    AX=B
    return X
Corrected Mass flows=X
for All MFCs do
    mass flow mfc=abs(coeffmat[from reactor][to reactor])*X[from reactor]
```

Table 4.1: Local v/s Global solver properties

Solver Type	Chemistry Bookkeeping	Numerical Solver	Matrix treatment	Governing Equations	Time Integration	Advancing by Newton´s method
Local	Cantera	SUNDIALS	Dense	In-built Cantera	BDF (CVODES)	No
Global	Cantera	Sci-Py	Sparse	Custom written	No	Implemented

4.4. IMPLEMENTED SOLVER ALGORITHM

The system of ODEs is characterized by non-linearity and stiffness. The stiffness of the system is attributed to the wide range of time scales for the reactions involved. Some reactions, such as those responsible for heat release are much faster than those for minor species formation such as that of NO. This makes it difficult to integrate as the fast reactions require a small time step to be captured whereas the slow reactions need to be integrated up to a large absolute time. One of way of tackling this issue is to initially advance the system using small time steps till the fast reactions reach a steady state and then switching over to large time steps to cover the slower reactions. Further extending this idea, one can use certain methods to push the system towards the steady state solution by advancing slowly in time and once it is close enough, the solver switches to a Newton's method which can take more rapid leaps towards converging to the steady state. The Newton's method cannot be directly applied because it may be unstable at a point quite far off from the solution.

Two levels of solvers are implemented, local and global. The local solver solves each reactor individually, whereas the global solver solves all the reactors simultaneously as a system. Cantera can be used in the following ways:

1. As a chemistry bookkeeping tool, in which Cantera ensures a consistent physical and chemical state of the reactors in the form of their temperature, density and species mass fraction and storing the chemical reaction mechanism with all its thermodynamic properties.

2. It can also be used to solve a reactor network, in which Cantera calls SUNDIALS to perform ODE integration.

At the local solver level, both features are used, whereas at the global solver level Cantera is used only as a chemistry book keeping tool. This is because the governing equations are written explicitly and solved using SciPy to solve a sparse matrix equation due to Cantera's solver limitations of being unable to simultaneously handle large number of reactors, as mentioned earlier.

At the global solver level Cantera's role is especially useful to maintain the consistency of reactor states in which the sum of all mass fractions should be equal to 1 and the value of every species mass fraction(Y) should satisfy Equation 4.12.

$$\begin{aligned} \sum Y &= 1 \\ 0 \leq Y &\leq 1 \end{aligned} \tag{4.12}$$

This can be easily violated while performing Newton iterations as the method is not bound by inequality or equality conditions. Cantera self adjusts the values if the above conditions are violated, hence ensuring physical consistency. The difference between the two solvers is summarized in Table 4.1

4.4.1. LOCAL SOLVER

Using the local solver, the reactors are individually integrated in time in sequential order. The corresponding reservoirs are updated to the reactor states after all the reactors have been advanced by one time step and the process is repeated till convergence. The absolute time step is different for each reactor. It is defined as a multiple of the residence time of the reactor.

$$dt = \gamma t_{res} \tag{4.13}$$

$$t_{res,i} = \frac{\text{mass}_i}{\dot{m}_{out,i}} \tag{4.14}$$

For a large enough multiple of the theoretical residence time, a reactor would reach steady state condition. The multiplication factor, γ, is initialized as 1 and is incremented after every successful iteration, a successful

iteration being defined as one in which all reactors converge locally. The reactors are not directly integrated to a large final time in the first iteration because it may lead to large differences in composition between neighboring reactors and it was observed that it causes convergence issues for the Cantera reactor object. Iterative increment of γ, treats the system in a 'pseudo-collective' manner and allows the reactors to adjust to the changes in the system.

Cantera's 'advance()' function is used to implement the time-stepping integration. The parameter passed is the time up till which the integration needs to be performed from t=t_0, where t_0=0 by default. The function calls another function called step() which advances the reactor by small time steps till the reactor is advanced to the time specified. By default, whenever the advance() function is called, it solves the reactor from its current state starting from t=0. The implication of this is that if the time specified is less than the residence time of the reactor, it is artificially restricting the residence time of the reactor. In experiments with a single reactor it was seen that the size of the time step affected the final solution if time step was less than t_{res}. While running time stepping iterations, the time passed to advance() should be the latest cumulative time, so that the solver advances the reactor from t=0 to the latest time.

4.4.2. GLOBAL SOLVER

The global solver comprises of a Newton solver and a Time stepping integrator. The governing equations were explicitly coded in. The equations are as follows:

$$g(\omega) = -C\omega + f + R(\omega) \tag{4.15}$$

where g(ω) is the net rate of production of mass of species in a reactor, C is a $N_E \times N_E$ sparse matrix accounting for convection terms, ω is a vector of mass fractions of species in all reactors, f is a vector accounting for mass flows from external environment, i.e boundary conditions and R is a vector accounting for production terms due to local reactions within the PSR. N_E=$N_C \times N_R$, where N_C is the number of species and N_R is the number of reactors. The Newton method, also known as the Newton-Raphson method is a root finding algorithm which finds a 'y' such that 'f(y)=0'. The general Newton-Raphson Equation for a single variable is

$$y_{i+1} = y_i - \frac{f_i}{f_i'} \tag{4.16}$$

where f_i is the function value at the i^{th} iteration and $f_i' = \frac{df}{dy}$ at the i^{th} iteration. The objective of the Newton Raphson method is to find the solution to f(y)=0, i.e the solution is reached when the function value, f, is zero. This method is extended to a multivariate system by replacing the variables with vectors and the derivative by a Jacobian matrix,

$$\mathbf{y}_{i+1} = \mathbf{y}_i - \frac{\mathbf{f}_i}{J_i} \tag{4.17}$$

This can be re-written as

$$J_i \Delta \mathbf{y} = -\mathbf{f} \tag{4.18}$$

This is an $AX = B$ type of equation which can be easily solved using either direct or iterative solvers from the SciPy package. The aim of the Newton iterations is to obtain a ω for which $g(\omega) = 0$.

$$J_i \Delta \omega = -\mathbf{g} \tag{4.19}$$

The time integration is performed on a modified form of the governing equations. By definition,

$$m_k \frac{d\omega_{ki}}{dt} = g_{ki} \tag{4.20}$$

This equation is discretized and integrated using the BDF method.

$$\omega_{ki}^{n+1} = \omega_{ki}^{n} + \int \frac{g_{ki}^{n+1}}{m_k} dt \tag{4.21}$$

The BDF method uses implicit iteration, i.e the integral of g over the time step is calculated at n+1 iteration. For the final results, the time integrator was not used as in some small scale tests the implementation was found to be flawed and unreliable. Hence currently the software only uses the Newton's method for global iterations.

One of the limitations of Cantera's reactor network solver was its inability to handle large systems. In the global solver the Jacobian would be very large considering reactors of the order of 10^3 and each reactor has around 53 species, leading to a Jacobian of the size of around 53000×53000 which would lead back to the same memory consumption issue. Hence the Jacobian is expressed as a sparse matrix rather than a dense one and is solved using the sparse solvers in SciPy.

4.4.3. JACOBIAN CALCULATION FOR GLOBAL CALCULATION

The Newton's method involves calculating a Jacobian matrix at the current state. This section describes how it is done. The methods adopted are from [17] and are used in KPP. The Jacobian for the entire reactor network can be expressed as a combination of 2 Jacobian matrices, one having a contribution due to the inter-connectivity between neighboring reactors, J_s, and the other being the sensitivity of species production within the reactor species composition, J_w.

$$J = J_s + J_w \tag{4.22}$$

Both, J_s and J_w are expected to be sparse matrices. J_s is sparse because each reactor is connected to only a few other reactors, compared to the total number of reactors, hence it has a structure similar to the one shown in Figure 4.3. Each row represents the contribution of the convection terms of a species conservation equation in the reactor, the reactor being represented as a square with dark borders lying along the diagonal of the matrix. J_w is sparse and concentrated near the diagonal. This is because only the species present

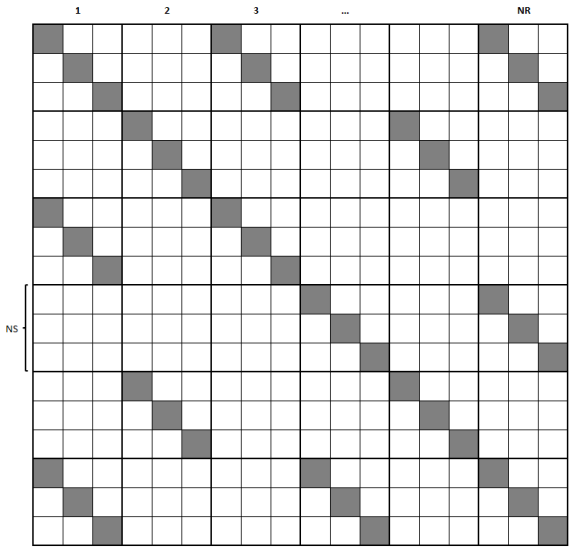

Figure 4.3: Sample structure of Jacobian due to reactor inter-connectivity(J_s), where NS is the number of species and NR is the number of reactors.

within a particular reactor can directly affect the reaction rate, hence the derivatives of the species production with respect to species in other reactors is zero. Usually, a reaction mechanism has more reactions than species. The numerical way of calculating J_w would be to vary each species and for each variation, calculate the change in production rates of the other species. The Jacobian may also be calculated analytically by calculating the change of reaction rates with respect to the reactants for each reaction. As each reaction has 2 to 3 reactants, the number of evaluations are small. This is highly valuable in speeding up the evaluation time especially for large mechanisms, which are expected for complex fuels such as kerosene and gasoline. The influence of the change in mass fraction of a particular species on another species within a reactor can be expressed as,

$$J_{\dot{\Omega}} = \frac{\partial \dot{\Omega}}{\partial Y} = \frac{\partial \dot{\Omega}}{\partial C} \times \frac{dC}{dY} \tag{4.23}$$

J_w is composed of many $J_{\dot{\Omega}}$ sub matrices, each one belonging a reactor in the network as shown in Figure 4.4. Equation 4.23 splits the derivative into two parts according to the chain rule. The first term relates the change in species production rates to change in concentrations of all the species and the second term relates change

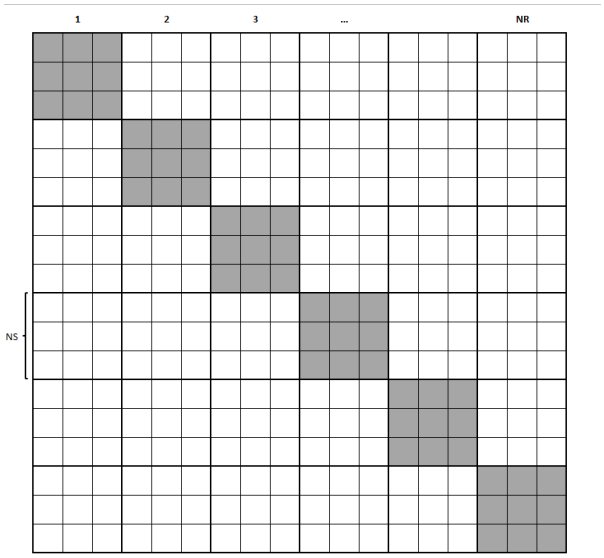

Figure 4.4: Sample structure of Jacobian due to reactions(J_w), where NS is the number of species and NR is the number of reactors.

in all the species concentrations to the change in that species' mass fractions.

$$\frac{\partial \dot{\Omega}}{\partial C} = A, \qquad \frac{\partial C}{\partial Y} = \Gamma \tag{4.24}$$

A chemical reaction can be generally expressed as:

$$\nu'_1 C_1 + \nu'_2 C_2 + ... \nu'_{n1} C_{n1} \rightleftharpoons \nu"_1 C_1 + \nu"_2 C_2 + ... \nu"_{n2} C_{n2} \tag{4.25}$$

The net rate of progress of reaction expressed in units of $\frac{kmol}{m^3 - s}$ is shown in Equation 4.26,

$$\begin{aligned} r &= r_f - r_b \\ r &= k' \prod_{i=1}^{n1} c_i^{\nu'_i} - k" \prod_{j=1}^{n2} c_j^{\nu"_j} \end{aligned} \tag{4.26}$$

where k is the rate constant given by Equation 4.27.

$$k = A(T) e^{\frac{Ea}{RT}} \tag{4.27}$$

The net rate of increase of species, $\dot{\Omega}$, involved can be obtained by multiplying 'r' by the stoichiometric coefficient, a constant α, and the volume of the reactor, where $\dot{\Omega}$ has the units of $\frac{kg}{s}$,

$$\begin{aligned} \dot{\Omega}_{ii,r} &= \alpha_i \times \nu_i \times r_i \times V_r \\ \alpha &= \begin{cases} -1 & \text{if i is a reactant species} \\ 1 & \text{if i is a product species} \end{cases} \end{aligned} \tag{4.28}$$

The derivative of 'r' with respect to a reactant species is of the form,

$$\begin{aligned} \frac{\partial r}{\partial C_\theta} &= \nu'_\theta k' c_\theta^{\nu'_\theta - 1} \prod_{i=1, i\neq\theta}^{n1} c_i^{\nu'_i} = \frac{\nu'_\theta}{c_\theta} k' \prod_{i=1}^{n1} c_i^{\nu'_i} \\ &= \frac{\nu'_\theta}{c_\theta} r_f \end{aligned} \tag{4.29}$$

Similarly, the derivative with respect to a product species is,

$$\begin{aligned} \frac{\partial r}{\partial C_\theta} &= -\nu"_\theta k" c_\theta^{\nu"_\theta - 1} \prod_{i=1, i\neq\theta}^{n2} c_i^{\nu"_i} = -\frac{\nu"_\theta}{c_\theta} k" \prod_{i=1}^{n2} c_i^{\nu"_i} \\ &= -\frac{\nu"_\theta}{c_\theta} r_b \end{aligned} \tag{4.30}$$

'A', in Equation 4.24, is a matrix that can be assumed to be a sum of the changes due to the different reactions(1 to I) occurring, as shown in Equation 4.31, where S_i is the contribution of coefficients related to the i^{th} reaction.

$$A = \frac{\partial \dot{\Omega}}{\partial C} = \sum_{i=1}^{I} S_i \frac{\partial r_i}{\partial C} \tag{4.31}$$

Thus, A has a unit of $\frac{kg-m^3}{kmol-s}$

$$\begin{aligned} C &= \frac{n}{V} \\ C &= \frac{n}{V}\frac{N}{N}\frac{MW_n}{MW_n}\frac{MW_N}{MW_N} = \frac{1}{V}\frac{n \times MW_n}{N \times MW_N}\frac{N \times MW_N}{MW_n} = \frac{1}{V}\frac{m_n}{m_N}\frac{m_N}{MW_n} \\ \therefore C &= \frac{Y_n}{V}\frac{m_N}{MW_n} \end{aligned} \tag{4.32}$$

Differentiating Equation 4.32 by mass fraction of the same species yields,

$$\frac{\partial C}{\partial Y} = \frac{m_N}{V \times MW_n} = \Gamma \tag{4.33}$$

The unit of Γ is $\frac{kg}{m^3 \frac{kg}{kmol}} = \frac{kmol}{m^3}$. This brings the overall Jacobian, $J = A\Gamma$ to the unit of $\frac{kg}{s}$.

The advantage of the analytic Jacobian is that exponential evaluation of the rate constants needs to be done only once at the beginning of the iterations, as the temperatures are kept constant while solving the CRN(isothermal reactors), whereas in the numerical Jacobian, the rate constants need to be re-evaluated for change in every species. This makes it a faster process and the gains are more on a larger mechanism.

Js is the Jacobian due to transport from neighboring reactors. It represents the rate of change of species mass in a particular reactor with respect to the change in mass fraction of the same species in that or other reactors. Consider the species conservation equation,

$$C_\omega = m\frac{dY_k}{dt} = \sum_{in} \dot{m}_{in}(Y_{k,in} - Y_k) + V\dot{\omega}_k MW_k = S + W \tag{4.34}$$

Differentiating the term for k^{th} species in i^{th} reactor with respect to to Y_{kj}, where j refers to neighboring inlet reactor index,

$$\frac{dC_{ik}}{Y_{ikj}} = \dot{m}_{in} = \alpha_{ij}\dot{m}_j \tag{4.35}$$

The general convention used in the representation of the governing equations is that all connecting mass flows are specified as those going out of a reactor, so all inlet mass flows are in fact outlet flows from neighboring reactors. α_{ij} is obtained from the coefficient matrix from the mass balance equation.

4.4.4. CONVERGENCE CRITERIA

The convergence is determined based on two residual conditions. The first one ϵ_s is based on the species mass fraction defined as

$$\epsilon_s = \max\left(\frac{Y_k - Y_{k_{old}}}{\max(Y_{k_{old}})}\right) \tag{4.36}$$

The second residual is ϵ_r, which is defined as the maximum rate of production of a species among all species present in all reactors. Theoretically, at steady state, rate of production/consumption of all species should be zero and the residual related to change in mass fraction should also be zero as once steady state is achieved there should not be a change between iterations.

ϵ_s should be less than 1e-09 or ϵ_r should be less than 1e-15 for convergence to be achieved. ϵ_s is a relative quantity an hence the lower threshold for convergence. The denominator in this residual is the maximum of all the mass fractions, else the criteria is too strict and takes significantly longer to converge without much benefit in absolute quantities. In this project, minor species pollutants were intended to be studied and are generally expected to be present at levels of the order of parts per million, i.e mole fractions of the order of 1e-06. But at the same time the maximum mass fractions of certain other species such as CO2 can be expected to be of the order of 0.1. If instead of maximum mass fraction, the mass fraction of that particular species is used, the maximum allowable change in mass fraction for convergence to occur is 1e-15(1e-06 × 1e-09) On

the other hand if maximum mass fraction is used, convergence can occur for a maximum difference of 1e-10. This is 1e-04 times less than the expected pollutant levels, which is an acceptable level of accuracy to call it a steady state. Of course the former case is more mathematically correct, but is an unnecessary constraint. The threshold values for convergence were taken based on the default values used for relative and absolute tolerance in Cantera.

Another important consideration for convergence is the reactor model used by the local solver. It was stated earlier that a combination of reservoirs, ideal gas reactors, mass flow controllers and valves is used to represent a PSR. The valves allow for a variable mass flow exchange between reactors, while the mass flow controller represents the fixed exchange. Once the residuals of species change, ϵ_s drop below 1e-06 continuously for 2 iterations, or the maximum mass flow through the valves relative to the fixed balance mass flow into the respective reactor is less than 1e-06, the model is switched to a fixed mass flow one by setting the valve coefficients to zero, effectively making the valves inactive. The aim of the CRN is not to obtain a perfect pressure distribution, but one that has a closer pressure condition to the constant pressure conditions. In the tests conducted on the case of an atmospheric combustion chamber, it was found that such an approach ensured the reactors were close to atmospheric pressure and reduced the convergence time. If there is an active valve present, the only way there is zero mass flow through it is if either the pressure is exactly equal on either side, which is difficult to achieve numerically, or the pressure difference is negative. Even a slight pressure difference will result in some mass flow through the valve and if the final solution converges with the presence of mass flows through valves, that would be physically inconsistent as the actual mass flows obtained from the CFD solver are modeled in the mass flow controllers and any other flows are in excess to that.

4.5. RECOMMENDATIONS

The software has been implemented to the level of proof of concept. This means that it has some limitations and scope for improvement. Some of the recommendations for future studies are:

- Temperature update: The temperatures are kept constant as the assumption is that the major species responsible for heat release should have been well predicted by CFD. Keeping temperature constant, helps in reducing the non-linearity of the system and enables faster convergence. This assumption would actually be necessary to solve a CRN with fixed mass flows because if the temperature change upon recalculation is large enough to affect the flow field, the mass flows between reactors should also be changed. On the other hand, Cuoci *et al.* [17] state that it may be possible that although the temperature differences between CFD and CRN with recalculation of energy may be small enough to not affect the flow, the production of minor species such as NO may be significantly affected as the value of E_a, in Equation 4.27, is quite high and has an exponential effect on the reaction rate constant. Hence it would be interesting to explore the effect of temperature re-calculation on the CRN results, but the equations of the global solver would have to be modified to include energy conservation and also the analytic Jacobian would have to calculate the rate constants at each iteration, due to the change in temperatures.

- Liquid fuels: The software has been shown to work with gaseous fuels, but the ultimate goal would be to extend it to liquid fuels such as gasoline and kerosene. As the software only deals with detailed chemistry and is not responsible for the fluid calculations, it should be possible to integrate it with a simulation done for spray combustion in ANSYS Fluent, but this may take some programming from the aspect of actually reading the right data from the file. In principle one can totally ignore the liquid phase and use only the gas phase for the chemistry, as this method has the assumption that the heat release and temperature should be accurately predicted by CFD. This assumption would consider that the evaporation of droplets is correctly predicted by CFD. The mass flow into the gas phase due to evaporation can be treated as a boundary inflow to the respective reactors, i.e included in the external source term, f_k, in Equation 4.10 and Equation 4.15. An issue that may come up is the actual computation power required because a mechanism for liquid fuels such as gasoline and kerosene can be much larger than that for methane. This would make it important to enable efficient computation for faster solution, although the system is capable of handling such a mechanism in its current state.

- Global Time stepping: The global time stepping was described earlier and was tested in the code for a reduced system of reactors(2 reactor CRN), and was found to lead to divergence of the solution. This made the implementation of the Time stepping ODE integration code unreliable and hence was not

used to solve the CRNs during this project. Time integration can help speed up the solver by not resorting to direct substitution, i.e local solver, when the global Newton's method becomes unstable. The recommended approach would be to integrate an ODE integration package such as SUNDIALS with the code, while making sure it does so by handling the system as a sparse one. The inability of the ODE integrators in SciPy to handle sparse systems was one of the major reasons why self implementation was attempted.

5

TEST CASE ANALYSIS

This chapter presents the combustion chamber design used as a test case for the research work. The chapter begins with some information on clean combustion technologies as a prelude to the type of combustion occurring in the test case. Results of experiments on this combustion chamber from literature are shown along with CFD results performed within the research group at TU Delft.

5.1. LOW NO_x COMBUSTION

Several technologies have been developed to reduce the amount of NO_x produced by combustion. The challenge is often a trade-off with the amount of CO produced, as usually NO_x is reduced by reducing the flame temperature which reduces NO_x production by the thermal pathway but leads to higher CO production due to reduced reactivity of the CO oxidation mechanism as shown in Figure 5.1. The extent of production and

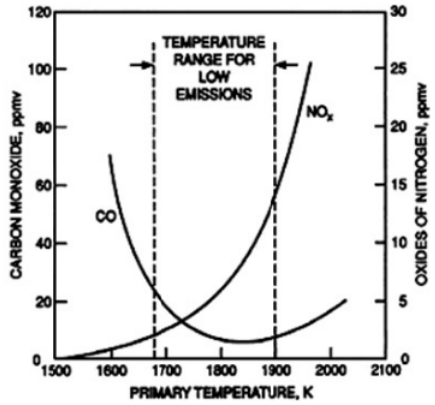

Figure 5.1: Effect of primary zone temperature on NO_x and CO emissions[23]

consumption of pollutant species also depends on the residence time of the combustor, which is the characteristic time for which the reactants are present in the combustor. This is influenced by the flow rate, geometry and density of the gases. A larger residence time allows for greater conversion of CO to CO_2 but it may also increase the amount of NO_x produced, hence it is an optimization problem.

There are 3 basic methods to achieve low emissions:

1. Water/Steam injection: Water is injected into the combustor to lower the flame temperature to produce lower NO_x. The usage of water injection provides several complications such as corrosion, increase in subsystems and the need to carry large amounts of water for continuous operation.

2. Catalytic treatment: The exhaust gases are treated with a catalyst to have lower CO and NO_x values. Such a catalytic converter can be expensive due to the catalyst material.

3. Dry Low NO_x burner: As the name suggests, there is no water injection and works only with air and fuel. These systems reduce emissions by achieving lower flame temperatures by optimizing the flow

field and having a lean burn ratio. This is currently the most widely used technology in gas turbines targeting lower emissions. There are several Dry Low NO_x(DLN) burner technology options that we can choose from:

- Rich burn Quick mix Lean burn (RQL)
- Lean Premixed (LP)
- Lean Premixed Prevapourised (LPP)
- Lean Direct Injection(LDI)
- Low Swirl Burner
- Flameless combustion

DLN is currently the preferred technology due to easier maintenance and the lower emission values that are achievable[61]. Flameless combustion in particular has been found to be a promising option for very low NO_x emission combustors showing less than 10ppm concentrations in most studies. It is also one of the current areas of research of the Propulsion group at TU Delft, Faculty of Aerospace Engineering. It shall be explained in later chapters that using a Flameless Combustion case for verification of the CRN method may be advantageous, which is why it is chosen as the specific concept to be used as the object of study.

5.2. FLAMELESS COMBUSTION

This is a combustion regime in which the fuel is burnt in a low oxygen(vitiated) environment. This results in a distributed reaction zone which makes the flame 'invisible' and leads to minimal temperature peaks. This technology is known by several names such as Flameless Combustion(FC), Flameless Oxidation(FLOX), Moderate or Intense Low oxygen Dilution(MILD) combustion, High Temperature Air Combustion(HiTAC). The regime is characterized by invisible flame, very low NO_x, CO emissions and negligible soot emissions[62][63]. One of the first references to Flameless Oxidation was by Wünning and Wünning [51], where in the conditions are described to have such combustion. A consensual definition of the flameless combustion regime has not yet been proposed, although there have been some attempts to define it. Cavaliere and De Joannon [64] define it by stating, "A combustion process is named Mild when the inlet temperature of the reactant mixture is higher than mixture self-ignition temperature whereas the maximum allowable temperature increase with respect to inlet temperature during combustion is lower than mixture self-ignition temperature (in Kelvin)."

$$T_{si} > T_{in} > \Delta T \tag{5.1}$$

Rao and Levy [65] give a comprehensive description through a combustion regime diagram. Figure 5.2 is an updated version of the diagram which has not been published as of the date of writing this report and was sourced internally from the research group. This diagram is presented with respect to gas turbine applica-

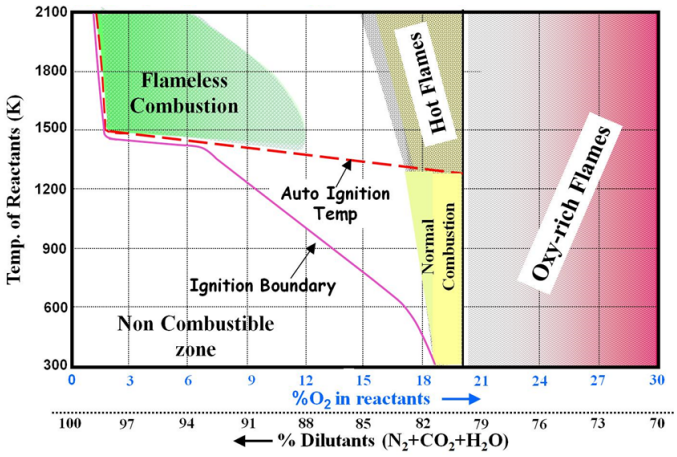

Figure 5.2: Different regimes of combustion

tions and was generated by a single ideal reactor(a Perfectly Stirred Reactor, PSR) using methane as fuel, in Chemkin. The concept of ideal reactors is explained in the next section. The authors also go on to mention the following characteristics of flameless combustion:

- Highly distributed combustion zone with uniform temperature.
- Spontaneous autoignition when the fuel-air mixture reaches above autoignition temperature.
- Highly transparent flame with low thermo-acoustic oscillation.
- Recirculation of combustion products also increases the chemical reaction time and therefore lowers the Damköhler number, a required condition for practically obtaining FC in a combustor, where Damköhler number (Da) is given by,

$$Da = \frac{\text{flow time scale}}{\text{chemical time scale}} \tag{5.2}$$

LOW OXYGEN

A low oxygen or vitiated environment causes an overall low adiabatic flame temperature because of the increase of specific heat of the gas mass. The vitiated air also allows the fuel to spread within the combustor under high strain rates without igniting instantaneously. This allows for a distributed reaction zone and a more uniform heat release. Hence vitiation effectively increases the chemical time scale and lowers the Damköhler number(Da).

HIGH INLET TEMPERATURE

The high inlet air temperature, above the autoignition temperature ensures that the fuel is ignited in the combustor without a concentrated flame region, by providing a suitable temperature for the reactions to proceed by having a high enough reaction rate constant(k=A$e^{-\frac{E}{RT}}$). This enables the reactions to take place in a distributed manner in space which causes lower temperature peaks, reducing thermal NO_x production.

PSR ANALOGY

As FC has been observed to take place under a distributed regime at low Damköhler numbers, the PSR approximation may be valid. Cavaliere and De Joannon [64] cite references of previous works on the subject and state that the phenomenon of fluid back mixing appears to be one of the key factors that enable a PSR consideration. Back mixing lowers the flow time scale, reducing the Damköhler number to approximately 1(Da≈1). This is closer to the ideal PSR condition of Da=0 as compared to conventional combustion modes. The authors also mention that a real combustor may be approximated to a PSR followed by a PFR as the PSR would represent the flameless regime and the PFR the post combustion zone in order to completely represent the combustion.

IMPLEMENTATION

FC was first discovered and explored in industrial furnaces. One of the earlier methods of creating FC was by regeneration. In this method a furnace would be operated in a bidirectional manner, such that the flow would be in one direction for sometime, then the flow direction would be switched as shown in Figure 5.3. This process would be repeated. This is done so that the exhaust gases heat up a regenerator. When the

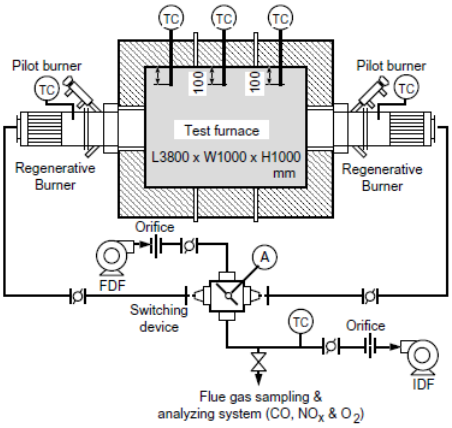

Figure 5.3: Schematic FC test rig[24]

cycle is switched the incoming gases get preheated by the heat stored in the regenerator before entering the combustion chamber. A vitiated environment is created by physically controlling the mixing of exhaust gas stream and fresh gases by valves before it enters the combustion chamber. Another method of creating a high temperature vitiated environment is to preheat the air by a heater and dilute it using another gas. This method provides more degrees of freedom to experiment with. A more practical oriented system is one by combining heat recirculation(regeneration) with hot combustion product recirculation to produce a vitiated environment within the furnace[24] as shown in Figure 5.4. This is also the strategy being employed for compact designs of FC combustors for gas turbines in research. In gas turbines, the space and weight constraints require the combustion chamber to have a simpler system design as well as be more compact. Some of the attempts are jet induced recirculation based combustors[25] and large recirculation zones in the chamber[66].

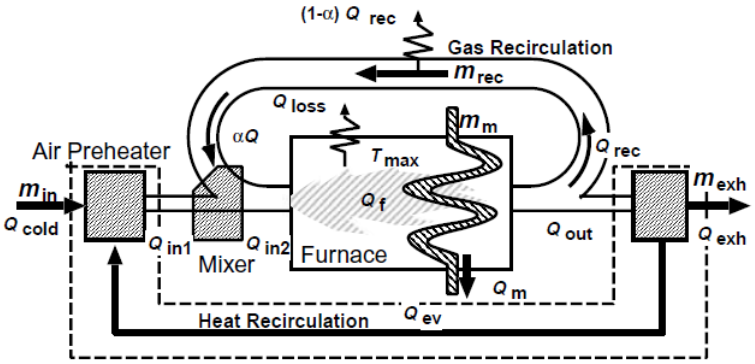

Figure 5.4: Schematic of model furnace with heat and gas recirculation[24]

5.3. TEST CASE

To validate the Automatic CFD-CRN method, a test case was required. This study requires understanding the effect of flow parameters on the pollutant prediction and hence it would be good to eliminate possible influence of modeling errors. The Flameless combustion concept involves a well distributed regime of combustion and hence comes close to an ideal PSR as explained in Section 5.2, which is the basic building block of a CRN. In the current CRN modeling, soot modeling is not included, so the fact that a flameless combustor produces lower soot[62] is an advantage as it would tend to produce less modeling error. Hence a combustor designed to operate in the flameless regime is chosen as the experimental object. It is a lab scale burner, located at the Mechanical Engineering Department,Instituto Superior Tecnico at the Technical University of Lisbon, operating on gaseous methane fuel(99.5% purity), for which experimental results in both conventional as well as flameless mode exist, according to the authors.

The combustion chamber is a quartz glass cylinder of 100 mm internal diameter and 340 mm length as shown in Figure 5.5. It has a burner at its top end with the exhaust nozzle at the bottom. The burner has a central hole of 10mm diameter for the air flow which is surrounded by 16, 2mm diameter, holes in a concentric circle of 30mm diameter for the fuel injection. The convergent nozzle is 150mm long and has an angle of 15^o. The inlet air is preheated to a temperature of 400^oC.

Experiments conducted on this burner by Verissimo *et al.* [25], report data of Temperature, O_2, CO_2, NO_x,HC, CO concentrations of the flue gas at locations within the combustion chamber. The availability of this data is one of the main reasons of choosing this particular experimental setup as a candidate for simulations. The combustor is run for different conditions of excess air(λ), called as Run 1 to Run 6 from lower λ to higher λ. It is found that it runs in flameless mode for lower excess air conditions and converts to a conventional lean combustion mode at higher excess air ratios. This can be observed in the images of the flame in Figure 5.7, where a,b,c,d,e,f are Runs 1,2,3,4,5,6 respectively. This possibly occurs due to the faster entrainment of fuel and burnt gas because of higher inlet air jet momentum, and higher concentration of O_2 in the entrained flue gases which leads to a less vitiated environment. The OH* images in Figure 5.6 indicate the main reaction zone to shift upstream for higher excess air ratios.

The NO_x and CO emissions are reported as shown in Figure 5.8. NO_x increases with increasing λ and then decreases beyond λ=1.9. The trend is counter intuitive as higher λ conditions would have lower adiabatic

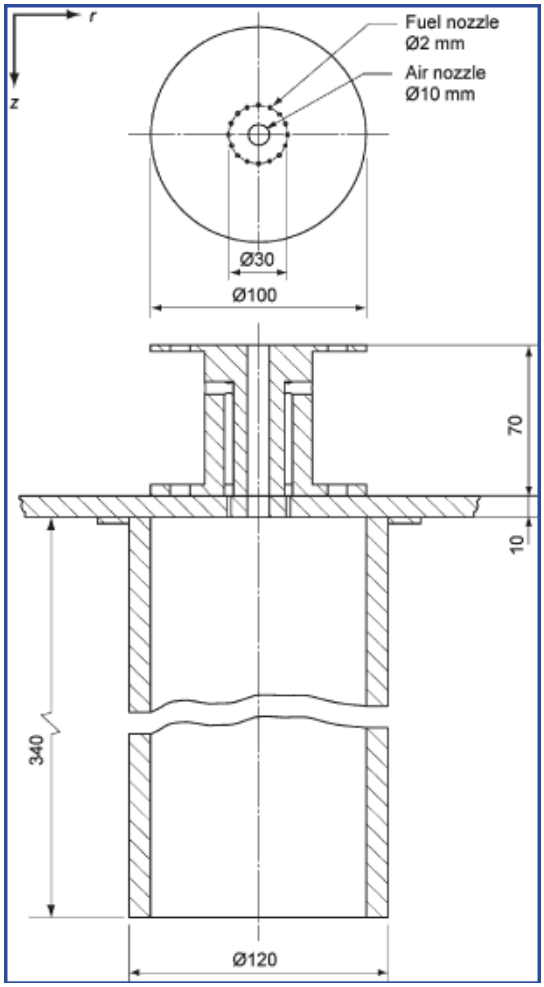

Figure 5.5: Schematic of Combustor[25]

flame temperature hence lower NO_x by thermal pathway. Verissimo *et al.* [25] attribute the low NO_x in Run 1 and 2 to flameless combustion mode which suppresses the Zeldovich mechanism, while the values above λ=1.7 follow the trend of conventional lean combustion. The plateau and reduction in NO_x in this range is due to lower adiabatic flame temperature and the supposed dominance of N_2O pathway. The trend for Run 3 and 4 is not explained. The authors also assert that the NO formation via the prompt mechanism is supposed to be insignificant due to the lean overall fuel-air ratio, and the formation of NO by the N_2O mechanism should have a relatively higher contribution. The CO concentration trend is mentioned to be as obtained by Luckerath *et al.* [67] and is said to have the same explanation. CO levels first decrease due to increasing oxygen content in the domain but increase above λ=1.9 until the lean extinction limit at λ=2.2. Luckerath *et al.* [67] state that as the flow field approaches the lean extinction limit, combustion becomes unstable and hence locally incomplete combustion occurs leading to increasing CO levels near the lean extinction limit.

In this particular case of combustion, one must take into account not only the overall air fuel ratio of the system, but also the level of dilutants being supplied to the flame via recirculation. According to the description provided in the paper, the variation in excess air ratio, λ, is achieved by varying the air inlet jet velocity, while maintaining the same mass flow and velocity of the fuel gas jet. This means that with increasing excess air ratio, there should be an increase in oxygen content in the recirculating stream, thereby reducing the dilution level of the flame. As shown earlier, flameless combustion relies on the presence of vitiation to delay the combustion process and hence have a distributed reaction zone. A reduction in vitiation makes the regime go away from FC and hence the gradual increase in NOx. The later reduction in NOx beyond λ=1.9, maybe due to the onset of unstable combustion which causes regions of local extinctions and hence lower NOx.

The CO levels are seen to drop with increasing excess air ratio up to λ=1.9. This is may be because there

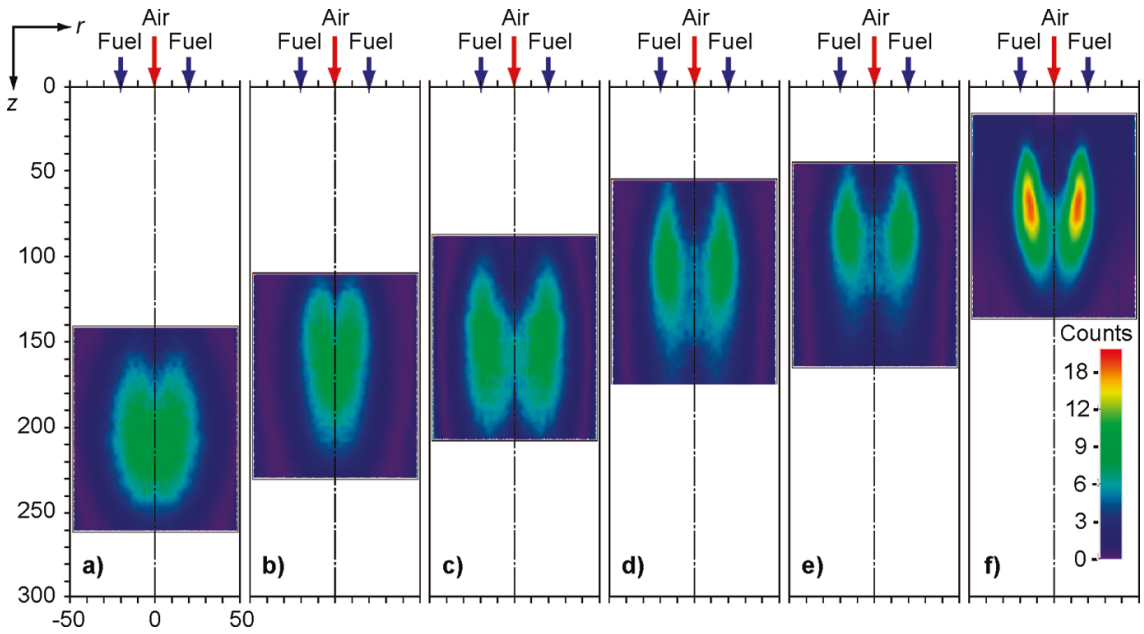

Figure 5.6: Mean OH* images at the combustor symmetry plane for various excess air ratios[25]

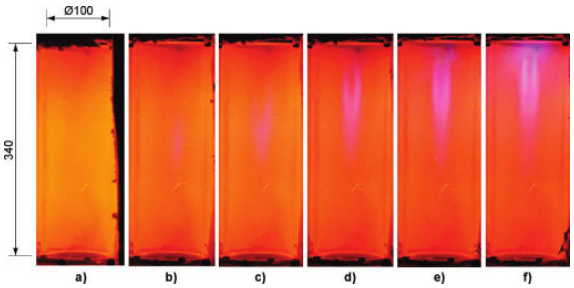

Figure 5.7: Appearance of combustion for different excess air coefficients[25]

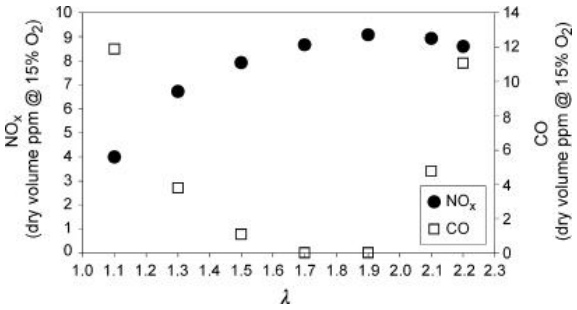

Figure 5.8: NOx and CO emission as a function of excess air coefficient[25]

is less vitiation and more oxygen in the flame zone allowing the CO molecule to oxidize. The trend reverses beyond a certain point and a probable reason may be reduced residence time in the combustion chamber due to increasing air flow which gives CO less time to oxidize. Another reason may also be the onset of unstable combustion which prevents complete oxidation of products.

The above explanations are hypotheses and do not have a clear proof. In this thesis, an attempt is made to explain this phenomenon. Verissimo *et al.* [25] do show and explain some of the phenomenon in Run 2 and Run 4, but there are no detailed results explaining the trend inversion.

This particular burner serves as a good candidate for performing simulations because of the availability of measurements of emissions within the combustor domain and operating points that lie within both, the conventional and flameless regime which would enable the development of a more general algorithm for the generation of CRNs.

5.4. CFD MODELING

The CFD-CRN process requires a CFD simulation as an input. Hence CFD simulations in ANSYS Fluent are done for the aforementioned combustion chamber(simulations courtesy Andre Perpignan), for which experimental data is available in open literature. The simulations are performed for an axisymmetric section of the cylindrical combustion chamber as shown in Figure 5.10. The turbulence is modeled by Reynold's Average Navier Stokes(RANS) approach using the k-ϵ turbulence model and the turbulence-chemistry interaction is modeled by the Flamelet Generated Manifold(FGM) method. The FGM is constructed from non adiabatic, non-premixed counterflow flamelets, the difference in flamelets being brought about by variation

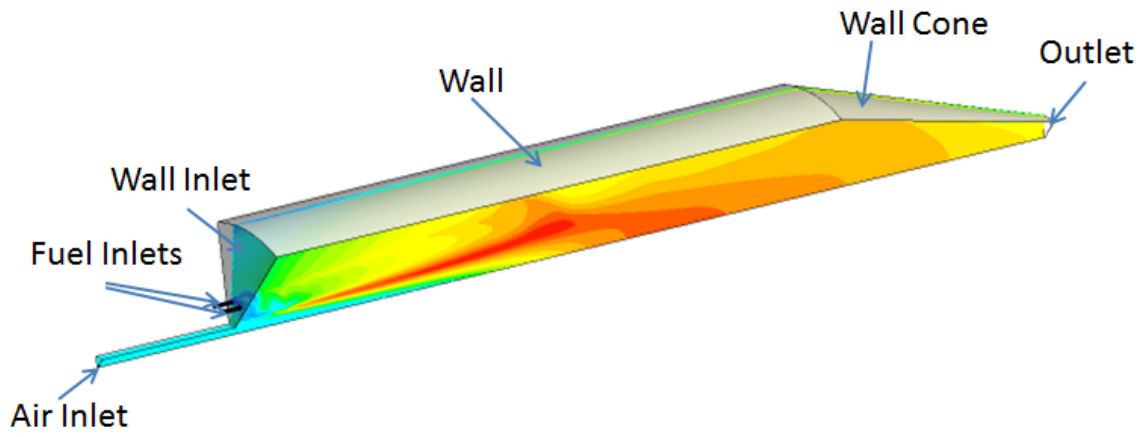

Figure 5.9: CFD simulation of combustion chamber

in strain rate. The effect of turbulence on chemistry is modeled by a presumed shape Probability Density Function(PDF), assumed to be a function,P(f), of the mixture fraction, f as shown in Equation 5.3 and 5.4.

$$P(f) = \frac{f^{\alpha-1}(1-f)^{\beta-1}}{\int f^{\alpha-1}(1-f)^{\beta-1}df} \tag{5.3}$$

where,

$$\begin{aligned} \alpha &= \bar{f}\left[\frac{\bar{f}(1-\bar{f})}{\bar{f'^2}} - 1\right] \\ \beta &= \left[\frac{\bar{f}(1-\bar{f})}{\bar{f'^2}} - 1\right] - \alpha \end{aligned} \tag{5.4}$$

The boundary conditions are that of fixed mass flows for air and fuel inlets and the outflow boundary condition is specified at the outlet, which is a condition for zero diffusion flux for all flow variables and an overall mass balance[40]. The walls are non-adiabatic with heat transfer being modeled by specifying a heat flux distribution along the wall. The value of total heat loss was determined based on the estimated inlet energy and the outlet temperature of flue gases obtained from experiments as mentioned in [25]. The assumption of complete combustion was made while estimating the values of heat loss. The wall heat flux was set as a linear profile along the wall with a step as shown in Figure 5.10, such that the total heat loss estimated was achieved in the simulation. Radiation loss is not modeled in the CFD simulation. One of the drawbacks in the heat

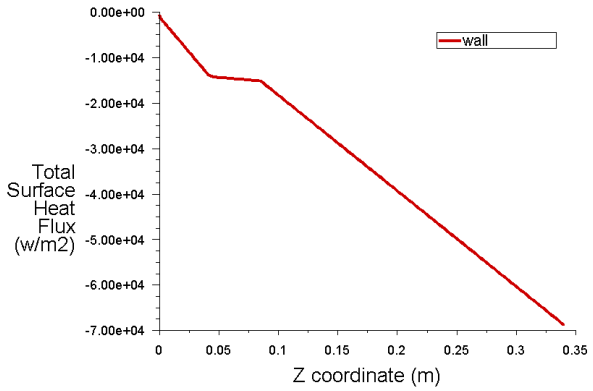

Figure 5.10: Wall heat loss profile

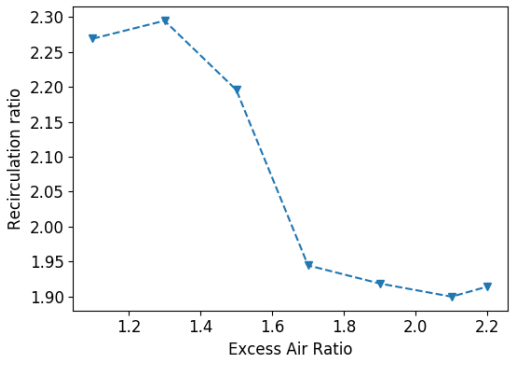

Figure 5.11: Recirculation Ratios from CFD

loss model is that a heat loss profile is enforced at the wall. This may not be true in reality, as there may be

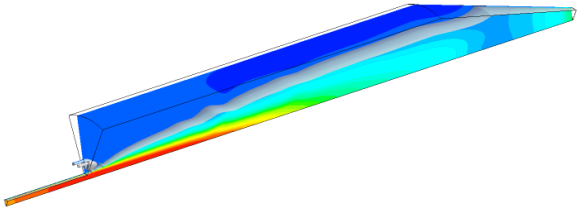

Figure 5.12: Iso-Surface of zero axial velocity

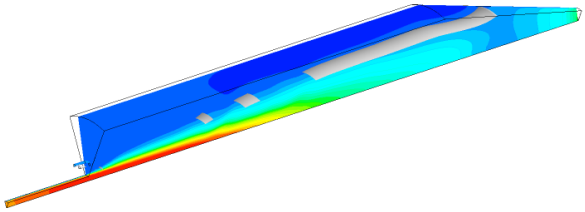

Figure 5.13: Surface through which there is radially outflowing mass

a different type of variation along the length of the wall depending on various features such as flow field and evolution of the flame within the combustion chamber. The lack of radiation modeling may also cause some temperature disparities with respect to the actual conditions. The NOx emissions were obtained by using the ANSYS Fluent NOx post processor. Fluent calculates the NOx concentrations in each cell while keeping the temperature and concentration of major species fixed as calculated during the CFD simulation. A Beta PDF model was used while post processing to capture the effect of fluctuations on NOx production.

5.5. RECIRCULATION

As described by the experiments, the momentum of the inlet air jet is expected to setup recirculations in the combustion chamber. To further quantify this recirculating mass, the CFD results were post processed accordingly. An iso-surface of zero axial velocity is created as shown in Figure 5.12. This is done in order to have a surface passing through the center of any vortices having a predominant vorticity in the tangential direction. Next, sections from the iso-surface are extracted as shown in Figure 5.13, such that these sections have a radially outward flow through them, decided by the value(positive/negative) of radial velocity. These sectioned surfaces are referred to as recirculation surface henceforth. The figure indicates multiple sectioned surfaces, which implies the presence of multiple radially outward flow regions, hence indicating multiple vortices as shown in the velocity vector field plot. The velocity vector plots along with the multiple recirculation surfaces indicate that the recirculation takes place through multiple eddies along the length of the combustion chamber. In most of the cases the recirculation takes place towards the end of the chamber, near the beginning of the exit cone where the wall starts tapering, i.e about 300mm from the inlet wall and also near the middle of the chamber at around 150mm from the inlet wall, through several vortex structures. The mass flow from the recirculation surface was calculated for each operational condition and the recirculation ratio was calculated using the formula

$$R = \frac{m_s}{m_{in}} \tag{5.5}$$

where R is the recirculation ratio, m_s is the mass flow through the recirculation surfaces and m_{in} is the total inlet mass flow into the combustion chamber. The recirculation ratio is plotted against excess air ratio in Figure 5.11, which shows a mostly decreasing trend. There are small increases from Run 1 to 2 and from Run 6 to 7. One may expect that an increasing air jet momentum would lead to an increase in recirculation ratio, but that is not the case. It must be noted that the characteristics of recirculation are heavily dependent on the different models used in this simulation, so it may as well be possible that the trend is an artificial facet of the simulation and not an exact representation of reality. It is also seen that the ratio for Run 1, 2 and 3 is distinctively higher than 5,6 and 7 with 4 being in the intermediate range. The relatively large drop in recirculation ratio after Run 3 maybe the reason for transition of the regime to conventional combustion from near flameless conditions.

5.6. HEAT RELEASE

The heat release during the process of combustion is gauged based on the Temperature and OH mole fraction contours across an axial plane. Figure 5.16 and Figure 5.17 show temperature and OH mole fraction distributions respectively. The highest temperatures are prevalent in a more spread out pattern in Run 1 and Run 2, i.e the conditions span over a large area. On the other hand, Run4-Run7 have a more concentrated region of higher temperatures. The two different distributions may be an indication of flameless and conventional lean combustion respectively. Upon inspection of the OH mole fraction contours, it is seen that in Run 1 and Run 2, the highest values are spread out axially, further downstream in the chamber, whereas in Run 3-Run 7, the distribution is more receding towards the inlets and concentrated in smaller zones. As OH is generally

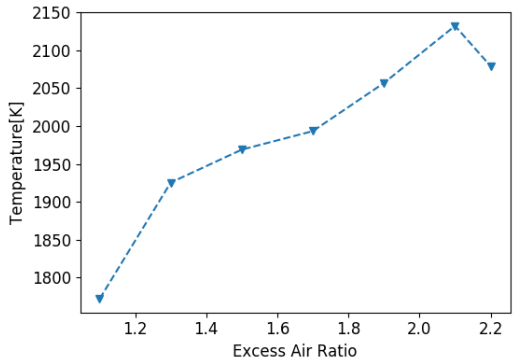

Figure 5.14: Peak temperature in combustor for different excess air ratios

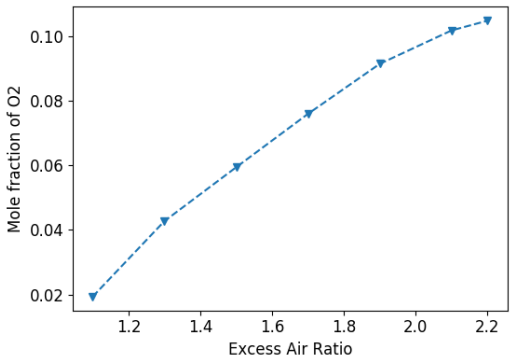

Figure 5.15: Average mole fraction of O2 through recirculation surface

considered an important precursor to the heat release reactions[68], it is also considered an indicator of the flame front or site of heat release in the flow. This may indicate that the flame in Run 1 and 2 is further spread out axially and is formed more downstream whereas in the other cases the flame shifts upstream as the oxidizer ratio is increased. One of the reasons cited in [25] for the shift in flame is the increase in excess air ratio, achieved by increasing the air mass flow and hence the air jet momentum, causes faster entrainment of fuel and hence earlier heat release.

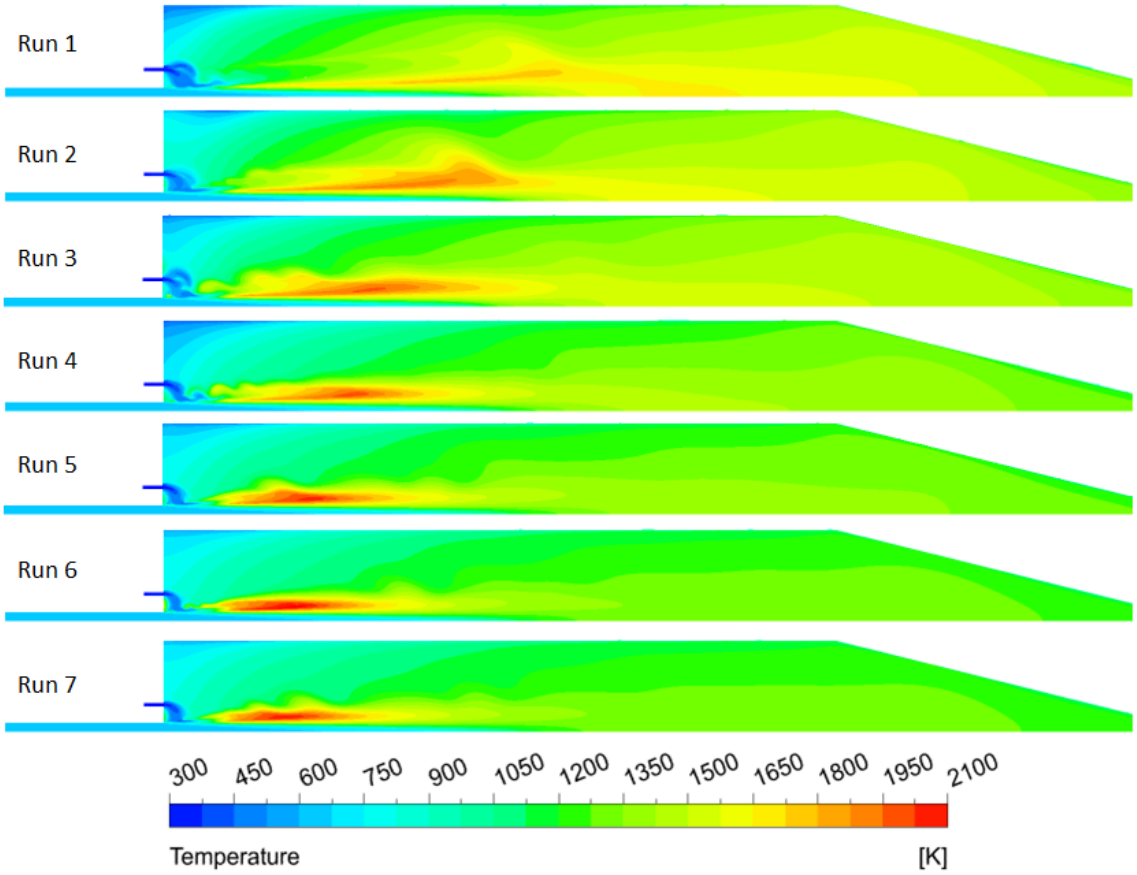

Figure 5.16: Temperature contours

From the analysis in the previous section, it is also seen that the recirculation ratio decreases with increase

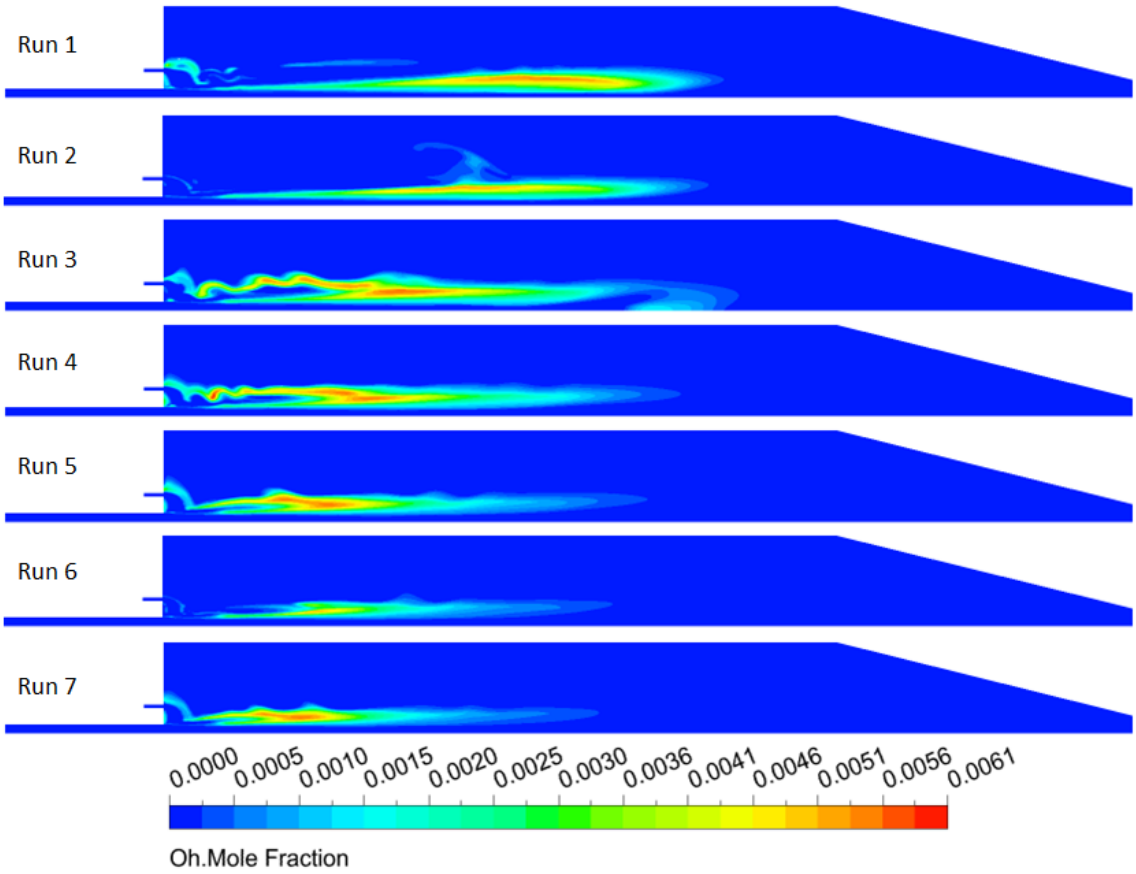

Figure 5.17: OH mole fraction contours

in excess air ratio. This leads to less flue gas being fed back into the flame, hence less vitiation. The recirculation also has a higher oxygen content as shown in Figure 5.15, with increasing excess air ratio. The lack of vitiation due to reduced recirculation and increased oxygen content of the recirculating mass chemically may contribute to the shift from flameless to conventional combustion. The increasing jet momentum also leads to early entrainment of fuel, leading to a richer air fuel mixture locally, which may also be the reason behind the increasing peak temperatures with excess air ratio as shown in Figure 5.14

5.7. EMISSIONS

The CO and NOx emissions are calculated during the CFD simulation. The production of these two emissions are typically characterized by slower chemical reactions. CO is calculated directly from the FGM tabulation, whereas NOx is calculated using the ANSYS Fluent NOx post processor.

The NOx emissions as shown in Figure 5.18, are much lower than the experimental values. This may be attributed to the NOx post processor which uses the equilibrium method of calculation for O atoms required to calculate NOx, as mentioned in the ANSYS Theory guide[37]. The increasing NOx may be due to increasing peak temperatures. Also in Run 5-7, the heat release occurs in a more concentrated region. This along with increasing excess oxygen supply both at the inlet and in the recirculation flow promotes NOx production. The experiments show a decrease in NOx in Run 6 and 7. This is not captured in the CFD results. Analyzing the CFD results, it is seen that the average temperature of the mass recirculated into the main flow keeps decreasing. The addition of low enthalpy flow to the main flow should be useful in causing auto-ignition delay such that the reaction takes place over a more spread out region. On the other hand increasing EAR causes a high air jet momentum which provides a suction on the fuel jet, causing it to mix earlier and have an earlier reaction evolution, along the axis. From the experiments it seems that when EAR is increased, the later phenomenon is predominant but as EAR is further increased, the former phenomenon seems to take over causing a decrease in peak temperature and reduction in NOx. This change in trend is not captured by

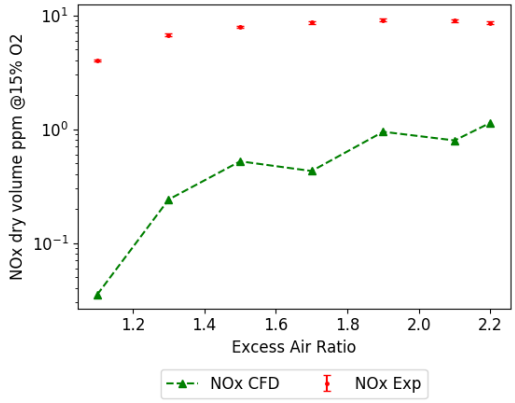

Figure 5.18: NOx at outlet, on log scale

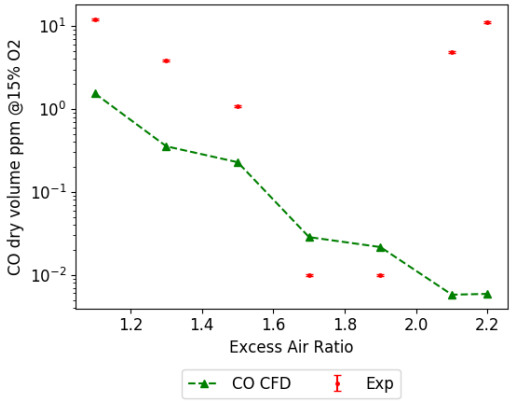

Figure 5.19: CO at outlet, on log scale

the NOx post processor, but the flow field seems to have the characteristics to be able to predict it, if given a full detailed chemical mechanism.

The increasing peak temperatures may occur due to earlier fuel air mixing because of entrainment of fuel jet due to the increasing air jet momentum and another reason may be the decreasing recirculation ratio. As there is less recirculating mass flow, the same amount of enthalpy release would lead to higher gas temperatures, but for run7 the peak temperature is seen to drop which corresponds to an increase in recirculation ratio as seen in Figure 5.11, which causes an increased addition of low temperature flue gas to the flame, which in principle should show a decrease in NOx but that is not seen in the ANSYS post processor.

CO emissions obtained from the CFD simulation are a result of direct FGM calculations. The values decrease monotonically with increasing EAR. The experiments show that the CO value first decreases then increase after run5. An increase in EAR causes an increase in O_2 content in the recirculation mass flow as well as the inlet mass flow, leading to higher chance of complete oxidation of CO to CO_2. Also, due to the phenomenon explained earlier, there is a higher peak temperature which promotes the oxidation. This causes a drop in CO. It must be noted that the FGM is generated using 1D flamelets which have an underlying assumption that the chemistry is faster than the turbulent fluctuations. This means that the oxidation of CO which is a slow reaction process, is inherently considered to be faster, leading to lower than real CO values. This may possibly be the reason why the increase in CO is not captured. In the experiments, it is stated that the rise in CO levels at very high EAR is due to the proximity to the lean extinction limit due to which combustion becomes unstable. This is a chemical kinetics phenomenon but also the turbulence plays an important role. The lack of being able to capture this trend may also indicate some modeling drawbacks of turbulent fluctuations driving the chemistry in the CFD simulation.

Thus it can be seen that that the implementation of a detailed chemistry may be able to better predict NOx and CO, even from the same reacted flow field.

5.8. CONCLUSIONS

Following conclusions can be made from the experiments and CFD results:

- Recirculation seems to play an important role in determining flame type.
- Increase in CO for leaner conditions may be due to combustion instability, hence chemical kinetics and turbulence would play an important role to capture it in simulations.
- NOx not well captured in CFD and a detailed mechanism may be required.
- CO may be under-predicted due to fast chemistry in flamelets

6

EMISSIONS BY CHEMICAL REACTOR NETWORKS

This chapter presents results and analysis of CRN calculations done for the test case mentioned in the previous chapter. It begins with a description of the formulation used to correct the emissions obtained from simulations(CFD and CRN) such that they are in a standard form so that different cases are comparable. Next an analysis of emissions obtained at the combustor exhaust by CFD-CRN simulation is presented. This data is used to study the sensitivity of emissions prediction to choice of clustering criteria. Further, the pollutant formation mechanism within the combustion chamber is analyzed using the data from the CRN along with an explanation for deviation from experimental results. Finally, a comparison of results from the Automatic CFD-CRN method to standard methods of emissions prediction is shown.

6.1. EMISSIONS CORRECTION

In order to represent the emission concentrations as a standard form such that they are comparable with emissions obtained at different conditions and relative concentrations with other major species, certain corrections are applied. NOx and CO mole fractions are expressed as parts per million in a dry volume at 15% O_2. This means that the species is represented in an equivalent domain where there are no H_2O molecules and the mole fraction of O_2 is 0.15.

$$X_i = \frac{N_i}{N_{mix}} \tag{6.1}$$

Let x be the percentage of O_2 in the corrected mixture.

$$(\frac{x}{100})N_{\text{mix-corr}} = N_{O_2 corr} \tag{6.2}$$

$$N_{O_2 corr} + (N_{\text{mix}} - N_{O_2}) = N_{\text{mix-corr}} \tag{6.3}$$

$$\frac{x}{100}N_{\text{mix-corr}} + (N_{\text{mix}} - N_{O_2}) = N_{\text{mix-corr}} \tag{6.4}$$

$$N_{\text{mix-corr}} = \frac{N_{\text{mix}} - N_{O_2}}{1 - \frac{x}{100}} \tag{6.5}$$

$$X_{i,O_2 corr} = \frac{N_i}{N_{\text{mix-corr}}} \tag{6.6}$$

$$X_{i,O_2 corr} = \frac{N_i}{N_{\text{mix}} - N_{O_2}}(1 - \frac{x}{100}) \tag{6.7}$$

$$\tag{6.8}$$

For dry volume mole fraction the formula is,

$$X_{i,\text{dry}} = \frac{N_i}{N_{\text{mix}} - N_{H_2O}} \tag{6.9}$$

Combining the above equations,

$$X_{i,\text{dry volume},O_2 corr} = \frac{N_i}{N_{\text{mix}} - N_{H_2O} - N_{O_2}}(1 - \frac{x}{100}) \tag{6.10}$$

Dividing numerator and denominator by N_{mix},

$$X_{i,\text{dry volume},O_2 corr} = \frac{X_i}{1 - X_{H_2O} - X_{O_2}}(1 - \frac{x}{100}) \tag{6.11}$$

where i may be any species such as CO or NOx.

6.2. CRN ANALYSIS

The CFD-CRN code is used to simulate a combustion chamber at different operating conditions. The conditions are varied by changing the mass flow of air entering the combustor while maintaining a constant fuel mass flow rate. CFD simulations were performed for the test case combustion chamber, as presented in Chapter 5 and CRNs were generated from these solutions using the CFD-CRN code. The operating conditions are listed in Table 6.1 and are listed as variation in Excess Air Ratio(EAR) and the equivalent Run number, which is used to refer to the conditions later on in this report. The CRN simulations are characterized by the

Table 6.1: Operating conditions of combustion chamber

Run	1	2	3	4	5	6	7
Excess Air Ratio	1.1	1.3	1.5	1.7	1.9	2.1	2.2
Recirculation Ratio from CFD	2.269	2.294	2.195	1.944	1.918	1.899	1.914

number of reactors specified, for the CFD grid to be reduced to, and the criteria used as a basis for agglomerating the CFD cells into reactors. A CRN represents a network of 0D reactors, hence the physics of the flow field, i.e momentum characteristics are lost and are not solved for. The only way the information of the flow field is maintained in the CRN is through the mass flow exchanged between different reactors. The connections between different reactors act as transition 'bridges' between different discrete states. When viewed as an aggregate these reactor points and bridges can represent a 3D flow, just on a coarser grid compared to that of CFD. A PSR, which is the building block of a CRN, has the assumption of homogeneous distribution of properties within it. Hence variation in properties may be represented by several PSRs having different physical and chemical states. This principle dictates the clustering process in which the idea is not only to group similar cells together but also to make sure that dissimilar cells are kept separated. If a particular property is determined to be important for chemical kinetics and its gradients need to be maintained in the CRN to simulate the chemistry accurately, it can be achieved by specifying that parameter as a clustering criterion. Cells of dissimilar values of the criterion would be clustered into different reactors, thereby better resolving the CRN in regions of higher gradients. By having these different values exist across multiple reactors, it would be possible to calculate chemistry effectively at those states of physical and chemical property, instead of having them all clustered into one reactor an have the chemistry calculated at an average of these states.

The choice of criteria may affect the resolution of the CRN in different regions and the physical and chemical state at which the reactors are initialized. This in turn may affect the chemical kinetic calculations resulting in an effect on the emission prediction from this computation. Hence a sensitivity analysis of the outlet emissions to the clustering criteria is a useful addition to the knowledge of the CFD-CRN method. One way of achieving good results from a CRN is to have as many reactors as possible, as that would retain more of the flow field and the gradients in it. A better way of doing so would be to have a good choice of clustering criteria such that critical phenomenon are retained in the CRN while being clustered from the CFD solution. This is a hypothesis and is explored by simulations. Several CRNs are generated by varying the combination of clustering criteria used and the details are provided in Table 6.2.

The emissions of the combustor for different operating conditions are calculated by the CFD-CRN method and analyzed along with the results obtained, at the combustor outlet, from experiments. The clustering criteria of Case 1 was determined based on the PSR model of having a homogeneous distribution of temperature and species. Hence, Temperature and mass fractions of major species pre and post combustion were chosen, i.e CH_4, O_2 and CO_2. A comparison is done between Case 1 and 3. Both have the criteria of Temperature, Mass fraction of CO_2, CH_4 and O_2 in common, while Case 1 has an additional criteria of Velocity Angle. 'Velocity

Table 6.2: CFD-CRN cases

Case	No. of Reactors	Tolerance	Static Temperature	RMS Temperature	CO_2	O_2	CH_4	OH	H_2O	C_2H_2	Mean Mixture Fraction	Progress Variable	Velocity Angle	Velocity Direction	Z Velocity
1	1000	1.26	■		■	■	■						■		
2	1000	1.4									■	■	■		
3	1000	0.27	■		■	■	■								
4	1000	1.31		■							■	■	■		
5	1000	0.4	■	■				■			■				■
6	1000	0.55	■	■				■			■			■	
8	5000	0.18	■	■				■			■			■	
9	1000	0.36	■	■				■			■				
10	1000	0.11	■											■	
11	1000	0.21	■	■										■	
12	1000	0.11	■		■									■	
13	1000	0.11	■						■					■	
14	1000	0.14	■					■	■					■	
15	1000	0.14	■		■			■						■	
16	1000	0.15	■					■	■	■				■	
17	5000	0.04	■					■	■					■	
18	5000	0.05	■					■	■		■			■	
19	5000	0.05	■					■	■	■				■	

Angle' is the angle between the velocity vectors of the cells and using it as a clustering criterion is expected to capture the directions of flow and hence the recirculation, by representing regions of the flow in different directions by separate reactors in the CRN. The NOx and CO are shown in Figure 6.1 and Figure 6.2 respectively. Case 3 seems to over-predict NOx but captures the trend of increase and then decrease in NOx to a certain extent. Case 1 on the other hand has closer absolute values, except for in Run 5. The CO levels in Case 3 are higher than experiments whereas those in Case 1 are closer to the experiments while also capturing the trend better.

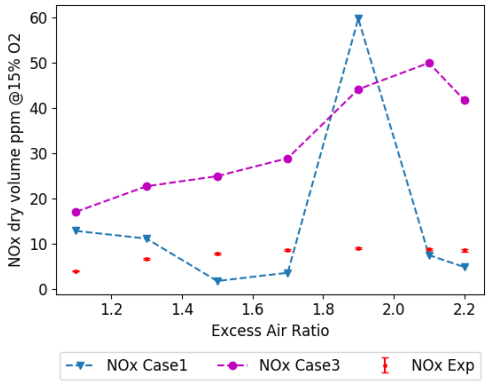

Figure 6.1: NOx v/s Excess Air Ratio at combustor outlet, Case1 (T, CO_2, O_2, CH_4, Velocity Angle) and 3 (T, CO_2, O_2, CH_4, Velocity Angle)

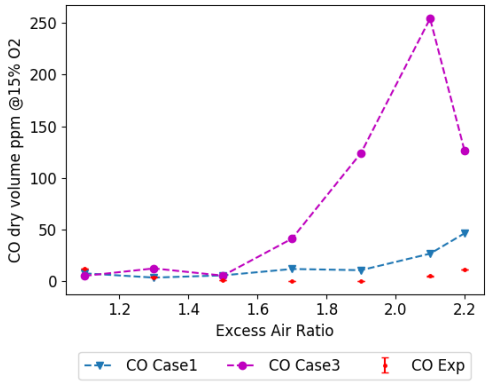

Figure 6.2: CO v/s Excess Air Ratio at combustor outlet, Case1 (T, CO_2, O_2, CH_4, Velocity Angle) and 3 (T, CO_2, O_2, CH_4, Velocity Angle)

In order to get a better understanding, some more results from Case 2 and 4 are analyzed. Case 2 and 4 both have Mean Mixture fraction, Progress variable and Velocity Angle as common criteria, in addition to which, Case 4 has RMS temperature to take into account effects of turbulent fluctuations. The NOx trends, as shown in Figure 6.3 show an apparently random pattern for both runs. On the other hand, the CO plot in Figure 6.4, shows a trend similar to the experiments, although the rise in CO occurs earlier, i.e at a smaller EAR in the CRNs than in the experiments. From these observations it can be seen that the NOx emissions from CRNs with Velocity Angle as a criteria(Case 1, 2 and 4) have a more random trend whereas the CO emissions

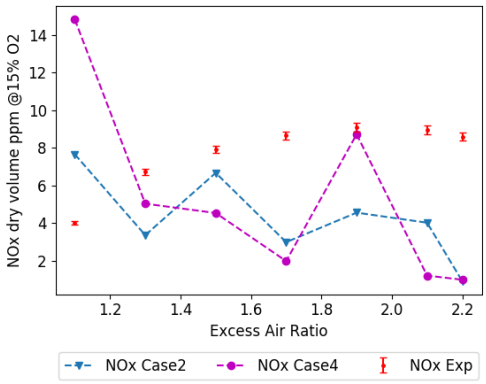

Figure 6.3: NOx v/s Excess Air Ratio at combustor outlet, Case2 (Mean Mixture Fraction, Progress Variable, Velocity Angle) and 4 (RMS T, Mean Mixture Fraction, Progress Variable, Velocity Angle)

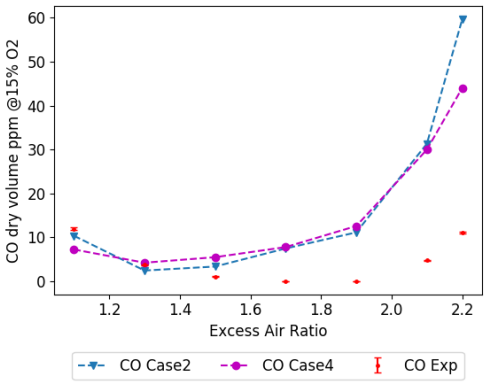

Figure 6.4: CO v/s Excess Air Ratio at combustor outlet, Case2 (Mean Mixture Fraction, Progress Variable, Velocity Angle) and 4 (RMS T, Mean Mixture Fraction, Progress Variable, Velocity Angle)

from these CRNs are closer to the experiments, both in trend and absolute value.

The quality of the CRN can be partially gauged by the tolerance value. In order to determine the Fitness of a cell/reactor for clustering, the value of the clustering criterion of the cell is compared to that of the clustering center. If the absolute difference between these values is less than a threshold value, the cell/reactor is clustered. This threshold value is a product of a tolerance, which is a non dimensional quantity(ϵ), and the difference between the maximum and minimum value of the clustering criteria in the CFD domain as shown in Equation 3.1. To obtain networks with lesser number of reactors, the value of tolerance is relaxed, i.e increased, conditionally after every iteration of clustering. This would generally imply that the smaller the network, the larger the tolerance, as more cells need to be clustered together, which would mean that the resultant reactor has an average value of the clustering criteria that is further away from that of its constituent cells in the original CFD solution.

The tolerance averaged over all 7 runs for the different cases is shown in Figure 6.5. From this it can be seen that the parameter is much higher for Case 1,2 and 4 compared to Case 3. The implication of this is that cells with more dissimilar conditions are clustered together in effect leading to a temperature and species condition that has a higher deviation from that of the individual constituent cells. This can be termed as an over relaxation which leads to inaccurate reactor conditions. A reason for this may be that the Velocity Angle is a very strict criteria for clustering, which would require higher relaxation to pass the Fitness test in order to achieve the desired number of reactors. On the other hand, the parameter seems to capture the CO emissions better than in Case3. This may imply that the recirculating mass is quite important for accuracy in CO levels, probably because the oxidation of CO is influenced by the residence time of the molecules in excess oxygen environment and the recirculation helps in extending this time period. This may be why in Case 3, which does not have Velocity Angle as a criterion, the CO levels are much higher, especially in the leaner conditions, where conventional combustion is expected to occur. NOx on the other hand is highly sensitive to temperatures, probably because of the thermal NOx mechanism, and over relaxation causes the values of reactor temperature to deviate from that of the constituent cells.

A comparison is made for Case 5 and 6 as shown in Figure 6.6 and Figure 6.7. The CRN quality, expressed by the average tolerance is higher for Case 6 than for Case 5 although, both are much lower than Case 1, 2 and 4 as seen in Figure 6.5. Case 6 uses Velocity Direction as a criterion which clusters cells only with the same sign of Z velocity, so as to better separate cells in different parts of the recirculation vortex. This criterion is used in order to maintain low tolerance levels as it should be easier to satisfy than the condition of Velocity Angle. It is also expected to better capture the recirculation as compared to the criteria of Z Velocity used in Case 5, which clusters cells based on value and may cluster positive and negative Z velocity values, as long as they lie within a threshold limit of each other. This can be seen in the CO plots in Figure 6.7 wherein Case 5 has much higher values for the very lean runs. This may be because the CFD predicts lower recirculation for these Runs which make them more sensitive to deviations in recirculation ratio in the CRN. The NOx plots in Figure 6.6 have a generally higher value than experiments and do not follow the trend.

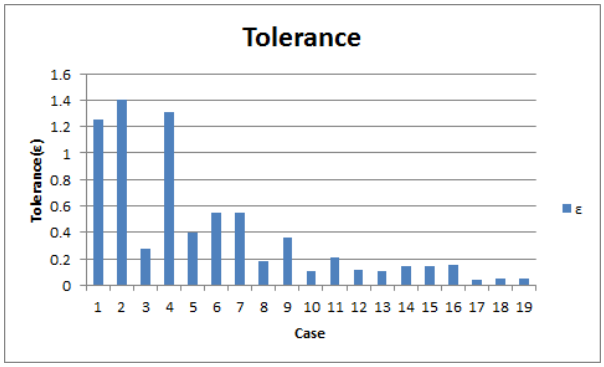

Figure 6.5: Comparison of Clustering relaxation between different cases

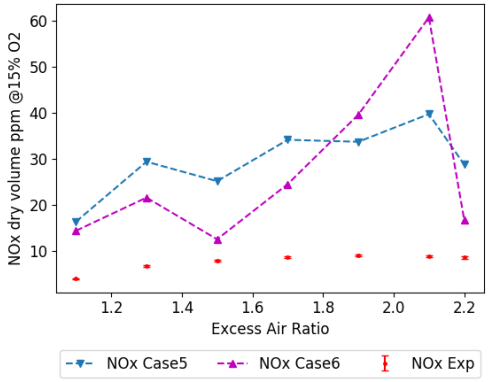

Figure 6.6: NOx v/s Excess Air Ratio at combustor outlet for Case5 (T, RMS T, OH, Mean Mixture Fraction, Z Velocity) and 6 (T, RMS T, RMS T, OH, Mean Mixture Fraction, Z Velocity) and 6 (T, RMS T, OH, OH, Mean Mixture Fraction, Velocity Dir)

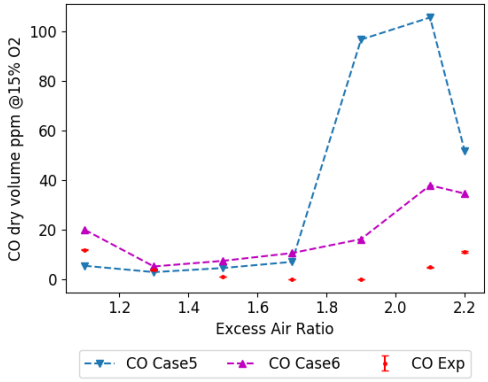

Figure 6.7: CO v/s Excess Air Ratio at combustor outlet for Case5 (T, RMS T, OH, Mean Mixture Fraction, Velocity Dir)

6.2.1. SENSITIVITY TO CLUSTERING CRITERIA

The cases used for this analysis were ensured to have a low tolerance while clustering. This was done by decreasing the increment steps used to relax the tolerance during successive iterations.All cases starting from Case 10 till 19 had this implementation. Fewer criteria are used in the simulations presented ahead because more criteria make the Fitness condition more difficult to satisfy thereby leading to a higher tolerance value for a given number of reactors. If the tolerance needs to be reduced under such a condition, the number of reactors needs to be increased, hence it is a trade off. Most of the simulations were done with 1000 reactors which took about 2.5 hours to solve and some cases were simulated with 5000 reactors which took about 26 hours to solve. It may be observed that the simulation time does not scale as a multiple of the number of reactors, and this is because an increase in number of reactors also causes an increase in the number interconnecting massflow controllers between them which increases the convergence time.

The analysis starts with a basic criteria of Temperature and Velocity Direction. This is to be able to capture high NOx production zones(high temperatures) as well as capture the recirculation zones which were found to be important for CO oxidation. The next cases chosen are Case 12 and 13 which in addition to the criteria in Case 10 have the criterion of 'Mass fraction of CO_2' and 'Mass fraction of H_2O' respectively. This is to capture the chemical composition that differentiates burnt and unburnt states. Also it may be possible that there are regions within the domain that have a similar temperature but different chemical composition, thereby having the possibility of different types of reactions taking place in those regions. It may be noted from Table 6.2 that the tolerance does not increase from 10 to 12 and 13 even though a criterion is added. This may be because Temperature and CO_2/H_2O are interdependent due to the heat release by chemical reactions and hence the same number of reactors are redistributed in a different manner while maintaining the same tolerance. A comparison of the NOx values from Case 10, 12 and 13 in Figure 6.8, shows an inversion of trend from a 'W' like shape to an 'M' like one. In general it seems the inclusion of combustion products as criteria in addition to temperature and direction of axial velocity, causes an increase in NOx values, although the change

was relatively less for Run1 which is also claimed to be the one in Flameless mode in the experiments. This may suggest that for most of the operating conditions, the NOx prediction is sensitive to inclusion of a major combustion product as a criterion. The CO trends as seen in Figure 6.9, follow the experiments in general, although there are deviations for some runs. It appears that the trend is best captured in Case 10 amongst the 3 presented cases. The deviations are seen in Case 12 which has 'Mass fraction of CO_2' as one of its criteria as opposed to Case 13 which has 'Mass fraction of H_2O' as its criteria which may indicate a sensitivity of CO prediction towards the major product species choice of criterion.

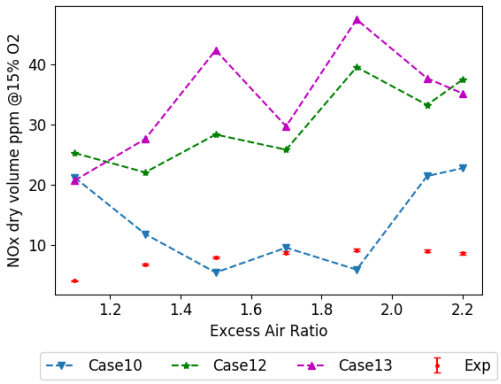

Figure 6.8: NOx v/s Excess Air Ratio at combustor outlet for Case10 (T, Velocity Dir), 12 (T, CO_2, Velocity Dir) and 13 (T, H_2O, Velocity Dir)

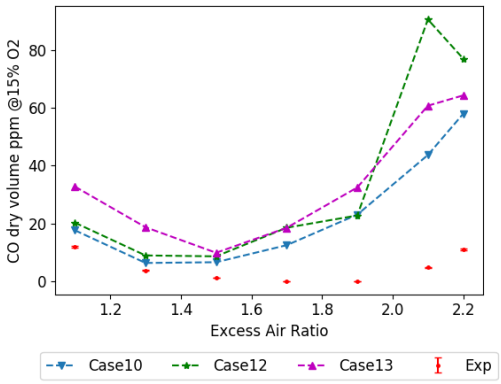

Figure 6.9: CO v/s Excess Air Ratio at combustor outlet for Case10 (T, Velocity Dir), 12 (T, CO_2, Velocity Dir) and 13 (T, H_2O, Velocity Dir)

Next, mass fraction of OH is added as a criteria to Temperature, Velocity Direction and CO_2/H_2O. This is because OH is involved in the oxidation of combustion intermediates that lead to the formation of CO and CO_2 which are responsible for the major heat release in combustion. Hence including 'Mass fraction of OH' as a criterion may help in getting better resolution of the CRN in the reaction zone of the flame, giving a better estimate of intermediate radicals. A comparison of Case 12 and 15 is done to demonstrate the effect of 'Mass fraction of OH', when CO_2 is used as a major species criterion. There is a change in NOx trend, mainly because Run4 has a higher relative value to the other runs in Case 15 as shown in Figure 6.10, compared to Case 12. The absolute values of NOx also have a significant deviation from Case 12 to Case 15 indicating that the NOx prediction is sensitive to OH gradients. The CO plots in Figure 6.11 display similar trends indicating a lower sensitivity of CO prediction trend on OH gradients, although the absolute values do have a deviation of about 10 ppm, which is comparable to the NOx deviations.

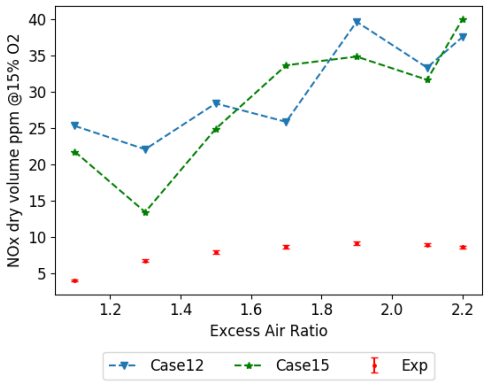

Figure 6.10: NOx v/s Excess Air Ratio at combustor outlet for Case 12 (T, CO_2, Velocity Dir) and 15 (T, CO_2, OH, Velocity Dir)

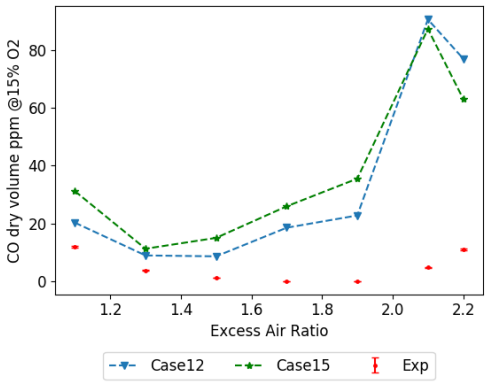

Figure 6.11: CO v/s Excess Air Ratio at combustor outlet for Case 12 (T, CO_2, Velocity Dir) and 15 (T, CO_2, OH, Velocity Dir)

The effect of inclusion of 'Mass fraction of OH' as a criterion is further studied in a case where H_2O is used as a major species criterion instead of CO_2. The NOx plots in Figure 6.12 show a comparison of Case 13, 14

and 16. Case 13 use Static temperature and Mass fraction of H_2O as criteria, Case 14 uses the same criteria as Case 13 along with Mass fraction of OH and Case 16 has Mass fraction of C_2H_2 in addition to the criteria of Case 14. Considering Case 13 and 14, a significant difference in NOx predictions is seen. The trend inverts for Run 5, 6 and 7 from decreasing to increasing upon the addition of OH as a criterion. This observation is in agreement with the previous one wherein NOx prediction was found to be sensitive to the gradients of OH. A comparison of CO prediction by Case 13 and 14 as shown in Figure 6.13, indicates similar trends with deviations for Run 4 and 6.

In the same plots, the addition of C_2H_2 as a criterion is also demonstrated as Case 16. C_2H_2 is chosen as a criteria because it was one of the species available in the CFD solution that is not a typical combustion product or reactant species but is a precursor to the formation of CH_x radicals formed during the oxidation of methane, which facilitate the Prompt NOx pathway. The gradients of C_2H_2 may be a possible indicator of intermediate reactions taking place during combustion ignition and may be useful in better predicting radical concentrations important for Prompt and NNH pathway of NOx formation. This is because, the H-C bonds in CH_4 are very strong and hence CH_3 radicals formed in the induction zone, may not decompose into CH_2 and CH radicals but instead react to form CH_2O and other higher hydrocarbons which leads to generation of radical pool that initiates the process of combustion[68]. From Figure 6.12 it can be seen that it significantly affects the trend line of NOx prediction. Comparing Case 14 and 16, the trend from Run 1 to 4 transforms from an arch to a nearly monotonically increasing curve while there is a drop in NOx from Run 5 to 7 in Case 16 as opposed to a monotonic increase in Case 14. The CO profile in Figure 6.13 for Case 16 follows a similar trend as that of Case 14, with the exception of a high over prediction for Run 6.

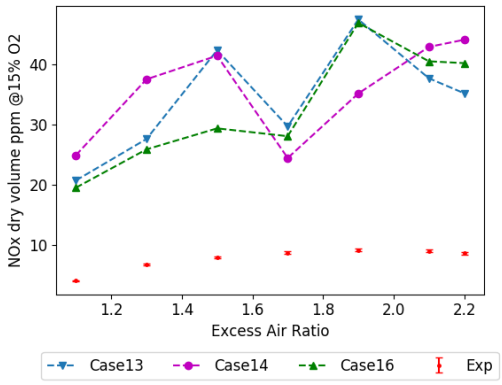

Figure 6.12: NOx v/s Excess Air Ratio at combustor outlet for Case 13 (T, H_2O, Velocity Dir), 14 (T, H_2O, OH, Velocity Dir) and 16 (T, H_2O, OH, C_2H_2, Velocity Dir)

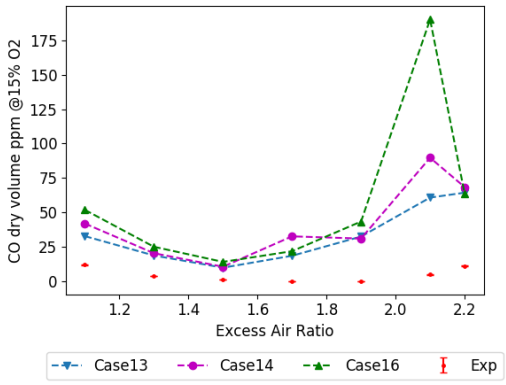

Figure 6.13: CO v/s Excess Air Ratio at combustor outlet for Case 13 (T, H_2O, Velocity Dir), 14 (T, H_2O, OH, Velocity Dir) and 16 (T, H_2O, OH, C_2H_2, Velocity Dir)

Increasing the number of reactors should help increase overall resolution and hence better capture gradients and mass flows. It should also result in lower values of tolerance as the clustering process would require less successive relaxations. A comparison of Case14, which has 1000 reactors, is made to Case17, which has the same criteria as 14 but has 5000 reactors. Figure 6.14 and Figure 6.15 show the NOx and CO profiles respectively. The NOx emissions of Run1 and 2 are not quite affected by the increase, while the other Runs have a deviation. This causes a change in trend along Run 2, 3 and 4. The CO levels decrease and have lesser deviation from the general trend. This may be as a result of better resolution due to increase in number of reactors. It can be seen from Figure 6.5 that Case17 has a much lower tolerance value,0.04, than Case14, 0.14, which should lead to more accurate clustering with less internal deviation of constituent cells. Tolerance seems to significantly affect the magnitude of CO predictions, but the NOx levels seem to be affected in terms of trend but vary within the same region of magnitude. A similar observation is seen in the comparison of Case 16 and 19, which has C_2H_2 as an additional criteria and Case 16 has 1000 reactors, whereas Case 19 has 5000 reactors. There appears a slight change in trend of NOx as seen in Figure 6.16 by the increased NOx prediction for Run 1, 2 and 3 in Case 19 as compared to Case 16. From Figure 6.17, it may be seen that Case 19 has lower CO values and lower deviation from trends. Referring back to Figure 6.5, the tolerance of Case 19, 0.05 is lower than that of Case 16, 0.15, and hence provides lesser deviation of clustered values and higher resolution in regions of high gradients.

A comparison of cases with larger number of reactors, i.e 5000 reactors, is done for different combination

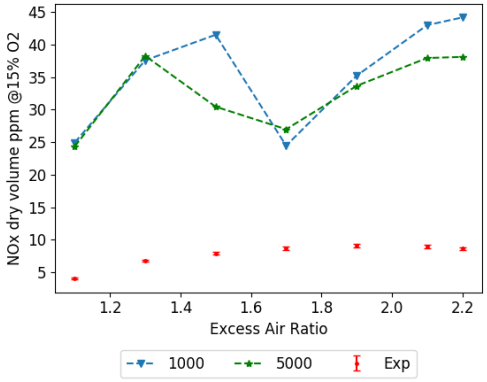

Figure 6.14: NOx v/s Excess Air Ratio at combustor outlet for Case 14 (T, H_2O, OH, Velocity Dir, 1000 reactors) and 17 (T, H_2O, OH, Velocity Dir, 5000 reactors)

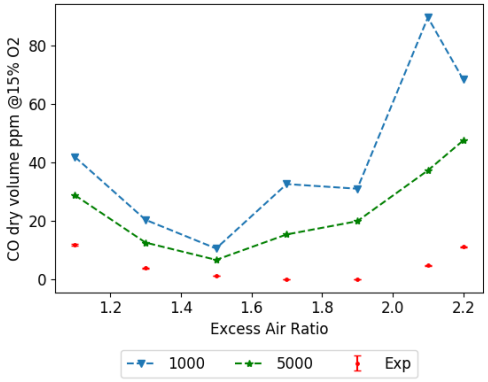

Figure 6.15: CO v/s Excess Air Ratio at combustor outlet for Case 14 (T, H_2O, OH, Velocity Dir, 1000 reactors) and 17 (T, H_2O, OH, Velocity Dir, 5000 reactors)

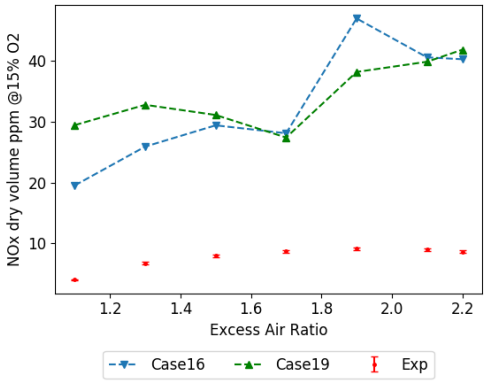

Figure 6.16: NOx v/s Excess Air Ratio at combustor outlet for Case 16 (T, H_2O, OH, C_2H_2, Velocity Dir, 1000 reactors) and 19 (T, H_2O, OH, C_2H_2, Velocity Dir, 5000 reactors)

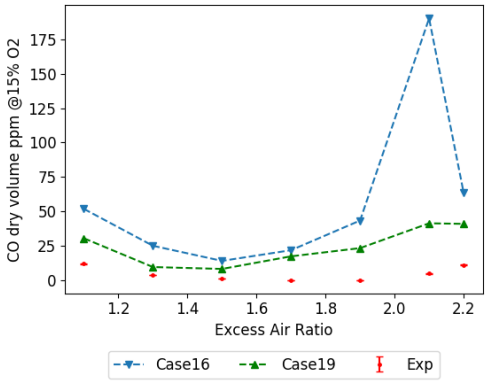

Figure 6.17: CO v/s Excess Air Ratio at combustor outlet for Case 16 (T, H_2O, OH, C_2H_2, Velocity Dir, 1000 reactors) and 19 (T, H_2O, OH, C_2H_2, Velocity Dir, 5000 reactors)

of clustering criteria. The cases are Case 17, 18, 19 respectively. Case 17 uses Static temperature, mass fraction of H_2O and mass fraction of OH as clustering criteria while Case 18 uses the same criteria as case 17 along with an added criterion of Mean Mixture fraction, which is a non dimensional quantity varying from 0 to 1 that depicts the amount of matter originating from the fuel stream, 1 being entirely originated from the fuel stream. Case 19 has the same criteria as Case 17 in addition to which mass fraction of C_2H_2 is used. The NOx plots in Figure 6.18 show that the NOx values deviate with a similar magnitude from the experimental values for all 3 cases, indicating that the difference may be attributed to the deviation of the underlying flow field, as predicted by CFD, from experiments rather than a clustering criteria choice. On the other hand the choice of criteria does influence the trend to a certain extent.

Taking Case 17 as the base case a further comparison is done. The initial rise in NOx from Run1 is seen to continue up to Run3 in Case 18 as opposed to a drop after Run2 in Case 17. The rise in NOx after Run4 is higher in Case 18 but then there is a switch in trend at Run7 where NOx decreases. Case 19 has a similar trend to Case 17, but the initial rise in NOx from Run1 to 2 is lower and the later increase after Run4 is higher. The values for Run 1 are similar for Case 18 and 19 and higher than that in Case 17. The values for Run4 are similar for all 3 cases and Run3 is similar for Case 17 and 19. The criteria of Mean Mixture Fraction and C_2H_2 may lead to better resolution of fuel rich zones or regions having high carbon bearing radical content. This is probably why Cases 18 and 19 have higher NOx beyond Run4 where the high entrainment of fuel by the increased air jet momentum leads to higher Prompt NOx formation. The CO trends are similar for all 3 cases as seen in Figure 6.19, except for a reduction at Run7 in case 18 and 19. The rest of the trend is similar to the experimental data with the difference being that the rise in CO takes place earlier, i.e at Run4 compared to

that at run6 in the experiments.

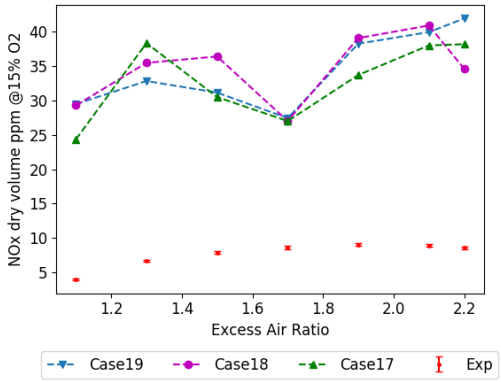

Figure 6.18: NOx v/s Excess Air Ratio at combustor outlet for Case 19 (T, H_2O, OH, C_2H_2, Velocity Dir, 5000 reactors), 18 (T, H_2O, OH, Mean Mixture Fraction, Velocity Dir, 5000 reactors), 17 (T, H_2O, OH, Velocity Dir, 5000 reactors)

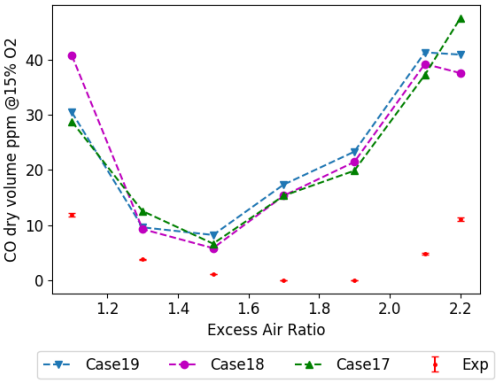

Figure 6.19: CO v/s Excess Air Ratio at combustor outlet for Case 19 (T, H_2O, OH, C_2H_2, Velocity Dir, 5000 reactors), 18 (T, H_2O, OH, Mean Mixture Fraction, Velocity Dir, 5000 reactors), 17 (T, H_2O, OH, Velocity Dir, 5000 reactors)

These comparisons show that increasing the number of reactors does cause a change in solution. It is expected that the further increase in reactors should lead to an improvement in solution due to improved resolution of flow field in the CRN, but the improvement should reach an asymptotic limit beyond which an increase in number of reactors will not lead to an improvement in emissions prediction. This is because once the gradients influencing minor species formation are well resolved, a further increase in reactors would be the equivalent of splitting one reactor into many and calculating them all at the same thermo-chemical state which has no added benefit. This is also seen in Figure 6.20 and Figure 6.21, in which the values of NOx and

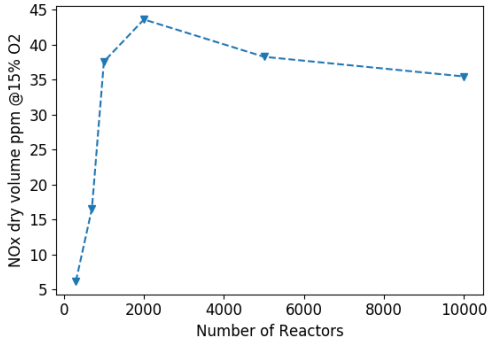

Figure 6.20: NOx v/s Number of reactors for Run2 using T,H_2O and OH as criteria

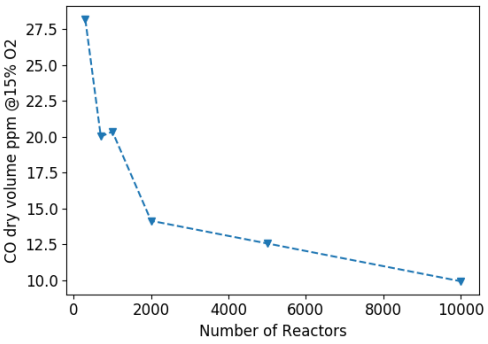

Figure 6.21: CO v/s Number of reactors for Run2 using T,H_2O and OH as criteria

CO seem to reach an asymptotic value if the trend is continued further for more number of reactors. The simulations were done up-to 10000 reactors due to time constraints[1]. It is recommended to solve for greater than 10000 reactors, but first the solver should be improved in order to reduce the computation time.

The values of NOx and especially the trend is sensitive to choice of species chosen as criteria. CO trends on the other hand are seen to be less sensitive to species and more dependent on recirculation prediction. This may be because NOx production is dependent on several pathways that are slow and depend on different intermediate radical species to be produced. CO on the other hand is produced relatively quickly but the exhaust emissions are due to the CO molecules that fail to oxidize in the combustion chamber to CO_2. This is more dependent on residence time of the molecules in the chamber which is influenced by the recirculation and other internal flows and temperature, which is one of the basic criteria chosen for clustering.

[1]The Case with 10000 reactors took 47 hours

The magnitude of difference in values introduced by criteria variation reduces for higher number of reactors, indicating a reduced sensitivity to clustering criteria, but this remains an optimization problem as with increase in number of reactors, solution time also increases and probably the number of reactors required for criteria independent solutions would also scale with the size of the chemical mechanism used.

This analysis does shed light on the influence of clustering criteria choice on the emissions prediction, but the CRN data is significantly higher than the experiments. The reason for this difference and the underlying mechanism of NOx and CO formation in this test case combustion chamber is not yet fully understood as the data analyzed is that at the exit of the chamber. Hence, detailed analysis is presented further which explores the pollutant formation mechanism.

6.3. CRN VALIDATION

The previous data presented is that at the exit of the combustion chamber. The experiments also provide values of species and temperature at discrete points within the combustion chamber for Run2 and Run4. These values are compared to those obtained from the CRN in Case 17, to better understand the inherent difference between the simulation and experiments. A comparison of Temperature, CO_2, CO, NO and O_2 is shown in Figure 6.22 and Figure 6.23 for Run2 and Run4 respectively. The distribution is along a line along the axis of the combustion chamber and the plots are for lines at a distance of r=0, 10,25 and 45mm from the central axis. The reader is encouraged to refer back to Figure 5.5 in order to get a better picture of the locations. The axis of the chamber is the z axis in the figure. In the plots presented, the simulation data points represent the trend along fixed points. The CFD cell centers lying between these points along the axis and having the same radial distance from the axis, are mass averaged to represent the previous point. The values of quantities used are that of the reactor in the CRN to which these cells belong. The experimental data starts at the inlets at 0mm and ends at around 300mm. The region from 300mm to 500mm contains the latter part of the cylinder and the exit cone. The temperature plots for both Run2 and Run4 show a lower CRN value near the boundary wall and also near the axis. The temperature near the wall may be a result of over prediction of heat loss in the CFD near the early sections of the chamber as a result of which the recirculating gases are colder. The region at r=0mm may be colder due to improper mixing as predicted by CFD along with the lack of radiation modeling in the CFD. The CO peak from CRN as seen at r=10mm is much higher than the experiments. This may be due to an improper prediction of recirculation which would have brought

Table 6.3: Excess Air ratio from Experiments(at z=300mm) and CRN(at outlet). Calculations shown in Appendix A

	Run2 Exp	Run4 Exp	Run2 CRN	Run4 CRN
O_2(dry %)	5.9	9.1	5.09	8.57
CO_2(dry %)	8	6.3	8.72	6.78
CO(dry ppm)	140.8	65.8	14.02	16.51
EAR wet	1.368	1.722	1.292	1.632
EAR design	1.3	1.7	1.3	1.7

in more vitiation which would make the environment less conducive for rapid fuel oxidation. This peak in CO coincides with a temperature peak which is higher than the experiments. It may also be seen that the CO_2 values at 300mm are higher than experiments while the O_2 values are lower for Run 2 and Run 4 which suggests that there is less excess air being fed to the system in the CRN than experiments. Table 6.3 presents the Excess Air Ratio expected to be fed to the system by calculations based on the amount of O_2, CO_2 and O_2 at z=300mm for the experiments as those were the last reported points and at the outlet, z=500mm, for the CRN. It is seen that the CRN has a lower EAR (EAR wet) than the experiments which means it is effectively being calculated at a richer mixture, hence the higher carbon species content. This may be due to convergence to a higher threshold value. Despite that, it is also seen that he EAR of the experiments are higher than the expected design value. It may be possible that there was an error in the regulation of air or fuel flow during the experiments which resulted in such a condition. The NO values are higher in general for the CRN which may suggest that a higher NO is being predicted during the formation stage in the CRN.

The analysis from this section indicates that there may be some differences between predictions and experiments due to convergence errors in the CRN as well as unreported errors in the experiments, but the prediction of the flow field by the CFD simulation is also flawed and may be resulting in significantly different values for the minor species. A further analysis of species formation in each run is required to understand the NO and CO production mechanisms and what factors of the CFD-CRN simulation may be influencing them.

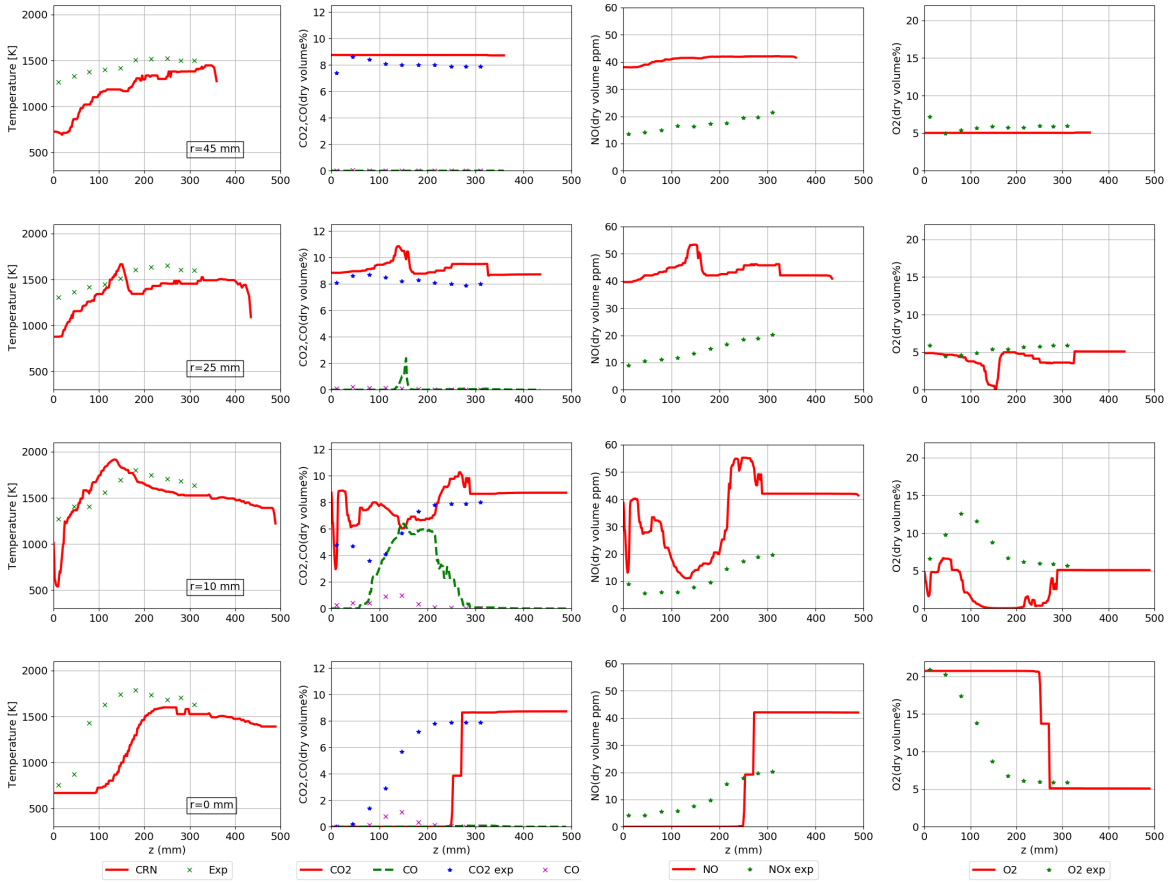

Figure 6.22: Comparison of Experiments and predictions by CRNs of Temperature, CO_2, CO, NO and O_2 for Run2

6.4. POLLUTANT FORMATION

One of the main aims of this research is to understand the influence of clustering criteria on the prediction of emissions from the CFD-CRN process. From the previously presented cases, there is an evident change in results with the use of different criteria and the CRN predicted emissions are much higher than the experiments. To better understand why the differences are being caused, the mechanisms of NO and CO formation within the combustion chamber need to be understood. This can be done by looking at the variation of species and their formation rates along the length of the chamber. This analysis also provides an opportunity to demonstrate the utility of having a network of large number of reactors, which increases the resolution to which such variation of quantities in space can be observed. Case 17 was chosen as the case to be analyzed in detail to understand how pollutant emissions of NOx and CO are formed in the different operating conditions of this combustion chamber. This particular Case was chosen because it had the lowest value of tolerance and a large enough number of reactors to be confident that the results would be less distorted due lack of resolution of the CRN.

The data is first visualized in the form of contours by projecting the CRN back to the CFD domain. A suitable plane from the CFD domain, along the axis of the combustion chamber, is chosen for the analysis such that it intersects with one of the fuel inlets and the air inlet as shown in Figure 6.24 and Figure 6.25. The equation of the plane is used to obtain the cells that lie on that plane in the CFD domain. Next, the cells that form the plane are assigned properties/values based on the reactor in the CRN to which they belong. Hence it is possible to analyze the properties of the reactors through their constituent cells in the plane.

The outlet NOx values and the contour of NO in the CRN are shown in Figure 6.26 and Figure 6.27 respectively. From the NO contours, it can be seen that the NO concentration is more distributed in Run1 and 2 even though Run2 has a high NOx at the outlet. The other runs have a high NOx concentration in a region that appears to be the post flame zone. The flame zone can be defined as the regions of highest temperatures as seen in Figure 6.30. Higher concentrations of NO are seen in regions where the flame zone and air jet meet,

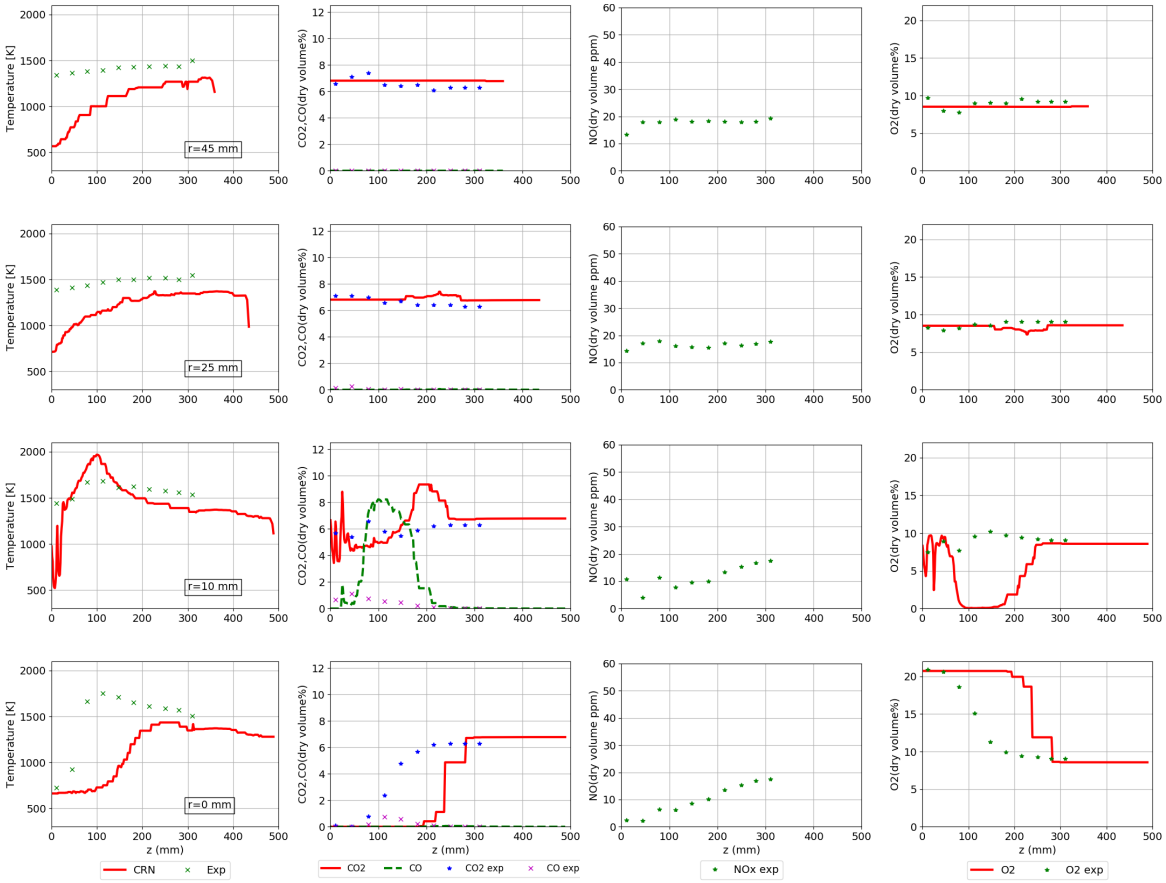

Figure 6.23: Comparison of Experiments and predictions by CRNs of Temperature, CO_2, CO, NO and O_2 for Run4

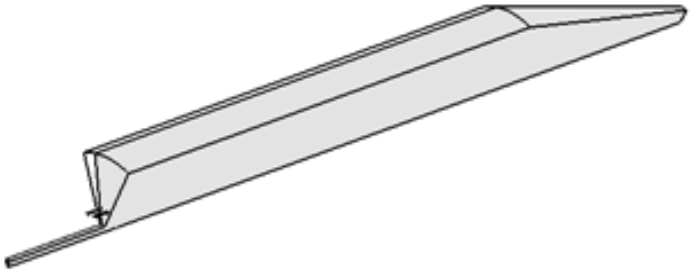

Figure 6.24: CFD domain of combustion chamber

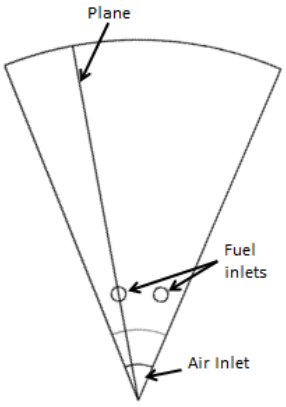

Figure 6.25: Cross section of CFD domain indicating analysis plane

the air jet being the fluid stream of lower temperature, closest to the central axis.

Similarly, the CO levels at the outlet are shown in Figure 6.28 and the CO contours in the CRN are shown in Figure 6.29. From the contour plots it can be seen that the region of high CO gradient, in which the CO concentration reduces due to oxidation towards the later part of the combustor, shifts upstream as excess air ratio increases, i.e from Run1 to 7. This may be due to the faster entrainment of fuel due to higher suction caused by a higher air jet momentum. This leads to faster mixing and earlier heat release reactions , leading to lower CH_4 penetration in the domain as seen in Figure 6.31. Thus CO formation reaches its maximum

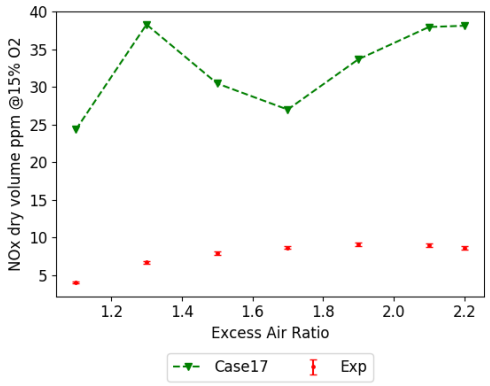

Figure 6.26: NOx at outlet, Run1-7 from left to right

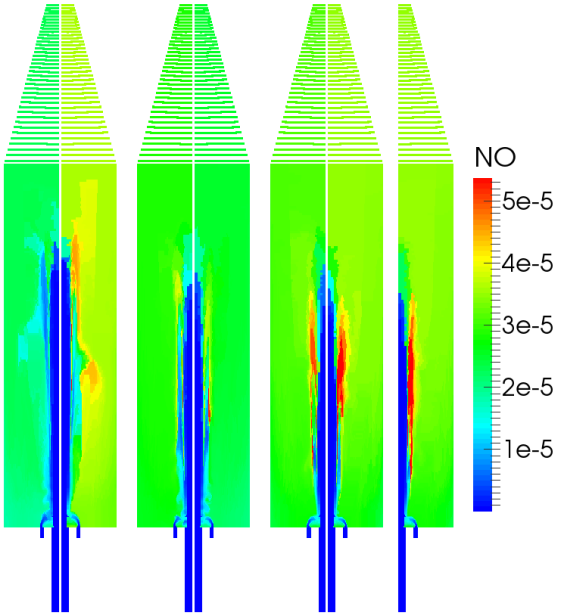

Figure 6.27: NO distribution, Run1-7 from left to right

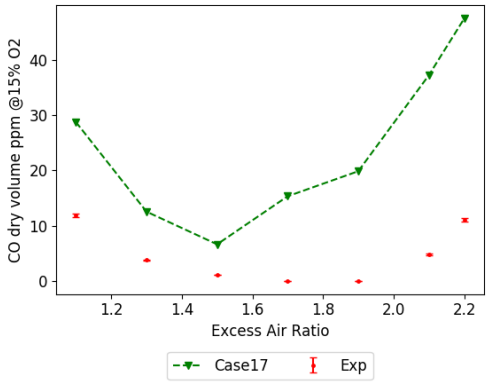

Figure 6.28: CO at outlet, Run1-7 from left to right

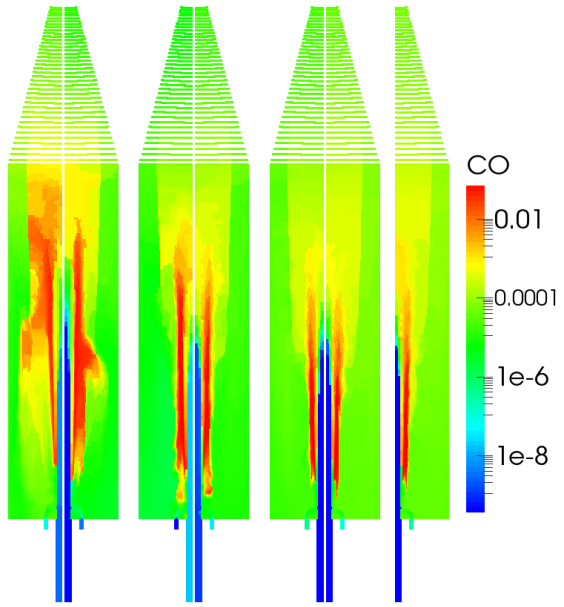

Figure 6.29: CO distribution, Run1-7 from left to right

point earlier along the axis with increasing excess air ratio.

The contours of HCN are shown in Figure 6.32, in which high HCN concentration is seen near the flame zone. The values are comparable to that of the NO formed as seen in Figure 6.27. This may indicate that the prompt and reburn pathway of NOx play a role in this case as HCN is an important product in the initiation reaction of both of these processes. It is difficult to comment on which pathway is more dominant based on composition only and hence more insight into the rate of formation of NO through these pathways is required. The contours of O as shown in Figure 6.33 depict an increase of O just after the flame zone. The regions of highest value of O mole fraction happen to be those where the excess air from the air jet near the central axis, mixes with the flue gases after the flame zone. From the contour plots of NO, CO, temperature, HCN and O, it can be seen that most of the chemical kinetic activity of interest occurs along the axis at a location radially between the air jet and fuel jet.

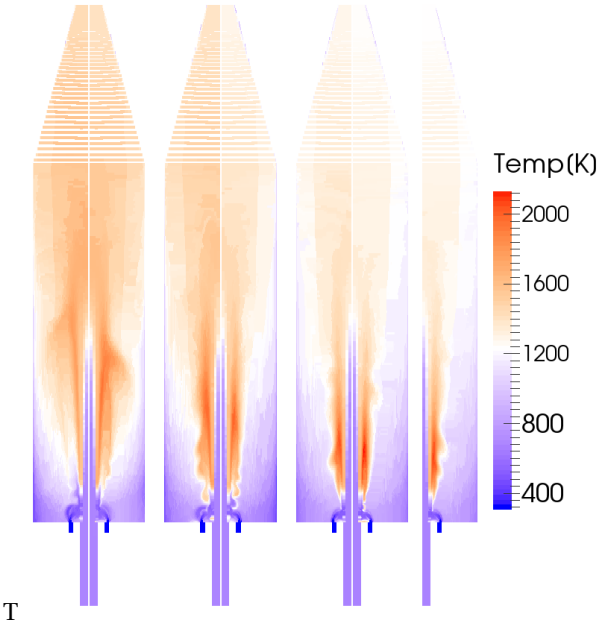

T

Figure 6.30: Temperature distribution, Run1-7 from left to right

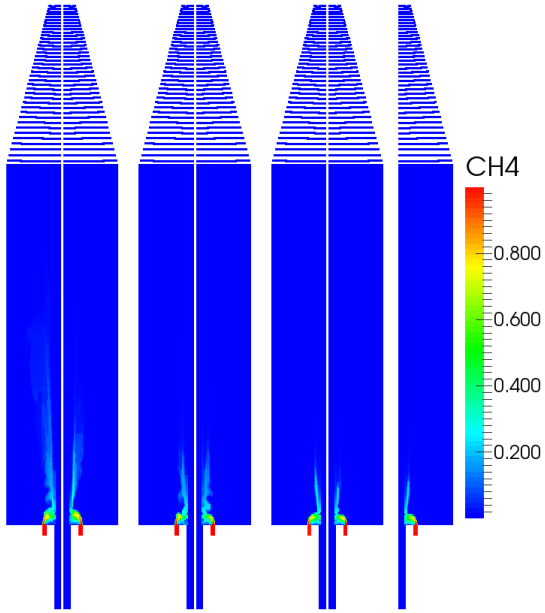

Figure 6.31: CH_4 distribution, Run1-7 from left to right

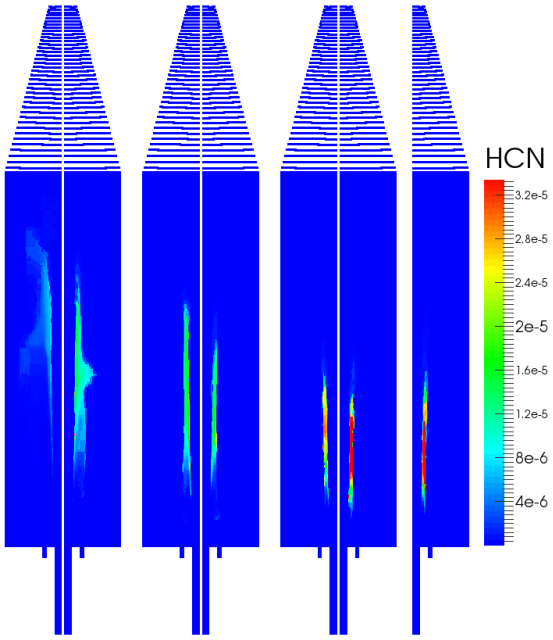

Figure 6.32: HCN distribution, Run1-7 from left to right

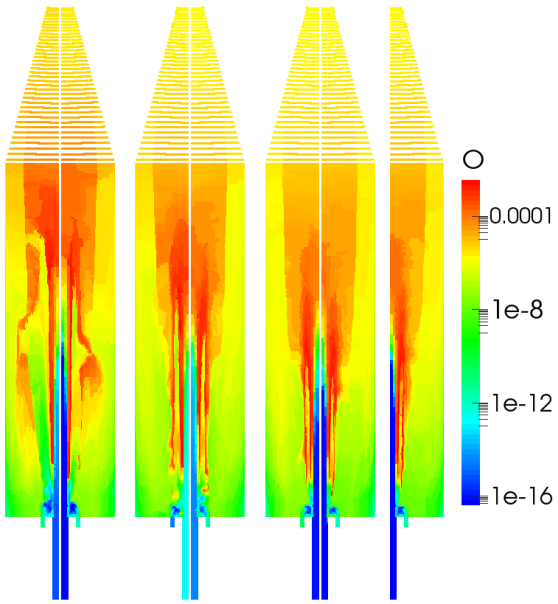

Figure 6.33: O distribution, Run1-7 from left to right

The CRN data is plotted along a line parallel to the central axis at a radial distance of 10mm from the axis for further analysis, the fuel jet being located at a radial distance of 15mm from the axis. The formation rates of NO are presented for the different production pathways, i.e the Thermal, Prompt, NNH and N_2O pathways along with the NOx destruction by the Reburn pathway. The initiation reactions of these pathways are usually the rate limiting reactions and hence the rate of those reactions is considered during the calculation. Reactions of these pathways are explained in Section 1.3.2 and the most important ones are presented further.

Thermal pathway:

$$O + N_2 \rightleftharpoons NO + N \tag{6.12}$$

Prompt pathway:

$$CH + N_2 \rightleftharpoons HCN + N \tag{6.13}$$

NNH pathway:

$$NNH \rightleftharpoons N_2 + H \tag{6.14}$$

N_2O pathway:

$$O + N_2 + (M) \rightleftharpoons N_2O + (M) \tag{6.15}$$

Reburn pathway:

$$CH + NO \rightleftharpoons HCN + O \tag{6.16}$$

The reburn pathway leads to destruction of NO and converts it into HCN and other N-C-H species which may be oxidized back to NO under the right conditions of O and temperature. For the prompt and reburn pathway, there are many more such similar reactions taken into account in the actual calculation, but for the sake of concise presentation only, the main reaction is shown.

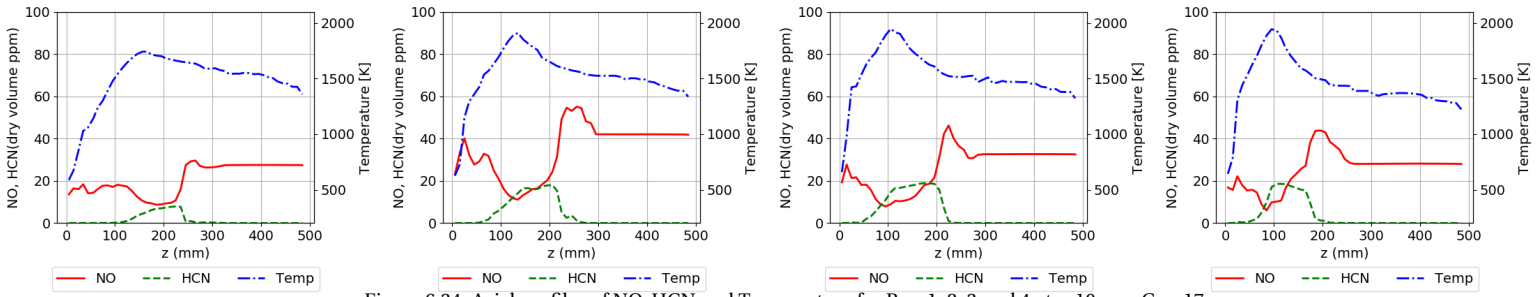

Figure 6.34: Axial profiles of NO, HCN and Temperature for Run 1, 2, 3 and 4 at r=10mm, Case17

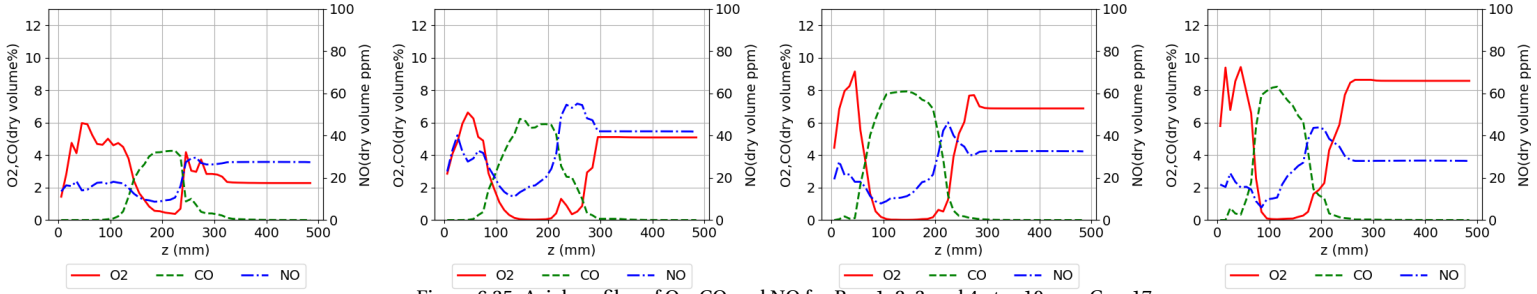

Figure 6.35: Axial profiles of O_2, CO and NO for Run 1, 2, 3 and 4 at r=10mm, Case17

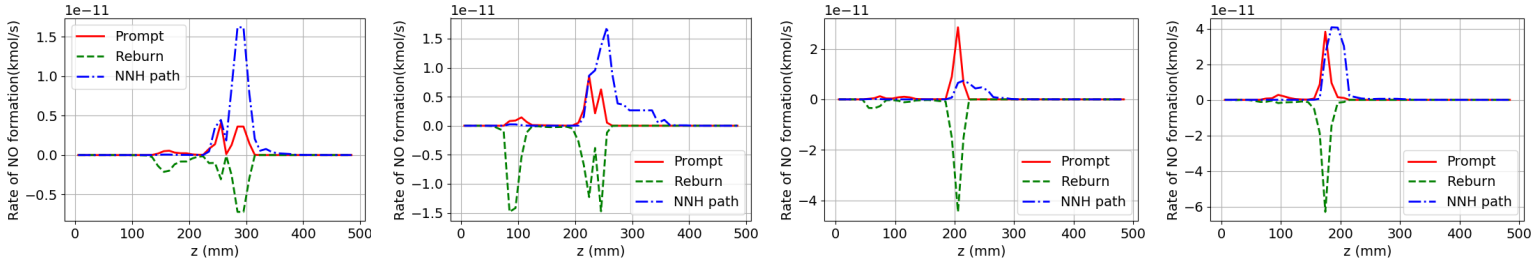

Figure 6.36: Axial profiles of rate of NO formation for Run 1, 2, 3 and 4 at r=10mm, Case17

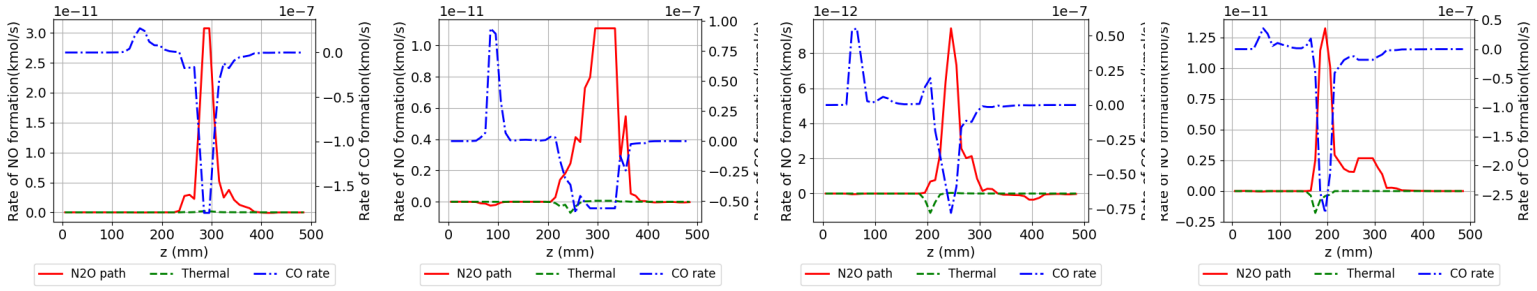

Figure 6.37: Axial profiles of rate of NO and CO formation for Run 1, 2, 3 and 4 at r=10mm, Case17

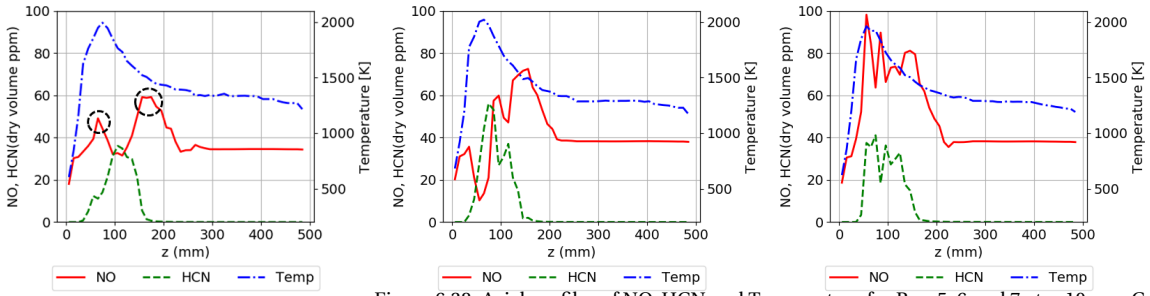

Figure 6.38: Axial profiles of NO, HCN and Temperature for Run 5, 6 and 7 at r=10mm, Case17

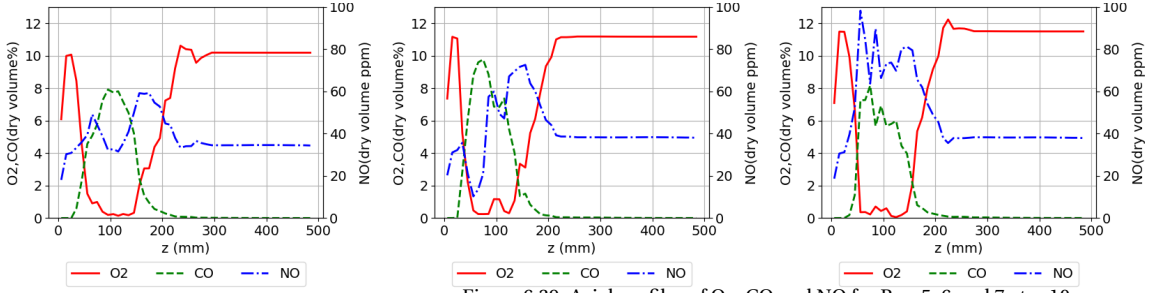

Figure 6.39: Axial profiles of O_2, CO and NO for Run 5, 6 and 7 at r=10mm

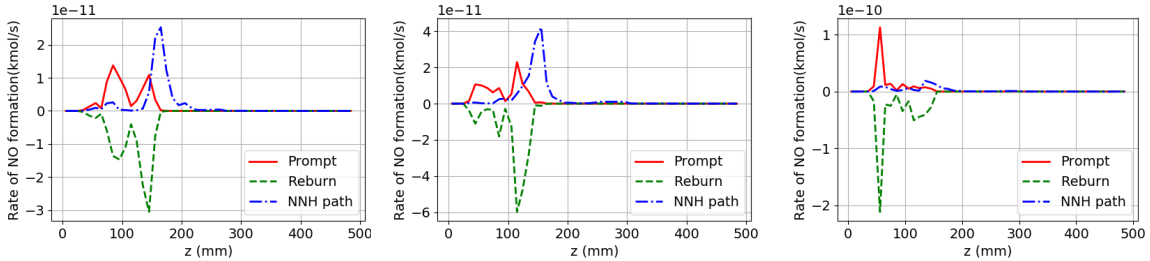

Figure 6.40: Axial profiles of rate of NO formation for Run 5, 6 and 7 at r=10mm, Case 17

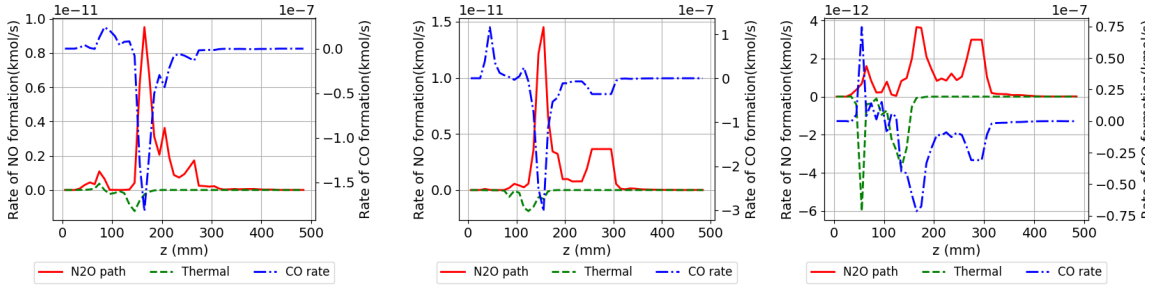

Figure 6.41: Axial profiles of rate of NO and CO formation for Run 5, 6 and 7 at r=10mm, Case17

Run1(EAR=1.1)
This is the run with least excess air and high recirculation ratio. There is a noticeable level of NOx near the inlet region, z=0mm in Figure 6.34. From the plots of rate of NO formation in Figure 6.36 and Figure 6.37, there appears to be no active mechanism and hence it may be concluded that this NO is a result of transport, most likely from the recirculation flow. There is a drop in NO and rise in HCN at z=100mm as seen in Figure 6.34, which is a result of increase in reburn rate as seen in Figure 6.36. At around z=210mm, there is an increase in NO and drop in HCN, which coincides with the point where O_2 starts increasing and CO decreases as seen in Figure 6.35. Referring to the rates of formation, CO seems to have a negative rate, which may indicate oxidation due to the excess O_2 inflow in the region. The oxidation of CO leads to release of H and O radicals as shown in Equation 6.17.

$$\begin{aligned} CO + OH &\rightleftharpoons CO_2 + H \\ CO + O_2 &\rightleftharpoons CO_2 + O \end{aligned} \tag{6.17}$$

The H and O atoms contribute towards the NNH and N_2O pathways of NO formation respectively, which can be seen by the increase in rates of NO formation through these pathways in the plots in Figure 6.36 and Figure 6.37 respectively. The N_2O pathway in particular is also enhanced by the presence of CO_2 and H_2O which act as third bodies. It also seems that there is an increase in prompt NO rate after the CO peak. The formation of CO takes place through CH_2O as an intermediate. The CH_2O levels build up by the reaction of CH_x radicals with OH and O radicals as shown in Equation1.11, and this intermediate oxidizes to CO. Thus a drop in CO levels may also mean that CH_x radicals in the domain are not being used for CH_2O formation and are hence available for the slower Prompt pathway. The high recirculation seems to provide some vitiation which prevents intense heat release thereby limiting the maximum temperature to around 1700K while maintaining the temperature at around 1500K beyond z=100mm. This prevents high temperatures and large temperature gradients which limits thermal NO formation which has a negligible rate of formation. The relatively higher temperatures, 1500K, in most of the combustion chamber allows for conversion of fuel to CO and subsequently oxidation to CO_2. The influx of O_2 downstream at z=250mm, is the excess air from the air jet that mixes with the flue gas and causes rapid oxidation of CO and leads to formation of H and O radicals contributing to NO formation.

Run2(EAR=1.3)
There is an increased air jet momentum compared to Run1 which causes higher fuel entrainment. This is seen in Figure 6.31, where there is lower penetration of CH_4 into the domain indicating early consumption to form radicals and products. The early mixing of more fuel leads to higher temperatures and higher CH_x radicals in the domain which leads to an increase in NO reburn rate, seen by increase in HCN and reduction in NO. As the temperature is significantly high and the region has low N2 content, the reburn pathway is much more dominant than the prompt pathway, even though both require excess CH_x in the domain. This run has the highest predicted recirculation rate and hence maintains a well distributed temperature, even after having a higher fuel entrainment, but the entrainment has the effect of making the temperature peak sharper and higher than in Run1. There is higher O_2 near the inlet than in Run1 which may be due to recirculation from the later part of the chamber. Higher fuel air mixing leads to earlier CO production along the axis which causes the sharp temperature peak. There is an influx of O_2 at around z=200mm that oxidizes CO to CO_2 and the resultant radicals, H and O as explained earlier, lead to increase in NNH and N_2O pathway rates that lead to an increase in NO. There is also a rise in reburn and prompt pathway rates which indicates a region of excess CH_x, which is present as a result of not being fully oxidized to CO. This is proven by the decreasing CO formation rate in this region. Prompt NO also increases due to increasing N2 content brought in by the fresh mixing air. The reduction in CO is as expected, as the excess air entering the system increases leading to better CO oxidation.

Run3(EAR=1.5) and Run4(EAR=1.7)
The further increase in air jet mass flow causes higher suction but there is also the effect of higher oxygen concentration in the recirculating stream. These two runs also seem to have an unsteady interface between the main flow and the recirculation seen by the wiggles near the inlet, as seen in the temperature and CH_4 contours in Figure 6.30 and Figure 6.31 respectively, which probably cause more recirculating flue gas to be entrained with the fuel stream. This causes dilution of NO concentration near the inlet, i.e at z=0mm and also suppress prompt NO formation by using the CH_x radicals for CO formation. Both the Runs follow the same NO formation mechanisms in the later part of the chamber where the increase in O_2 due to the mixing causes CO oxidation and NO formation by N_2O, NNH and prompt pathways. The cumulative rates for the NO pathways for these runs are higher than Run2 but they have lower NO , probably because of the

increased mass flow rate which results in a lower residence time in the reactors. The initial rise in NO, near z=100mm is just before CO reaches its peak, which may be due to the oxidation of N bearing species due to some O/OH radicals being available. It is also the point where CO formation rate reaches 0.0 after its first peak. In summary Run3 and 4 have a reduction in NO due to suppression of prompt NOx early in the chamber and a narrow axial region of NO formation due to rapid mixing of O_2 with the flue gases. These effects are larger in Run4 due to higher air jet momentum, resulting in a lower NO level. The rapid mixing of O_2 with flue gases along with the higher excess air in Run 4 leads to a reduction of temperature to below 1500K at around z=250mm, which is earlier than that in the previous Runs. There is also a decrease in recirculation ratio as mentioned in Table 6.1, but more importantly the temperature even at r=0 mm is lower than the experiments in the CRN as shown in Figure 6.23. This is due to the over prediction of wall heat loss in the early sections of the combustion chamber which leads to an over cooled recirculating flow mixing back with the main flow, leading to lower enthalpy addition to the main air flow by the recirculating mass. This causes colder excess air to mix with the flue gases downstream. hence a rise is seen at Run 4 instead of at Run 6 as shown in the experiments in Figure 6.28.

Run5(EAR=1.9) and Run6(EAR=2.1)
These operating conditions have higher excess air ratio and a higher air jet momentum which results in a early fuel entrainment and mixing with the air. There is an early increase in temperature due to early CO formation which results in heat release and a temperature high enough for radical build up which leads to increase in NO, NNH and N_2O pathways as seen in Figure 6.40 and Figure 6.41. The high temperatures also result in some thermal NO activity. This results in the first NO peak just after z=0mm. As temperature increases and CO formation increases, there is a CO peak which result in a drop in NO due to radicals being pulled towards CO formation. Further downstream of the CO peak, CO drops due to lower formation rate and dilution by transport of other species. This results in excess CH_x radicals which lead to Prompt pathway increase and a rise in NO. At around z=140 to 150 mm, there is an inflow of excess O_2 as seen in Figure 6.39, leading to CO oxidation and the H and O radicals released cause NO formation by NNH and N_2O pathway. Hence the 2nd NO peak is initiated due to prompt pathway but reaches its highest level due to high NNH and N_2O formation. Out of the 2 runs, Run6 has more entrainment due to higher suction by the increased air jet momentum, causing faster mixing and heat release resulting in a sharper and higher temperature peak. The increased mixing of fuel and air leads to a more fuel rich region in Run 6 than Run 5 in the earlier part of the chamber causing a higher Prompt NO rate in the fuel rich zone. There is also a much higher NNH pathway rate due to higher H radical concentration produced by oxidation of CO. These effects lead to higher NO in Run6 than Run5. There is a further increase in CO levels because the higher excess air entering the domain is not heated enough by the recirculating mass due to the excessive heat loss near the inlet region which causes a lower enthalpy stream of air to mix with the flue gases downstream causing a more rapid cooling, making the conditions less suitable for CO oxidation.

Run7(EAR=2.2)
Rapid mixing of fuel and higher O_2 content due to higher air jet momentum leads to early CO formation in the combustion chamber. The mixing is so high that CO is formed under very rich fuel conditions leading to a simultaneous increase in Prompt NO formation rates. The Prompt formation rate is significantly higher than other pathways and seems to dominate the NO production process. The CO levels increase due to the same explanation as in Run 5 and Run 6. The general increase in CO for higher EAR may also be attributed to the reduction in residence time of species in the combustion chamber due to the increase in inlet mass flow. The residence time may be extended by increasing the recirculation ratio but in this case it does not seem to compensate for the increase in mass flow.

The above analysis gives an insight into the pollutant formation mechanism in this combustion chamber. Run1 has the least amount of NO due to the lower temperature peak and more spread out temperature distribution brought about by the high recirculation ratio and vitiation relative to the incoming air flow. Prompt NO formation in the early regions of the combustion chamber is limited by vitiation and the later region of high NO formation is limited to a narrow axial region by rapid oxygen mixing with the flue gas. Run2 has higher NO due to higher NNH and N_2O pathway rates for longer axial region because of extended O_2 mixing region and hence a larger CO oxidation region. This may be a detrimental effect of higher recirculation ratio at an increased inlet air mass flow or the increase in recirculation ratio is not high enough to compensate for the increase in air flow. Run 3 and 4 see a reduction in NO due to suppression of prompt NO in the early regions by excess air due to increased inlet air mass flow into the system. Run5, 6, and 7 result in a monotonic increase due to increased fuel entrainment due to increasing air jet momentum resulting in increased Prompt NO formation.

In summary, the NO formation mechanism seems to vary from Run1 to Run7. The rate of formation is high in the later part of the combustion chamber for the runs with low excess ratio and transitions to NO formation in the early as well as latter region(2 point of formation) as excess air ratio increases due to early fuel entrainment and finally ends with NO formation at only the early part of the combustion chamber for the run with the highest excess air ratio. The NOx formation occurs mainly through NNH and N_2O pathway for the runs with lower excess ratio and the combination of prompt and NNH pathway is dominant for runs with higher excess ratio.

It appears that high prompt and NNH pathways may be leading to the NO prediction being higher than experiments in general. One of the reasons for the CRN to over predict the prompt pathway may be that it is effectively running at a lower excess air ratio, and hence a richer condition than the experiments. This is shown in Table 6.3, in which the EAR values for Run 2 and Run 4 are compared to experiments. This may be occurring due to low convergence threshold parameter. Another reason may also be that the recirculation predicted by the CFD may be lower than the experiments. A higher recirculation mass would reduce the concentration of the radicals associated with these pathways, thereby reducing the rate of formation of NO. The reduction in NO in Run3 and Run4 due to the 'wiggles' which enhance mixing with the recirculating flow might be proof of that. As mentioned in Section 6.3, the temperature near the walls and at the axis seem to be too low compared to experiments, possibly due to over prediction of heat loss in the early regions of the combustor as well as the lack of radiation modeling within the gases, which might lead to redistribution of heat within the chamber. This may be leading to incorrect fluid properties in this region, thereby affecting the recirculation ratio calculated.

6.4.1. EFFECT OF CRITERIA

Using the knowledge of the pollutant formation mechanism in this combustion chamber, the effect of adding C_2H_2 as a clustering criterion is analyzed in detail using Case 19. A comparison of emissions from Case 17 and Case 19 is shown in Figure 6.18 and Figure 6.19. The NO formation rates through NNH and N_2O pathway, in Run1, are more axially spread out in Case 19, as seen in Figure 6.44 and Figure 6.45, than in Case 17. This is possibly due to the earlier mixing of excess air with the flue gas in Case 19, at 200mm instead of 230mm, and occurs over a longer axial distance, as seen in Figure 6.43. The introduction of C_2H_2 as a criterion creates a better resolved CRN in this region where O_2 mixes as it also coincides with C_2H_2 gradients as Run 1 is an operating condition with relatively distributed reactions and heat release. The existence of high NO formation rates over an extended region results in higher NOx for Run 1 in Case 19 than Case 17. Run2 has lower NOx value in Case 19, shown in Figure 6.42, due to lower peaks of Prompt and NNH pathway formation rates seen in Figure 6.44.

In Run5, a much higher Prompt pathway peak, seen in Figure 6.48, results in higher NO concentration peak near the inlet, shown in Figure 6.46. A similar effect is seen in Run6 which has higher prompt formation pathway peak value than in Case 17. Thus Run5 and 6 have a higher NOx value in Case 19 due to higher Prompt pathway prediction. This may be because of better resolution of fuel and carbon radical rich zones brought about by C_2H_2 as a clustering criterion.

Run7 has a different mechanism responsible for higher NOx than Case 17. The initial prompt pathway peak is actually lower in Case 19 than Case 17 which might be as a result of better resolution of CRN in the fuel rich zone which captures the slight increase in recirculation ratio better as shown in Table 6.1. On the other hand, higher NNH and N_2O pathway peaks are seen. The O_2 mixing with flue gases seems to be slightly earlier in Case 19, at around 100mm as opposed to about 125mm in Case 17. This may be responsible for early CO oxidation leading to the formation of radicals that enhance the NNH and N_2O pathway under higher temperature conditions. The early oxidation of CO gives the CO molecules more residence time in higher temperature regions where oxidation is faster. Hence Case 19 predicts higher NOx for Run7 but lower CO values. The mixing of O_2 may be predicted to be earlier due to lower number of reactors in this zone as more reactors were used near the inlet, fuel rich region, where C_2H_2 gradients may exist. This may also be seconded by the tolerance of Case 19 being slightly higher, 0.05 than that of Case 17, 0.04.

To sum up the comparison to Case 17, in Case 19, Run1 is affected by changes in the NNH and N_2O pathways, Run 2 is affected by variation in NOx production of Prompt and NNH pathways, Run 5 and 6 have higher Prompt pathway predictions along with similar levels of NNH and N_2O pathway in the later part of the chamber. Run7 on the other hand has a different NOx formation mechanism than Run 7 in Case 17 by increased NNH and N_2O pathways which contribute to NOx formation downstream, i.e the second NO peak is higher than the first. This is different from Case 17 in which prompt NOx near the inlet is most dominant and leads to the highest first peak and subsequent drop in NOx till the outlet.

Regarding the effect of criteria, with limited number of reactors, the choice of criteria can influence the pollutant formation mechanism. For example, in the above mentioned results, the addition of C_2H_2 as a criterion is expected to lead to better resolution of C_2H_2 gradients from the CFD solution in the CRN. As C_2H_2 is a precursor to CH_x radical formation, it may be said that resolving its gradients separates regions conducive to CH_x radical formation in the CRN. This in turn leads to a variation in the NOx formation mechanism within the combustion chamber for different operation conditions.

Hence the influence of clustering criteria on emissions prediction is partly due to better resolution of regions of certain dominant reactions but also due to the loss of resolution in some regions because of refinement elsewhere, as the number of reactors are fixed. There is also the effect of increasing tolerance with addition of more criteria as it increases the constraint on the clustering. Hence, to be sure of obtaining a good solution from the CFD-CRN code, one must attempt to cluster to higher number of reactors but also try to limit the tolerance by choosing clustering criteria keeping in mind the pollutant formation mechanisms in the combustion chamber. As a good practice guideline, it is also recommended to run the CFD-CRN code for different combinations of clustering criteria which include some of the species involved in the CO and NOx formation pathways. The different cases should be compared before deciding on a final solution.

It should be noted while using the CFD-CRN code that mass diffusion of species is not modeled. The inclusion of diffusion may help in countering the flaws of clustering and may be important in regions of counterflows within the domain. On the other hand, it would lead to variable mass flows between reactors which would require the mass balance calculation to be repeated for every iteration, adding to computation expense. The CRN is also highly dependent on the detailed chemical mechanism used, and in essence is only as good as the kinetics modeled by the mechanism. Hence, not only should the mechanism be chosen based on the fuel, but one must also keep in mind that the mechanism is also a model of the reactions and may have some errors.

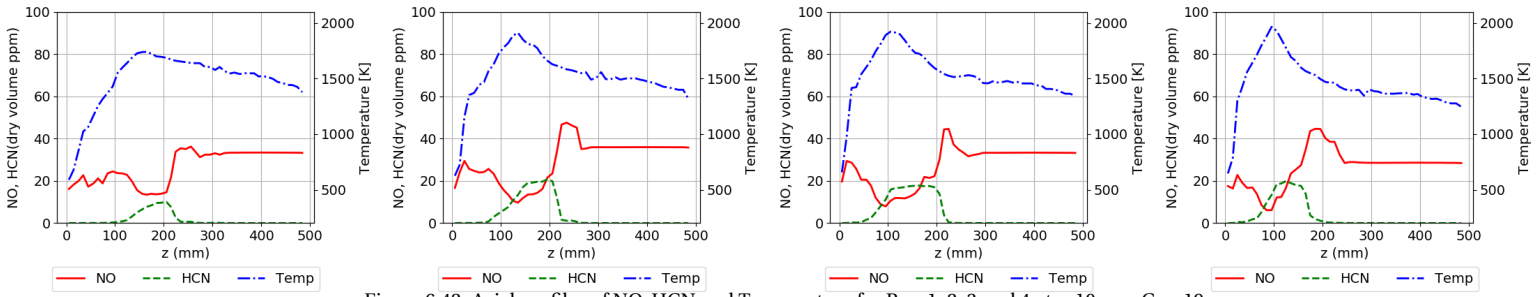

Figure 6.42: Axial profiles of NO, HCN and Temperature for Run 1, 2, 3 and 4 at r=10mm, Case19

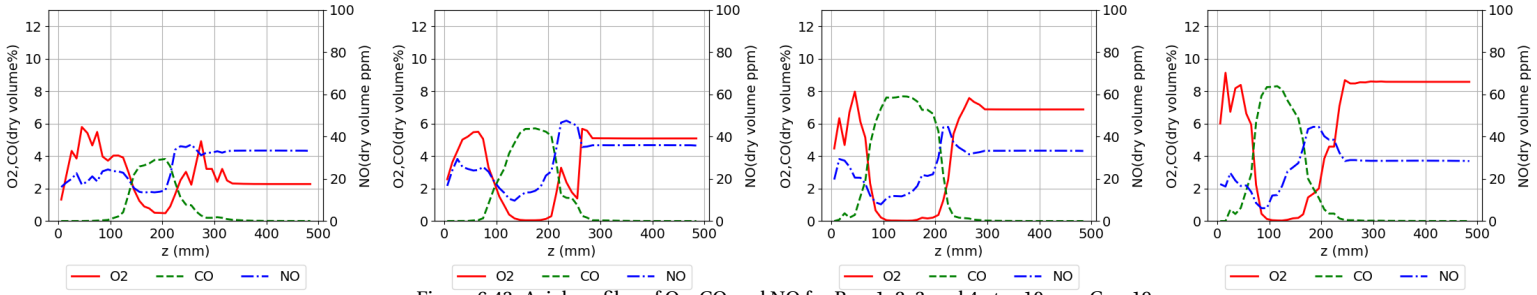

Figure 6.43: Axial profiles of O_2, CO and NO for Run 1, 2, 3 and 4 at r=10mm, Case19

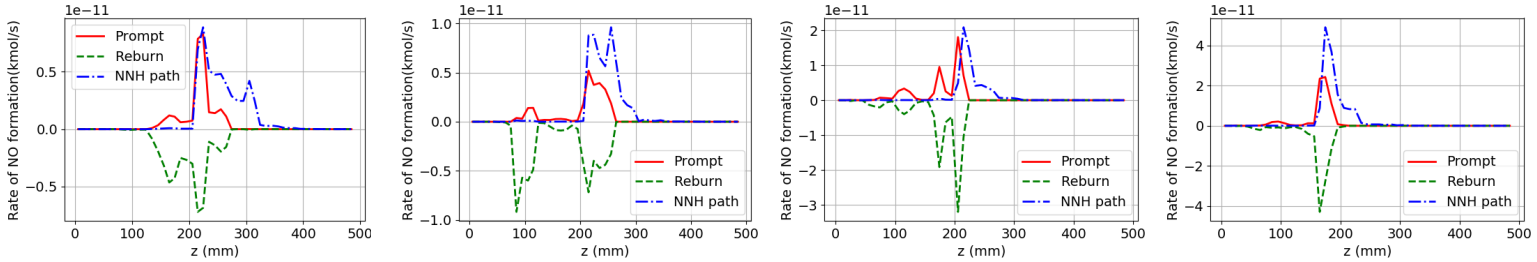

Figure 6.44: Axial profiles of NO formation rate for Run 1, 2, 3 and 4 at r=10mm, Case19

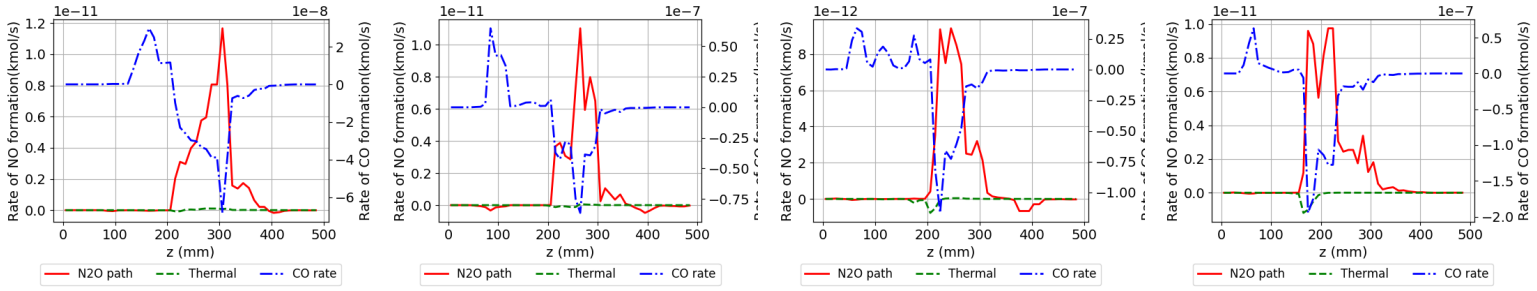

Figure 6.45: Axial profiles of NO and CO formation rate for Run 1, 2, 3 and 4 at r=10mm, Case19

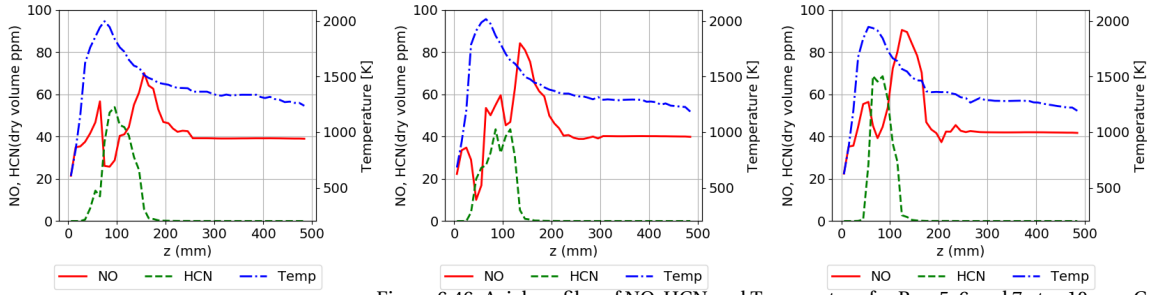

Figure 6.46: Axial profiles of NO, HCN and Temperature for Run 5, 6 and 7 at r=10mm, Case19

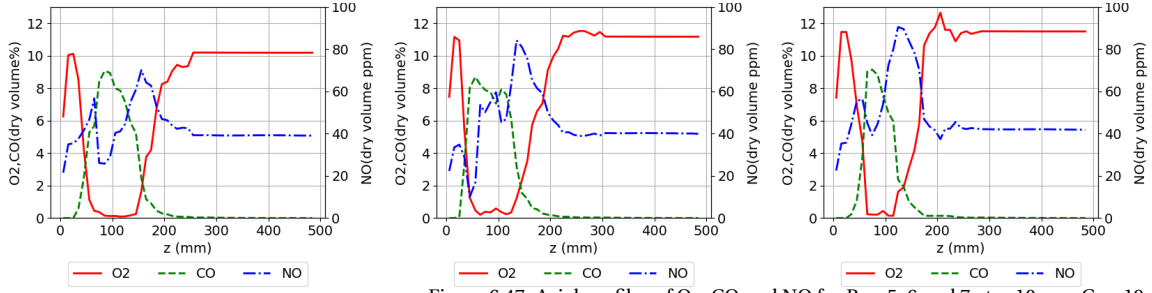

Figure 6.47: Axial profiles of O_2, CO and NO for Run 5, 6 and 7 at r=10mm, Case19

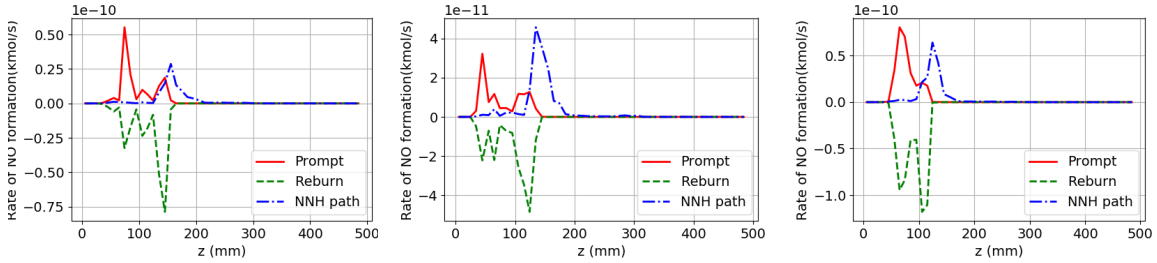

Figure 6.48: Axial profiles of NO formation rate for Run 5, 6 and 7 at r=10mm, Case19

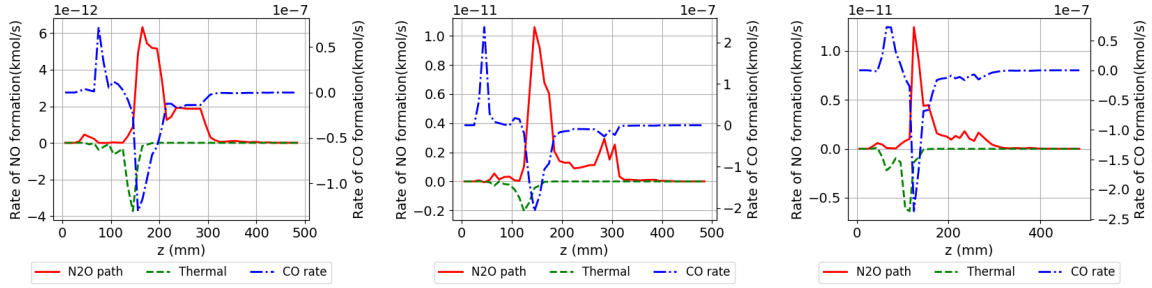

Figure 6.49: Axial profiles of NO and CO formation rate for Run 5, 6 and 7 at r=10mm, Case19

6.5. CRN PREDICTION COMPARISON

The emissions prediction from the Automatic CFD-CRN method are compared to results obtained from CFD and Manual CRN.

6.5.1. COMPARISON WITH CFD

The results of Case 17 are taken as the final results from the CRN study and are compared to the emissions predicted from CFD. The results of NOx are shown in Figure 6.50 and the CRN results are over-predicted compared to the experiments but are closer in value than the CFD results. The CFD emissions are very low, probably because of the NOx post processing model in ANSYS Fluent, which has been mentioned to under predict the NOx levels due to the equilibrium models used to estimate O species levels[40]. The CO emissions are shown in Figure 6.51, in which the CRN values capture the trend from the experiments, of decreasing and then increasing levels, although the increase occurs at a lower EAR. The early increase is attributed to the over prediction of heat loss in the early sections of the combustion chamber which leads to an insufficient addition of enthalpy to the air stream by the recirculating mass. This causes a low enthalpy stream of air to mix with the flue gases downstream causing a rapid reduction in temperature and leading to an environment less suitable for CO oxidation. There is also the factor of increase in inlet mass flow and decrease in recirculation ratio which leads to a net reduction of residence time of the CO molecules in the combustion chamber, giving them less time to oxidize. The experimental values for Run3 and Run4 are significantly lower than the rest as they were reported to be 0.0, which is probably because the actual values were less than the least count of the measuring instrument and hence for the sake of plotting on a log scale, a minimum value of 0.01 dry volume percent is used. The CFD on the other hand has a constantly decreasing trend of much lower value which, as mentioned in Section 5.7, may be due to the assumption of chemistry being faster than mixing in the flamelet model which causes the CO oxidation to be over predicted. This shows that using a detailed chemical kinetic mechanism in a CRN generated from a CFD solution can give better emissions prediction than that calculated directly in the same CFD simulation.

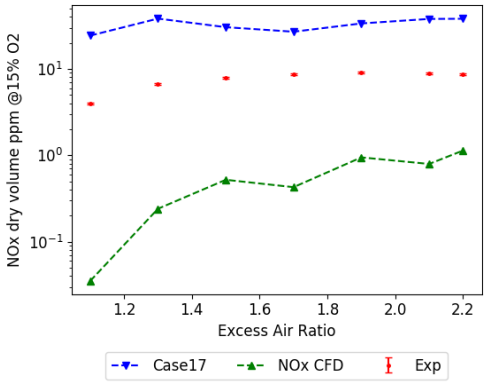

Figure 6.50: NOx v/s Excess Air Ratio at combustor outlet

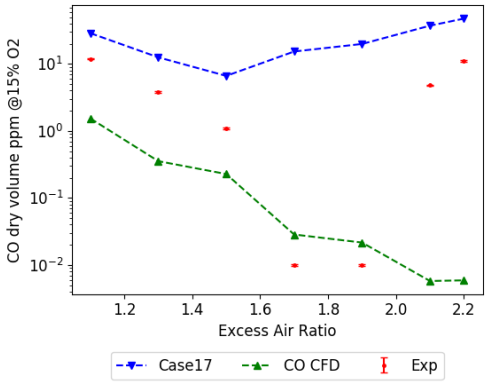

Figure 6.51: CO v/s Excess Air Ratio at combustor outlet

6.5.2. COMPARISON WITH MANUAL CRN

The combustion chamber is also modeled using a manual CRN approach, in which 7 PSRs are manually arranged and solved using the direct Reactor Network solver of Cantera. The mass flows are assigned based on the inlet mass flows and the recirculation ratio estimated from CFD. This study was carried out to compare results obtained from Automatic and Manual CRN as the latter is the more common approach to modeling chemical kinetics in combustion chambers with the specific purpose of emissions calculation[12][21]. Manual CRNs are typically smaller systems in terms of number of reactors and are hence faster to solve. On the other hand the distribution of volumes and mass flows is based on operator analysis of the flow field which makes the process less objective and repeatable. The limitation to fewer number of reactors also prevents the Manual CRN from resolving gradients to the extent of an Automatic CRN. It should be noted that the Manual CRN implemented is relatively simple and could be improved upon, but as it was not the focus of the project, variations in the model were not tested. The comparison of emissions is shown in Figure 6.53 and Figure 6.54. The NOx trend is monotonically decreasing with increase in EAR, similar to a conventional

premixed combustor. This is different from the increasing trend of the experiments and the Automatic CRN although having a much higher value than experiments, does capture the increase in NOx with increase in EAR in sections of the operating conditions. Run1 which is supposed to be in flameless condition and expected to have the lowest NOx is predicted to have the highest NOx. This may indicate the advantage of the Automatic CRN of having resolved gradients of temperature and composition for accurate NOx prediction. On the other hand, the CO values from the manual CRN are closer in value to the experiments and follow the trend better than the automatic CRN. This may be attributed to the heat loss modeling, which in the manual CRN is done by simply dividing the total expected heat loss by the number of reactors with a wall equally, five in number and the energy equation is also solved during the solution process. This leads to a higher exit temperature in the Manual CRN as seen in Figure 6.55, which leads to higher oxidation of CO resulting in lower exhaust CO than the automatic CRN. The Automatic CRN on the other hand, derives its temperatures from the CFD simulation and it seems that the heat loss model of the CFD over predicts heat loss in the earlier parts of the combustion chamber as shown in Section 6.3, which leads to lower temperatures than experiments. This may be leading to incomplete CO oxidation as explained earlier and hence the higher than experiment values. Even though both CRN types have the same total heat loss, the exit temperatures differ, possibly because of the different distribution of heat flux across reactors. This causes differing temperature distributions between the two CRN types and as specific heat capacity, C_p, is a function of temperature and composition, it also has a different distribution. Hence, the product of C_p and T, i.e specific enthalpy, at the exit may be the same, but the individual quantities may differ.

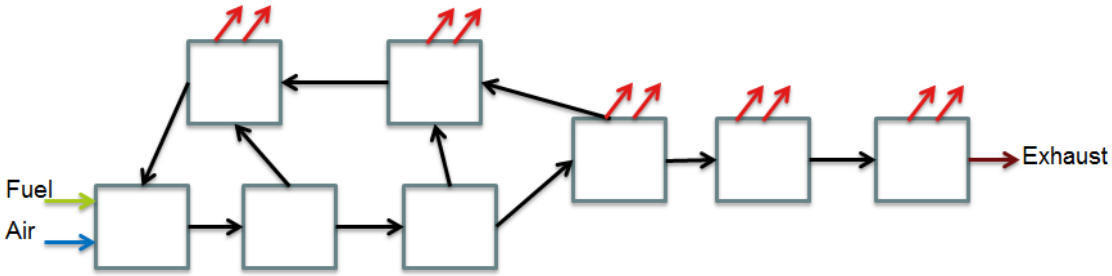

Figure 6.52: Manual CRN arrangement

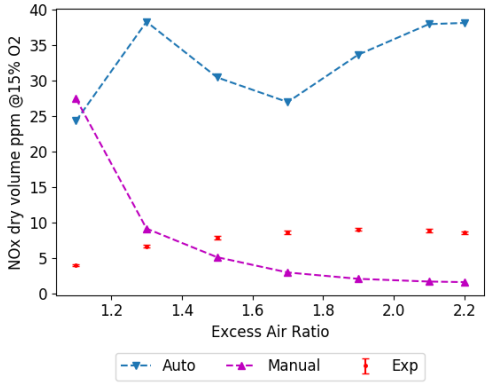

Figure 6.53: NOx v/s Excess Air Ratio at combustor outlet for Automatic and Manual CRN

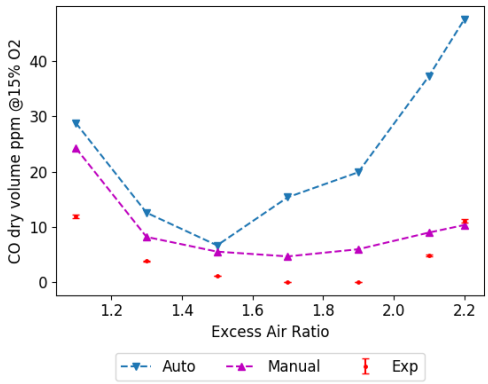

Figure 6.54: CO v/s Excess Air Ratio at combustor outlet for Automatic and Manual CRN

6.5.3. CONCLUSION FROM COMPARISON

The Automatic CFD-CRN method appears to give better predictions of NOx and CO than that obtained directly by CFD. This comparison may indicate the utility of the method in accurately predicting emissions by implementing a detailed chemical kinetic mechanism. The comparison with Manual CRN shows that the Automatic CFD-CRN gives a better trend for NOx, although the values are higher. The better prediction of trend may indicate the advantage of Automatic CRN in resolving species and temperature gradients. CO on

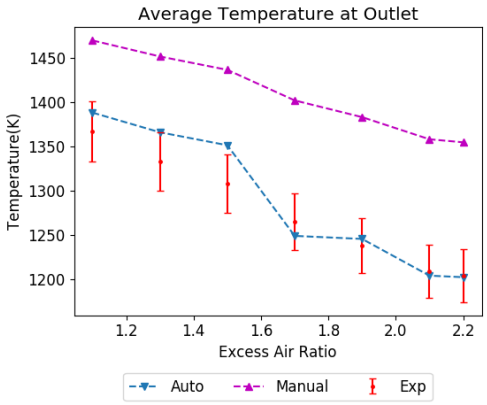

Figure 6.55: Temperature v/s Excess Air Ratio at combustor outlet for Automatic and Manual CRN

the other hand is better predicted by the Manual CRN, but that is attributed to the errors in wall heat loss model in the CFD simulation from which the Automatic CRN was generated.

7

CONCLUSION

The research was initiated with the goal of developing a computational tool that would accurately predict emissions, such as NOx and CO, from combustion chambers of gas turbines. This was due to the shortcoming of current CFD methods in doing so, within reasonable computational expense. The Automatic CFD-CRN method was found to be suitable for this application, and was seen to have been researched in open literature. The method decouples calculation of fluid dynamics and detailed chemistry. First a CFD simulation using simplified chemistry is performed to estimate the flow field. The chemistry is just detailed enough to predict the heat release within the domain. Next the CFD grid is reduced to a Chemical Reactor Network(CRN) by agglomerating similar cells together into Perfectly Stirred Reactors(PSRs). The simplified fluid dynamics of the PSR model allows one to implement a detailed chemical kinetic mechanism for the calculation of species which would have otherwise been prohibitively expensive in the CFD simulation itself. This should allow for more accurate calculation of emissions from a combustion chamber. The entire process has an underlying assumption that the pollutant species do not contribute significantly towards heat release and hence do not affect the flow field. However there was a gap in literature wherein the effect of criteria used to cluster CFD cells into PSRs to form a CRN was not studied. This was determined to be the research question for this thesis.

Does the clustering criteria have an effect on the emissions predicted by the CFD-CRN method and how does this effect vary with the choice of criteria?

A Python code capable of executing the CFD-CRN process was developed, using the solver algorithms of KPPSMOKE, a software implementing the Automatic CFD-CRN method, as a reference. KPPSMOKE was not used directly because it lacked the flexibility of implementing different criteria and did not have the option of further changing the type of ideal reactors used. The code developed, implements a clustering algorithm that uses the Breadth First Search algorithm to traverse through a graph representing the CFD cell centers and cluster cells in successive iterations to reduce the CFD domain to a Chemical Reactor Network of a smaller size. The CRN is solved using two levels of solvers, local and global, to optimize the solution time. Cantera is used as a chemistry solver in the local solver and as a bookkeeping tool in the global solver. The governing equations of the global solver are self coded so that the matrices can be handled in a sparse form. This makes it possible to handle large number of reactors with a detailed chemical mechanism, which was one of the major limitations of the Cantera default solver.

The code is used to calculate emissions from a test case. The case chosen is that of a lab-scale combustor, designed to operate in flameless regime. CFD simulations for 7 different operating conditions varying by excess air ratio are done for this case.

CRN analysis is done on this test case and the effect of clustering criteria on emissions is studied. During the process of investigation, it was found that the tolerance used to determine the Fitness of cells for clustering played an important role. The CO emissions were found to be highly sensitive to the capability of the CRN to capture recirculation and internal flow phenomenon and hence a sensitivity towards physical criteria such as Velocity Angle and Velocity Direction. The CO emissions also had a lower sensitivity to tolerance of clustering, although the reduction of tolerance by increasing the number of reactors did smoothen the spikes in CO curves. NOx on the other hand was highly sensitive to tolerance of clustering. It was also seen that along with the criterion of Temperature, the inclusion of species involved in reactions of major heat release such as

CO_2, H_2O and OH had an influence on the NOx trends. There was also an effect of intermediate species such as C_2H_2 which might influence radical formation that govern the different NOx formation pathways.

To get a better understanding of how choice of clustering criteria might affect the NOx and CO at the exhaust, the mechanism of pollutant formation in this combustion chamber was studied. The power of simulations is that one can not only predict the data at the outlet but also have a better look at phenomenon occurring within the domain, which may be difficult to measure during experiments. The CRN data is projected back onto the CFD domain and data at these cell centers is plotted. An axial line at a radial distance of 10mm from the axis is chosen for analysis. This line lies between the air and fuel inlets and is seen to be a region of main activity of heat release and flow phenomenon based on the CFD and CRN contour plots. The rate of formation of NO is high in the later part of the combustion chamber for the runs with low excess air ratio and transitions to NO formation in the early as well as later region(2 point of formation) as excess air ratio increases due to early fuel entrainment. Finally for the run with highest excess air ratio, NO formation takes place in only the early part of the combustion chamber . The NOx formation occurs mainly through NNH and N_2O pathway for the runs with lower excess ratio and the combination of prompt and NNH pathway is dominant for runs with higher excess ratio. It was found that the inclusion of C_2H_2 as a criterion changed the NOx formation mechanism in Run 7, going from Prompt dominant to similar weightage of Prompt and NNH pathways.

The predictions of CO on the other hand were found to capture the trend of the experiments of first decreasing with increase in EAR followed by an inversion of trend of increasing with increase in EAR. The increase was found to occur at a lower EAR than experiments and was attributed to the higher heat loss predicted by the CFD simulation in the earlier sections of the chamber. The higher heat loss causes a lower enthalpy addition to the main air flow by the recirculating mass and leads to a low enthalpy excess air stream mixing with the flue gases downstream. This leads to a rapid decrease in temperature, forming an environment less conducive to CO oxidation. CO was also found to be less sensitive to the addition of C_2H_2 except for a deviation in Run 7. This was attributed to the loss of resolution, in the region where excess air mixes with the flue gases downstream of the flame, due to higher tolerance upon addition of a criterion.

In conclusion, the choice of criteria does have an effect on the CRN predictions of emissions by influencing the pollutant formation mechanism. This effect is partly due to better resolution of regions of certain dominant reactions but also due to the loss of resolution in some regions due to refinement elsewhere. Also the addition of criteria makes the clustering process more constrained leading to higher tolerance. Hence, to be sure of obtaining a good solution from the CFD-CRN code, one must not only attempt to cluster to larger number of reactors but also try to limit the increase of tolerance by sparingly choosing clustering criteria keeping in mind the pollutant formation mechanisms in the combustion chamber. As it is seen that the inclusion of different species may have an effect on the trend of emissions under different operating conditions, it is recommended to perform simulations with different criteria and compare the results before finalizing a particular result.

Finally, a comparison of results from Automatic CRN to standard methods of emissions prediction is shown. In the comparison with CFD, the predictions from Automatic CRN of NOx and CO are found to be better, both in trend and absolute value, which demonstrates the advantage of using a detailed chemical mechanism for emissions prediction. Another comparison of results from Automatic CRN with those from Manual CRN shows the NOx trend to be better captured in the Automatic case, although the values are higher than those of experiments. This may be attributed to better modeling of gradients of species and temperature in the Automatic CRN due to the larger number of reactors and the algorithm used to generate it. CO on the other hand was better predicted in the Manual CRN. This was attributed to errors in the heat loss modeling in the CFD simulation used for the Automatic CRN, which may be causing an excessive temperature drop earlier in the combustion chamber leading to less oxidation of CO before it exits the chamber.

8

RECOMMENDATIONS

Based on the research and development work done during the course of this thesis, recommendations are made for further improvement of the tool, guidelines for tool usage and recommendations for improvement of the CFD simulation used as a test case.

8.1. TOOL IMPROVEMENT

- Temperature update: The temperatures of the reactors in the CRN are kept constant during the calculations, to reduce non linearity of the system of equations and achieve faster convergence. This is done under the assumption that the major species of heat release are correctly predicted in the CFD simulation. Hence, the predicted temperatures should be correct enough to determine the flow features and should not change much if recalculated by the CRN using a detailed chemical mechanism. However, the recalculation of temperature in the CRN may lead to a small deviation in temperature, which is too small to cause a significant change in flow features, but due to the sensitivity of NOx formation to temperature, it may lead to differences in prediction of NOx emissions. Hence, the tool should be extended to include temperature updates.

- Liquid fuels: The code has been demonstrated on gaseous fuels but tests should also be done on cases with liquid fuels, although slight modifications to account for mass flows due to evaporation of droplets may be required.

- Global Time stepping: The global time stepping is expected to speed up the simulation time by performing more global calculations rather than local ones when the global Newton solver becomes unstable. This module needs to be developed and added to the code

- Turbulence: It may be useful to investigate modeling of temperature fluctuations due to turbulence in the PSR as Cuoci *et al.* [17] did see an improvement in results by doing so.

- Complex geometries: Not tested on complex geometries. In theory it should be possible, but certain hard coded values of zone ids, should be re assigned depending on the simulation. The current code can handle only one Fluent fluid zone and that should be kept in mind while performing the required CFD simulation. For further development, it would be better to adapt the code to be able to handle multiple zones.

8.2. USER RECOMMENDATIONS

- One must perform a grid independence study to determine the minimum number of reactors required to accurately represent the domain. The more the number of reactors, the better resolved will the gradients be, but this would also lead to higher computational time.

- The number of reactors may be optimized by choosing criteria of species and physical conditions that influence the emissions production reactions.

- Using too many criteria may place a high constraint on the clustering process and would require a higher relaxation of tolerance to achieve a certain number of reactors. Hence the user should test different cases with various combinations of criteria and determine the most critical ones before finalizing on a result.

8.3. CFD IMPROVEMENT

The CFD simulation seems to have a higher heat loss prediction early on along the axis which may be influencing the fluid properties and hence incorrectly predicting the recirculation and mixing. It is recommended to improve the wall heat loss model used.

BIBLIOGRAPHY

[1] *Gas Turbine,* https://en.wikipedia.org/wiki/File:Jet{_}engine.svg, accessed on 01/02/2018.

[2] *Turbocharger,* https://auto.howstuffworks.com/turbo2.htm, accessed on 01/02/2018.

[3] T. Poinsot and D. Veynante, *Theoretical and Numerical Combustion,* Combustion and Flame , 534 (2005), arXiv:arXiv:1011.1669v3 .

[4] J. Warnatz, U. Maas, and R. W. Dibble, *Combustion: Physical and Chemical Fundamentals, Modeling and Simulation, Experiments, Pollutant Formation* (2006) pp. 1–378, arXiv:arXiv:1011.1669v3 .

[5] V. Fichet, M. Kanniche, P. Plion, and O. Gicquel, *A reactor network model for predicting NOx emissions in gas turbines,* Fuel **89**, 2202 (2010).

[6] G. L. Touchton, *An Experimentally Verified NOx Prediction Algorithm Incorporating the Effects of Steam Injection,* Journal of Engineering for Gas Turbines and Power-Transactions of the ASME **106**, 833 (1984).

[7] N. K. Rizk and H. C. Mongia, *Semianalytical Correlations for NOx, CO, and UHC Emissions,* Journal of Engineering for Gas Turbines and Power **115**, 612 (1993).

[8] T. Faravelli, A. Antichi, C. Callierotti, E. Ranzi, and D. Benedetto, *A kinetic study of an advanced reburning process,* Combustion Theory and Modelling **1**, 377 (1997).

[9] I. V. Novosselov, P. C. Malte, S. Yuan, R. Srinivasan, and J. C. Y. Lee, *Chemical Reactor Network Application to Emissions Prediction for Industial DLE Gas Turbine,* in *Volume 1: Combustion and Fuels, Education*, Vol. 2006 (ASME, 2006) pp. 221–235.

[10] A. Lebedev, A. Secundov, A. Starik, N. Titova, and A. Schepin, *Modeling study of gas-turbine combustor emission,* Proceedings of the Combustion Institute **32**, 2941 (2009).

[11] J. Park, T. H. Nguyen, D. Joung, K. Y. Huh, and M. C. Lee, *Prediction of NO x and CO Emissions from an Industrial Lean-Premixed Gas Turbine Combustor Using a Chemical Reactor Network Model,* Energy & Fuels **27**, 1643 (2013).

[12] G. A. Rao, Y. Levy, and E. J. Gutmark, *Chemical Kinetic Analysis of a Flameless Gas Turbine Combustor,* in *Volume 3: Combustion, Fuels and Emissions, Parts A and B* (ASME, 2008) pp. 487–496.

[13] A. G. Rao, *WHY AERONAUTICS SHOULD HAVE A CLOSER LOOK,* Leonardo Times (2015).

[14] D. Benedetto, S. Pasini, M. Falcitelli, C. La Marca, and L. Tognotti, *Emission Prediction from 3-D Complete Modelling to Reactor Network Analysis,* Combustion Science and Technology **153**, 279 (2000).

[15] T. Faravelli, L. Bua, A. Frassoldati, A. Antifora, L. Tognotti, and E. Ranzi, *A new procedure for predicting NOx emissions from furnaces,* Computers & Chemical Engineering **25**, 613 (2001).

[16] A. Frassoldati, S. Frigerio, E. Colombo, F. Inzoli, and T. Faravelli, *Determination of NOx emissions from strong swirling confined flames with an integrated CFD-based procedure,* Chemical Engineering Science **60**, 2851 (2005).

[17] A. Cuoci, A. Frassoldati, A. Stagni, T. Faravelli, E. Ranzi, and G. Buzzi-Ferraris, *Numerical Modeling of NO x Formation in Turbulent Flames Using a Kinetic Post-processing Technique,* Energy & Fuels **27**, 1104 (2013).

[18] A. Stagni, A. Cuoci, A. Frassoldati, T. Faravelli, and E. Ranzi, *A fully coupled, parallel approach for the post-processing of CFD data through reactor network analysis,* Computers & Chemical Engineering **60**, 197 (2014).

[19] D. Manca, G. Buzzi-Ferraris, A. Cuoci, and A. Frassoldati, *The solution of very large non-linear algebraic systems,* Computers and Chemical Engineering **33**, 1727 (2009).

[20] CharlesReid, *CharlesReid Wiki,* http://charlesmartinreid.com/wiki/Cantera{_}Outline{#}Overview{_}of{_}Cantera, accessed on 02/02/2018.

[21] A. A. V. Perpignan, M. G. Talboom, Y. Levy, and A. G. Rao, *Emission Modeling of an Interturbine Burner Based on Flameless Combustion,* Energy & Fuels **32**, 822 (2018).

[22] S. Lyra and R. Cant, *Analysis of high pressure premixed flames using Equivalent Reactor Networks for predicting NOx emissions,* Fuel **107**, 261 (2013).

[23] A. Lefebvre, D. Ballal, and D. Bahr, *Angewandte Chemie International Edition*, Vol. 40 (2001) p. 9823.

[24] A. Gupta and D. Lilley, *Chp 2 Combustion Phenomena of High Temperature Air Combustion,* in *High temperature Air Combustion* (2003).

[25] A. S. Verissimo, A. M. A. Rocha, and M. Costa, *Operational, Combustion, and Emission Characteristics of a Small-Scale Combustor,* Energy & Fuels **25**, 2469 (2011).

[26] S. R. Turns, *Mc Graw Hill*, Vol. 499 (Mc Graw Hill, 2000) p. 411, arXiv:arXiv:1011.1669v3 .

[27] *Gri-mech3.0,* http://combustion.berkeley.edu/gri-mech/overview.html, accessed on 02/03/2017.

[28] https://www.epa.gov/co-pollution, accessed on 02/03/2017.

[29] Nist, *NIST Chemical Kinetics Database, NIST Standard Reference Database 17, Version 7.0 (Web Version), Release 1.6.8, Data version 2015.12, National Institute of Standards and Technology, Gaithersburg, Maryland, 20899-8320.* http://kinetics.nist.gov, accessed on 01/03/2017.

[30] J. Santner, S. F. Ahmed, T. Farouk, and F. L. Dryer, *Computational Study of NOx Formation at Conditions Relevant to Gas Turbine Operation: Part 1,* Energy and Fuels **30**, 6745 (2016).

[31] J. A. Miller and C. T. Bowman, *Mechanism and modeling of nitrogen chemistry in combustion,* Progress in Energy and Combustion Science **15**, 287 (1989).

[32] J. WARNATZ, *Concentration-, Pressure-, and Temperature-Dependence of the Flame Velocity in Hydrogen-Oxygen-Nitrogen Mixtures,* Combustion Science and Technology **26**, 203 (1981).

[33] C. P. Fenimore, *Formation of nitric oxide in premixed hydrocarbon flames,* Symposium (International) on Combustion **13**, 373 (1971).

[34] J. W. Bozzelli and A. M. Dean, *0 + NNH: A Possible New Route for NOx formatio in flames,* International Journal of Chemical Kinetics **27**, 1097 (1995).

[35] P. C. MALTE and D. T. PRATT, *The Role of Energy-Releasing Kinetics in NO x Formation: Fuel-Lean, Jet-Stirred CO-Air Combustion,* Combustion Science and Technology **9**, 221 (1974).

[36] D. A. Goussis and U. Maas, *Model Reduction for Combustion Chemistry,* in *Turbulent Combustion Modeling*, Vol. 95 (2011) pp. 193–220.

[37] ANSYS, *ANSYS Fluent Theory Guide,* **15317**, 514 (2013).

[38] J. V. Oijen and L. D. Goey, *Modelling of Premixed Laminar Flames using Flamelet-Generated Manifolds,* Combustion Science and Technology **161**, 113 (2000).

[39] L. Ma, *Computational Modeling of Turbulent Spray Combustion*, Ph.D. thesis, TU Delft (2016).

[40] ANSYS, *ANSYS FLUENT User's Guide,* ANSYS FLUENT User's Guide **15317**, 2498 (2013), arXiv:arXiv:1011.1669v3 .

[41] J. A. Van Oijen and P. H. De Goey, *Predicting no formation with flamelet generated manifolds,* Proc. European Comb. Meeting , 810248 (2009).

[42] C. K. Westbrook and F. L. Dryer, *Chemical kinetic modeling of hydrocarbon combustion,* Progress in Energy and Combustion Science **10**, 1 (1984).

[43] N. K. Rizk and H. C. Mongia, *Three-Dimensional Gas Turbine Combustor Emissions Modeling,* Journal of Engineering for Gas Turbines and Power **115**, 603 (1993).

[44] A. Andreini and B. Facchini, *Gas Turbines Design and Off-Design Performance Analysis With Emissions Evaluation,* Journal of Engineering for Gas Turbines and Power **126**, 83 (2004).

[45] B. Rosati, *Prediction of Emissions from Combustion Systems Using 0D and 1D Reacting Flow Models,* Thesis , 153 (2015).

[46] M. G. Talboom, *Chemical Kinetics Study of the Hybrid Combustion System,* Thesis (2016).

[47] M. Falcitelli, L. Tognotti, and S. Pasini, *An algorithm for extracting chemical reactor network models from cfd simulation of industrial combustion systems,* Combustion Science and Technology **174**, 27 (2002).

[48] E. Ranzi, T. Faravelli, P. Gaffuri, A. Sogaro, A. D'Anna, and A. Ciajolo, *A wide-range modeling study of iso-octane oxidation,* Combustion and Flame **108**, 24 (1997).

[49] M. Falcitelli, S. Pasini, and L. Tognotti, *Modelling practical combustion systems and predicting NOx emissions with an integrated CFD based approach,* Computers and Chemical Engineering **26**, 1171 (2002).

[50] H. Schutz, R. Luckerath, T. Kretschmer, B. Noll, and M. Aigner, *Analysis of the Pollutant Formation in the FLOX® Combustion,* Journal of Engineering for Gas Turbines and Power **130**, 11503 (2008).

[51] J. A. Wünning and J. G. Wünning, *Flameless oxidation to reduce thermal NO-formation,* Progress in Energy and Combustion Science **23**, 81 (1997).

[52] A. KONNOV, *Detailed reaction mechanism for small hydrocarbons combustion. Release 0.5, (2000), available as Electronic Supplementary Material to: COPPENS, F.H.V., DE RUYCK, J. KONNOV, A.A., The Effects of Composition on the Burning Velocity and Nitric Oxide Formatio,* (2000).

[53] N. Dautov and A. Starik, *On the problem of choosing a kinetic scheme for the homogeneous reaction of methane with air,* Kinetics and Catalysis **38**, 185 (1997).

[54] S. Amzin and R. S. Cant, *Assessment of an Equivalent Reaction Networks Approach for Premixed Combustion,* Combustion Science and Technology **187**, 1705 (2015).

[55] J. Luche, *Obtention de modèles cinétiques réduits de combustion Application à un mécanisme du kérosène,* Ph.D. thesis, L'UNIVERSITE D'ORLEANS (2003).

[56] A. Cuoci, A. Frassoldati, G. Buzzi Ferraris, T. Faravelli, and E. Ranzi, *The ignition, combustion and flame structure of carbon monoxide/hydrogen mixtures. Note 2: Fluid dynamics and kinetic aspects of syngas combustion,* International Journal of Hydrogen Energy **32**, 3486 (2007).

[57] T. Faravelli, A. Antichi, C. Callierotti, E. Ranzi, and D. Benedetto, *A kinetic study of an advanced reburning process,* Combustion Theory and Modelling **1**, 377 (1997).

[58] David G. Goodwin and Harry K. Moffat and Raymond L. Speth, *Cantera: An Object-oriented Software Toolkit for Chemical Kinetics, Thermodynamics, and Transport Processes,* `http://www.cantera.org`, accessed on 02/03/2017 (2017).

[59] C. Cormen, Thomas H.; Leiserson, Charles E.; Rivest, Ronald L.; Stein, *Introduction to Algorithms(3rd ed.)* (MIT Press and McGraw-Hill, 2009).

[60] A. C. Hindmarsh, P. N. Brown, K. E. Grant, S. L. Lee, R. Serban, D. E. Shumaker, and C. S. Woodward, *SUNDIALS: Suite of nonlinear and differential/algebraic equation solvers,* ACM Transactions on Mathematical Software (TOMS) **31**, 363 (2005).

[61] G. F. C. R. Henry Cohen, H. I. H. Saravanamuttoo, *Gas Turbine Theory*, 6th ed. (Pearson Education, 2009).

[62] A. Effuggi, D. Gelosa, M. Derudi, and R. Rota, *Mild Combustion of Methane-Derived Fuel Mixtures: Natural Gas and Biogas,* Combustion Science and Technology **180**, 481 (2008).

[63] P. Coelho and N. Peters, *Numerical simulation of a mild combustion burner,* Combustion and Flame **124**, 503 (2001).

[64] A. Cavaliere and M. De Joannon, *Progress in Energy and Combustion Science*, Vol. 30 (2004) pp. 329–366.

[65] G. A. Rao and Y. Levy, *A New Combustion Methodology for Low Emission Gas Turbine Engines,* in *8th HiTACG conference,* July (2010).

[66] Y. Levy, V. Erenburg, V. Sherbaum, and I. Gaissinski, *Flameless Oxidation Combustor Development for a Sequential Combustion Hybrid Turbofan Engine,* in *Volume 4B: Combustion, Fuels and Emissions* (ASME, 2016) p. V04BT04A055.

[67] R. Luckerath, W. Meier, and M. Aigner, *FLOX[sup ®] Combustion at High Pressure With Different Fuel Compositions,* Journal of Engineering for Gas Turbines and Power **130**, 011505 (2008).

[68] W. Gardiner Jr., *Gas-Phase Combustion Chemistry*, 1st ed. (Springer, 2000).

A

Excess Air Ratio Calculation

The general equation for methane combustion under lean conditions can be written as

$$fCH_4 + a(O_2 + 3.76N_2) \longrightarrow pCO_2 + qCO + rH_2O + xO_2 + 3.76aN_2. \tag{A.1}$$

From the above equation, the conservation of atoms of elements on both sides of the equation results in the following equations:

$$\begin{aligned} p + q &= f \\ 4f &= 2r \\ 2p + q + r + 2x &= 2a \end{aligned} \tag{A.2}$$

Combing the equations in Equation A.2,

$$a = \frac{4p + 3q + 2x}{2} \tag{A.3}$$

Let Excess Air Ratio be represented by λ

$$\lambda = \frac{\frac{m_{air}}{m_{fuel}}}{\frac{m_{air}}{m_{fuel}}_{stoic}} \tag{A.4}$$

The stoichiometric combustion equation can be written as

$$fCH_4 + a(O_2 + 3.76N_2) \longrightarrow pCO_2 + qCO + rH_2O + 3.76aN_2. \tag{A.5}$$

$$\therefore a_{stoic} = \frac{4p + 3q}{2} \tag{A.6}$$

$$\begin{aligned} \therefore \lambda &= \frac{\frac{a}{f}}{\frac{a}{f}_{stoic}} \\ \lambda &= \frac{\frac{4}{f}}{\frac{a}{f}_{stoic}} \\ \lambda &= \frac{\frac{4p+3q+2x}{2(p+q)}}{\frac{4p+3q}{2(p+q)}} \end{aligned} \tag{A.7}$$

$$\therefore \lambda = 1 + \frac{2x}{4p + 3q} \tag{A.8}$$